Metallurgical and Physical Properties of Two Phase SiC_p/Al Composites Fabricated by Pressureless Infiltration Process

Thesis submitted for the degree of

Doctor of Philosophy

By

S. Santhosh Kumar

School of Physics

University of Hyderabad

Hyderabad – 500 046 India

June 2008

Dedicated

To

My Parents

DECLARATION

I hereby declare that the work reported in this thesis has been carried out by me under the joint supervision of Dr. T. Rajasekharan, Scientist 'F', Defence Metallurgical Research Laboratory and Professor V. Seshu Bai, School of Physics, University of Hyderabad, Hyderabad. I also declare that this has not been submitted to any University or Institution for the award of any degree/diploma.

Date:

Place: Hyderabad **S. SANTHOSH KUMAR**

CERTIFICATE

This is to certify that the research work compiled in this thesis entitled "**METALLURGICAL AND PHYSICAL PROPERTIES OF TWO PHASE SiC_P/Al COMPOSITES FABRICATED BY PRESSURELESS INFILTRATION PROCESS"** has been carried out by Mr. S. Santhosh Kumar under our supervision and the same has not been submitted for the award of any degree of any University.

Date:

Place: Hyderabad

Dr. T. RAJASEKHARAN
RESEARCH SUPERVISOR

Professor V. SESHU BAI
Co – SUPERVISOR

DEAN
SCHOOL OF PHYSICS

ACKNOWLEDGEMENTS

The research was carried out at The Defence Metallurgical Research Laboratory, Hyderabad and at University of Hyderabad, Hyderabad. I would like to express my sincere gratitude to my supervisor Dr. T. Rajasekharan, for his kind approval of the idea of writing this dissertation, his inspiration, continuous support during the entire course of my work, exceptional patience with critical reading, re-reading and correcting successive versions of my manuscript. Additionally I am benefited substantially from many meetings and discussions with him.

I would like to acknowledge my co-supervisor Professor V. Seshu Bai, for her support and co-operation at various stages of this work. I extend my thanks to her for the keen interest that she took during various measurements and subsequent discussions. This manuscript wouldn't have taken its complete form without the suggestions of Professor Seshu Bai. I also thank her, for her readiness in enabling me to work at different places by providing me with requisite assistance. I would like to extend my acknowledgements to Professor Seshu Bai for her patient and meticulous reading and re-reading of the manuscript and enabling it to reach a stage as presented here.

I owe my thanks to Professor Vipin K. Srivastava, Dean, Professor V. S. S. Sastry and Professor S. N. Kaul, former Deans of School of Physics, University of Hyderabad for various experimental facilities provided at the School. I wish to extend my thanks to the Central Instruments Laboratory that caters to various facilities involved in characterization. The Science Complex Workshop (SCW) has been a helping hand at different stages of experimental work. I convey my sincere thanks to the Officer-in-Charge and Staff of SCW. Further, not to be forgotten is role of Indira Gandhi Memorial Library (IGML) which has provided me with literature support that astronomical in its measure. I wish to extend my gratitude to the Chief Librarian and Staff of IGML.

I owe my thanks to Dr G. Malakondaiah, Director, Dr. A. M. Sree Rama Murthy and Dr. Dipankar Banerjee, former Directors of the DMRL for permitting me to work in DMRL and use the world class facilities available with them. I also thank all the Officers-in-Charge and Staff of Ceramics & Composites Group for enabling

me to use fabrication facilities, Metallography for help during microstructural characterization and Electron Microscopy for providing me with their exclusive facilities like SEM and EPMA. I also wish to acknowledge the help offered by Mechanical Behavior Group, headed by the Director for their support in mechanical characterization and Advance Materials Group for their help in thermal analyses. I would also like to acknowledge Dr. Amol A. Gokhale, Head of Light Alloy Foundry Group for providing me with alloys of required compositions and technical discussions. Further, the help rendered by the Workshop and Photography Group cannot be unnoticed. My thanks are also due to Shri Bijoy Sarma Head of Powder Metallurgy Group for timely help during the final stages of my work.

I extend my thanks to Dr. Roy Johnson of ARCI, Hyderabad, for helping me with Thermal Expansion measurements on my samples. Special thanks to Dr. T. Jayakumar and Shri K. V. Rajkumar of IGCAR, Kalpakkam for their assistance in ultrasonic velocity measurements followed by useful discussion. My thanks are also due to Dr. B. T. N. Sridhar of MIT, Chennai, for providing me with data on thermal conductivity of my samples. I express my thanks to the technical staff Mr. P. Kamalakar Rao and Mr. S. Suri for their willingness in helping at various stages of work. I wish to convey my sincere thanks to Mr. A. M. Job for machining my samples to a high precision and delivery of the same in stipulated time.

I wish to thank my senior Dr. K. Balkis Ameen, my colleagues Devendra, Swarup Raju, Satish, Ramudu, Parthasarathy, Kameswari and others, both at DMRL and School of Physics, for making my stay a pleasant and beneficial experience. I would like to thank my friends Satish, Praveen (s), Rizwan, Sudarshan, Samuel, Chandrajeet and Chaitanya for their continuous encouragement during all times of my life.

There are no words to express my gratitude towards My Parents who have borne patience and continuously supported me to make my desire a reality. I wish to extend my thanks to my Sister, Brother-in-Law, and convey my love to Vamshi and Gayathri. I wish to express my gratitude to Peddamama and Ninji Babai for their constant and voluntary support during the course. Financial assistance from DRDO in the form of JRF during 2003-2006 and SRF during 2006 and 2008 is greatly acknowledged.

Table of Contents

List of Tables

List of Figures

1. General Introduction

Two phase composite systems are of great interest for the benefit they offer over single phase materials in terms of physical and mechanical properties that are distinct from the constituent phases. A composite is a combination of two or more phases that differ substantially in their physical and/or mechanical properties. One of the two phases is continuous while the other phase is discontinuous and embedded in the continuous phase. The continuous phase is known as matrix and the dispersed phase is known as reinforcement. Effective properties of composite materials were found to depend on properties of individual phases and reinforcement size, reinforcement size distribution, shape and volume fraction of the reinforcing phase [1]. Among these parameters that affect the effective properties of two phase composite systems, the role volume fraction of the reinforcing phase is of significance. The effective physical properties greatly depend on the properties of individual phases and their volume fractions. The magnitudes of effective physical properties of a two phase composite system were found to fall within the magnitudes of respective physical properties. Efforts were made in the literature in order to determine and predict the effective physical properties of two phase composite systems.

Theoretical models such as Parallel [2] and Series [3] were proposed in order to determine the effective physical properties of two phase composites. A schematic view of the Parallel and Series models is shown in Figure 1.1. The bright regions represent the matrix phase denoted by ***m***, the dark regions represent the dispersed phase denoted by ***d*** and the arrows indicate direction in which a uniaxial stress is applied. These Parallel and

Series models were initially proposed to predict the effective elastic modulus of a two phase composite system.

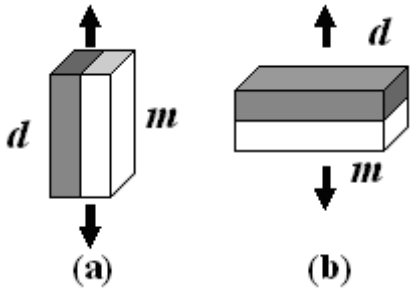

Figure 1.1 A schematic view of a composite material in (a) Parallel and (b) Series configurations.

If a stress is applied to a composite material in parallel configuration, the stress is parallel to the layers; a constant strain is experienced by each of the phases denoted by ***m*** and ***d***. In such case, for a composite material with matrix and dispersed phase volume fractions $V_{\boldsymbol{m}}$ and V_d and elastic moduli $E_{\boldsymbol{m}}$ and E_d respectively, the effective elastic modulus of the composite, E_C is given by the following relation

$$E_C = E_m V_m + E_d V_d \tag{1.1}$$

When the stress is applied normal to the layers, the stress is constant and the strain developed in the individual phases is different. For a composite material in Series configuration, the effective elastic modulus is given by the following relation.

$$\frac{1}{E_C} = \frac{V_m}{E_m} + \frac{V_d}{E_d} \tag{1.2}$$

Several experimental results for elastic modulus of composite materials were compared with the predictions of Parallel and Series model and it was observed that for

many of the two phase composite systems the experimental data falls in between the predictions of the two models at all volume fractions except V_f = 0.0 and 1.0 [4]. It was also observed that the predictions of the Parallel model are valid only on the condition that the Poisson's ratio of both the phases is equal. The Parallel model is often referred to in the literature as Rule-of-Mixtures. The disagreement between the experimental data and theoretical predictions can also be ascribed to intrinsic features of the material that affect the physical properties being measured and analyzed. Some of these features are porosity, microstructural inhomogeneity and differences in processing conditions; primary and secondary, methods used for evaluation of material parameters like volume fraction and the test conditions for the determination of physical properties of the material. Presence of porosity has great significance on mechanical properties and other physical properties such as CTE, ultrasonic velocity etc [5]. Thus, in order to understand the behavior of various physical properties it is necessary to analyze materials that are free from internal defects such as porosity.

The origin of porosity and microstructural inhomogeneity developed in a material can be traced back to the processing conditions employed in the fabrication of materials and in general composite materials. In the present context of two phase composite materials, several methods of fabrication are available depending upon various classes of composite materials. Two phase composite materials can be classified based on the features of matrix and reinforcement. Depending on the type of matrix, there are three classes of composite materials namely polymer matrix composites, metal matrix composites and ceramic matrix composites. Composite materials can also be classified based on the shape of the reinforcement into continuous fiber-, short fiber-, whisker-, platelet- and

particulate- reinforced composites as shown in Figure 1.2. Among several classes of composite materials obtained by matrix – reinforcement combinations, metal matrix composites have attracted considerable attention in view of its mechanical, thermal and physical properties. Composites with metallic matrices are preferred over polymer matrix composites for the high strength possessed by metals. Further stronger materials like ceramics could not be explored much owing to the very high temperatures required for processing. As a result, metal matrix composites have attracted large amount of research to explore the potential of high strength besides ease of fabrication.

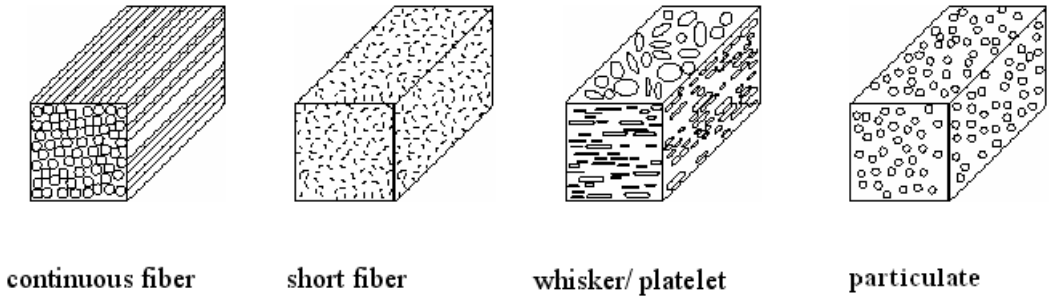

Figure 1.2 Classification of composites based on shape of reinforcement.

A metal matrix composite usually consists of a combination of metal and ceramic phases where the metal provides toughness, electrical conductivity, thermal conductivity and the ceramic provides higher strength, Young's Modulus, hardness and wear resistance. Some of the matrix materials are Al, Mg, Cu, Ni, Ti, Zn etc. the choice of which is based on the requirement of the application. These range from low density, high specific properties, high temperature capability, and high electrical conductivity to low coefficient of friction. These matrix materials are often reinforced with ceramic phases such as SiC, Si_3N_4, Al_2O_3, AlN, BN and sometimes refractory metals such as W, Mo etc.

The choice of reinforcing phase is dependent on significant physical and mechanical properties that these materials can offer in combination with their metallic matrix counterparts. Metal matrix composites have found applications in various industries such as automobile, electronics, aviation, defense etc.

Among several combinations of reinforcement – matrix systems that are possible, SiC_p/Al system has attracted attention of many researchers worldwide. One of the several interests behind this system is that the constituent phases are rather economical and possess superior physical and mechanical properties in their individual forms, among other raw materials. For example, the reinforcing phase of SiC possesses high specific strength, high hardness and low coefficient of thermal expansion which assure minimal dilatation in response to an applied stress. On the other hand, the matrix phase of Al possesses good ductility, low density and high corrosion resistance that are desirable for structural applications, especially in the field of aerospace. At the same time, it is to be noted that the matrix phase possesses high electrical and thermal conductivity, required for functional applications such as thermal management. Above all, the matrix phase offers great advantage with respect to fabrication. Besides several such interesting features, the constituent phases rank high in physical features – economy maps.

As a result, the two phases when combined would provide a composite material system with physical, mechanical, thermal, electrical properties that are otherwise not available in either of the constituent phases. The most common metal matrix composites are Aluminum alloys reinforced with SiC particulates. This system of metal matrix composites offers great promise from applications point of view, at almost all volume

fraction of reinforcement. SiC particulate reinforced Al alloy matrix composites with low volume fraction of the reinforcement find structural applications [6], specifically in the field of aerospace where low density of SiC_p/Al composites is the prime factor apart from high specific strength and ductility. A typical example of a structural MMC is SiC-17.5/6092 Al which is used as Fan exit guide vane blank with a double hollow construction as shown in Figure 1.3. Also shown in the figure is an assembled Fan exit guide vane mounted in the end cap. These components are being used in gas turbine engines of Pratt & Whitney 4084, 4090 and 4098. These composites possess tensile yield strength of 434 MPa, ultimate tensile strength of 490 MPa, a tensile modulus of 107 GPa and a corresponding strain to failure of 6 % [7].

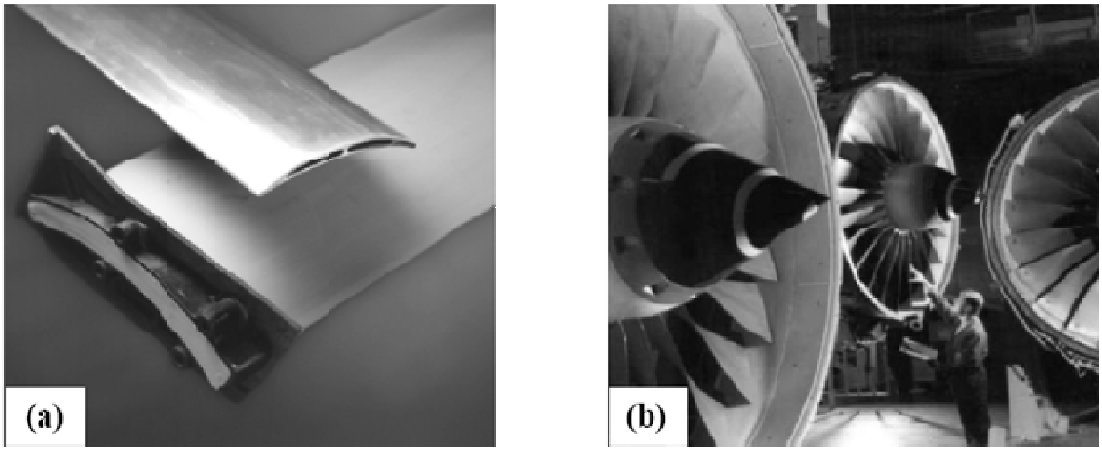

Figure 1.3 Structural application of low volume fraction SiC_p/Al MMCs. (a) Fan exit guide vane (FEGV) and (b) FEGVs assembled to Pratt & Whitney's gas turbine engine [7]. *Courtesy DWA Aluminum Composites Inc.*

Whereas SiC_p/Al composites with higher volume fractions of the reinforcement have relatively poorer mechanical properties such as low ductility, but are interesting functional materials with low coefficient of thermal expansion, high specific modulus of elasticity, hardness and high thermal conductivity. As a result, Al alloy matrix

composites with high volume fraction of SiC are suitable for electronic packaging applications [8]. A desirable feature for electronic packaging applications is low CTE to match that of semiconductor materials like Si and GaAs ($4 – 6 \times 10^{-6}$ K^{-1}). This would minimize thermal mismatch stresses between the semiconductor device and the electronic package and thus prevent failure of the device up on thermal cycling in service. Apart from low CTE, electronic packaging materials should possess high thermal conductivity for efficient dissipation of waste heat generated during operation of the device [9]. This aspect is becoming more important because of the need to pack a large number of high power devices within a small volume at present. SiC_p/Al composites are good alternatives to W/Cu composites and KOVAR in electronic packaging applications. However, W/Cu composites have high thermal conductivity (200 W/m. K) and also higher density (17.0 g/cc) in comparison with SiC_p/Al composite (3.0 g/cc) [10]. KOVAR that is extensively used in electronic packaging application suffers not only from higher density (8.2 g/cc) but also from low thermal conductivity (17 W/m. K) [10]. SiC_p/Al composites with CTE in the range of $9.2 – 6.4 \times 10^{-6}$ K^{-1}, i.e. volume fraction in the range of 0.55 – 0.75 of SiC, have promising applications as heat-sinks, electronic package, etc [8].

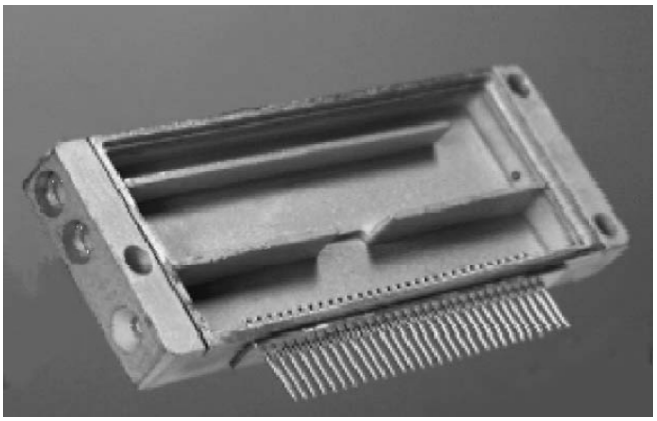

Figure 1.4 SiC_p/Al MMC used as a package for semiconductor electronics [10].

References:-

1. L. Holliday: *Advances in Materials*, Pergamon Press. (1965)
2. W. Voigt, *Lehrbuch der Kristallphysik*, Leipzig. (1928)
3. A. Reuss, *Z. Angew Math*. **9** (1929) 49.
4. C. L. Hsieh, W. H. Tuan and T. T. Wu, *J. Euro. Cer. Soc*. **24** [15-16] (2004) 3789.
5. F. P. Knudsen, *J. Amer. Cer. Soc*. **45** [2] (1962) 94.
6. J. P. Immarigeon, R. T. Holt, A. K. Koul, L. Zhao, W. Wallace and J. C. Beddoes, *Mater. Char*. **35** (1995) 41.
7. D. B. Miracle, ASM Handbook: Composites, D. B. Miracle and S. L. Donaldson, Eds., ASM International, 21 (2001) 1043.
8. G. J. Howell and A. Ball, *Wear* **181-183** (1995) 379.
9. D. D. L. Chung and C. Zweben, *Comprehensive Composite Materials*, Kelly, A., and Zweben, C. Eds., Pergamon Press, Oxford, UK, **6** (2000) 701.
10. Mark Occhionero, Richard Adams, Kevin Fennessy, and Robert A. Hay (1998), http://www.alsic.com/papers/imapsbos98.pdf

2. Literature Survey & Objectives

Particulate reinforced metal matrix composites have nearly isotropic properties. Discontinuously reinforced aluminum matrix composites have been of immense interest as heat sinks, electronic packages, truss structures, brake discs etc [1-3]. A typical Aluminum matrix composite with 25 vol. % SiC possesses a specific strength ~40 $MPa.m^3/Kg$ which is well above that of conventional materials such as steel and alloys of Al, Mg and Ti for which the specific strength ranges from 26 – 27 $MPa\text{-}m^3/Kg$ [4]. High thermal conductivity ~150 W/m. K with good wear resistance make the material suitable for applications as brake pads, brake discs, brake drums etc [5, 6]. Applications of the material have been extended to thermal management in electronics industry as heat sinks, electronic packages etc [7, 8]. SiC_p/Al composites with CTE in the range of 9.2 – 6.4 x 10^{-6} K^{-1}, i.e. volume fraction in the range of 0.55 – 0.75 of SiC, have promising applications as heat-sinks, electronic package, etc [7].

a) Fabrication Techniques:

In order to fabricate Aluminum matrix composites, several metallurgical processes that are based on solid state diffusion bonding, liquid metallurgy and vapor phase deposition are available. Several variants of these processes are discussed in brief.

Solid state diffusion bonding of materials is a process, in which a dense material is obtained as a result of bonding between neighboring particles due to mutual diffusion occurring between them in solid states at elevated temperature and under pressure [9]. Low temperatures used in solid state fabrication process are helpful to suppress the

formation of undesirable phases at the boundary between the matrix and dispersed phases. The process involves blending of constituent matrix metal and reinforcement powders to form a homogenous mixture which is then consolidated under pressure to form a compact. This green compact is then subjected to sintering, which is a method involving heat treatment to a high temperature below the melting point, when the material of the separate particles diffuse to the neighboring powder particles. In contrast to the liquid state fabrication of metal matrix composites, sintering method allows obtaining materials containing up to 50% of dispersed phase. The process of powder consolidation followed by sintering is shown in a pictorial form in Figure 2.1 and Figure 2.2. The metal matrix composites obtained in this manner can be subjected to deformation processes such as direct or indirect extrusion as a part of secondary processing.

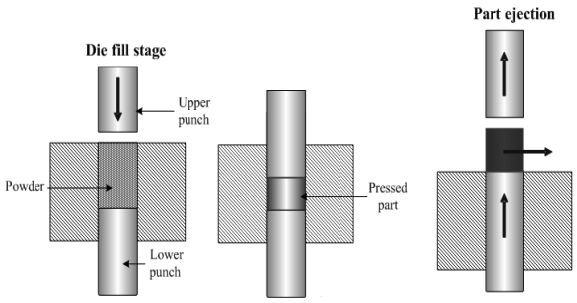

Figure 2.1 Schematic view of powder consolidation process.

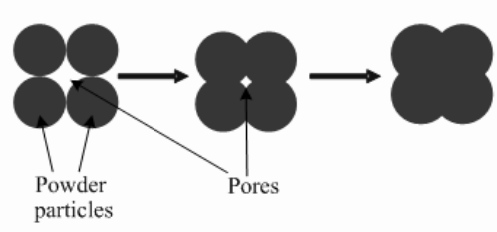

Figure 2.2 A pictorial representation of various stages in the process of sintering.

Liquid metallurgical processes are often preferred over solid state processes due the high cost of equipment involved in the latter, limitation on volume fraction and lack integrity between particle of reinforcement and matrix metal. Fabrication of metal matrix composites by liquid metallurgy techniques involves incorporation of dispersed phase into a molten matrix metal or vice-versa, followed by solidification. In order to obtain good mechanical properties, the interfacial bonding between the dispersed phase and the liquid matrix should be strong. Improved wetting can be achieved by coating the dispersed phase particles. Proper coating not only reduces interfacial energy, but also prevents chemical interaction between the dispersed phase and the matrix.

Stir casting is one of the simplest and is a cost effective method among several liquid metallurgical techniques used for the fabrication of Aluminum matrix composites [10]. Stir Casting is a liquid state method for fabrication of composite materials, in which a dispersed phase is mixed with a molten matrix metal by means of mechanical stirring. The liquid composite material is then cast by conventional casting methods which may also be subsequently processed by conventional metal forming technologies. However, in this method the reinforcement volume fraction is limited to 0.30 and distribution of the reinforcing phase is rather inhomogeneous. A difference in the densities of the two materials could cause segregation due to gravity. A close variant of the stir casting process is rheo-casting where the molten metal ceramic mixture is subjected to stirring at lower temperatures [11]. High viscosity of the semi-solid matrix material enables better mixing of the dispersed phase. Besides, disadvantages associated with stir casting process, the rheo casting process possesses additional demerits such as high power

involved in stirring a semi-solid mix and the corresponding wastage associated during casting.

In order to cope up with the limitations on maximum volume fraction of the dispersed phase, other methods were developed in course of time. It was observed that infiltration of molten metal into a compact can be used to obtain metal matrix composite upon solidification. The driving force of an infiltration process may be either capillary force of the dispersed phase **(**spontaneous infiltration**)** or an external pressure (gaseous, mechanical, electromagnetic, centrifugal or ultrasonic) applied to the liquid phase **(**forced infiltration**).** ***Gas Pressure Infiltration*** is a forced infiltration technique which uses a pressurized gas for applying pressure on the molten metal and forcing it to penetrate into a preform of dispersed phase [12]. A schematic representation of the gas pressure infiltration set up is shown in Figure 2.3. In contrast to the methods using mechanical force, Gas Pressure Infiltration results in low damage of the reinforcements.

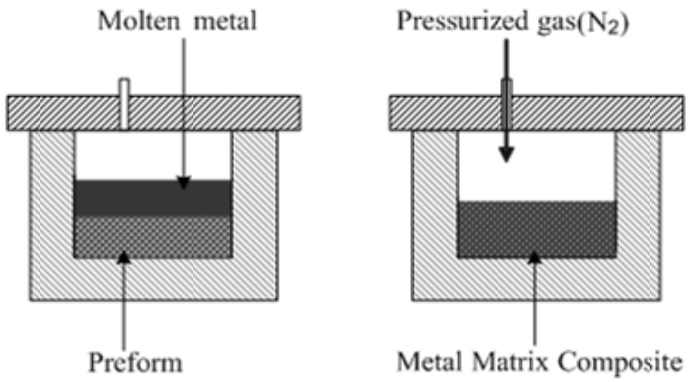

Figure 2.3 A schematic view of Gas pressure infiltration process [12].

Infiltration by ***Squeeze Casting*** is a forced infiltration technique among liquid phase methods developed for fabrication of metal matrix composites [13]. A movable

mold part (ram) is used for applying pressure on the molten metal and forcing it to penetrate into a preform of dispersed phase, placed into the lower fixed mold part. A schematic view of this process is shown in Figure 2.4.

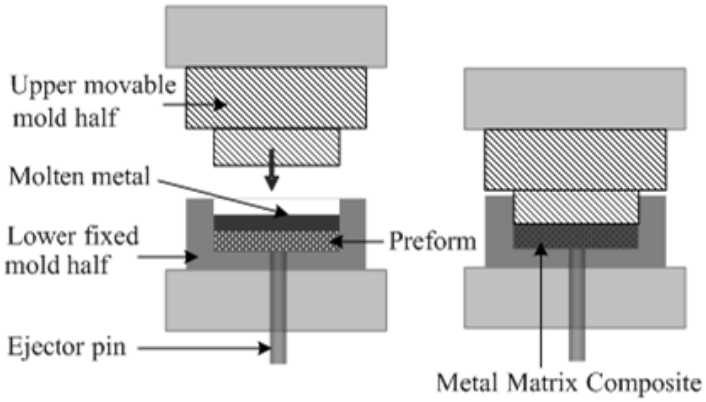

Figure 2.4 Schematic of infiltration by squeeze casting process [13].

Pressure Die Infiltration is a forced infiltration method used for fabrication of metal matrix composites, using a Die casting technology [14]. When a preform of dispersed phase is placed into a die (mold) which is subsequently filled with a molten metal entering the die through a sprue, the melt penetrates into the preform under the pressure of a movable piston. A schematic view of the process is shown in Figure 2.5.

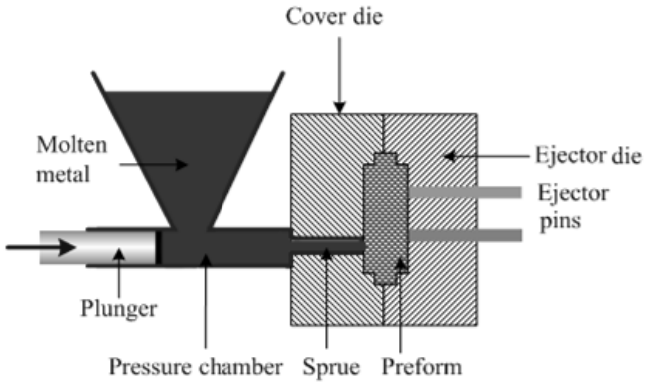

Figure 2.5 Schematic view of Pressure infiltration process [14].

Another equally promising fabrication technique is that of ***vacuum infiltration*** used for the fabrication of high volume fraction Aluminum matrix composites which are relatively defect free. A schematic of a vacuum infiltration process employed for the fabrication of SiC_p/Al composites is shown in Figure 2.6 [15]. In this method reinforcement powder compacts were prepared using vibratory compaction by aiming at different volume fractions. The compacts held in long stainless steel tubes and were immersed into a pool of Al melt under a cover of N_2 gas at a high flow rate. Following which, vacuum was applied in order to facilitate infiltration of molten Al into SiC compacts by developing a region of low pressure on the free end of the compact. The complexity of the system makes it quite un-economical for the purpose of mass production in the first case and poses a great limitation on the dimensions of the specimen and the number of composites that can be generated.

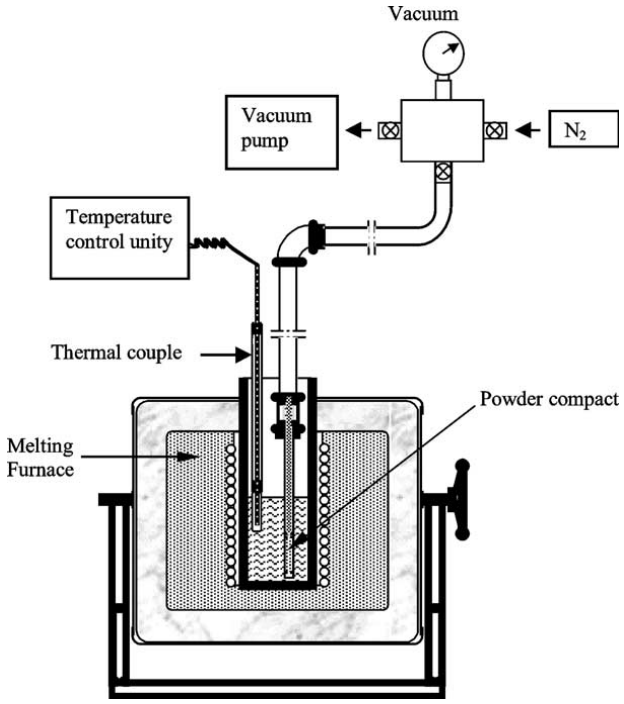

Figure 2. 6 A schematic view of vacuum infiltration process [15].

Pressureless infiltration technique is yet another method for the fabrication of Aluminum matrix composites with high volume fractions of the reinforcement [16]. The added advantage of the method is that no external force is applied on the molten metal to initiate and promote infiltration. The molten metal of suitable composition and under specific conditions of atmosphere and temperature infiltrates the preform of a refractory material to form a metal matrix composite. A schematic of experimental assembly required for pressureless infiltration is shown in the Figure 2.7.

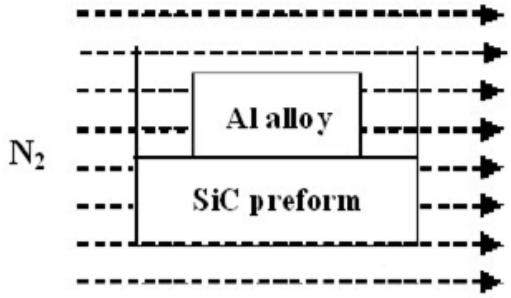

Figure 2.7 Schematic for pressureless infiltration process.

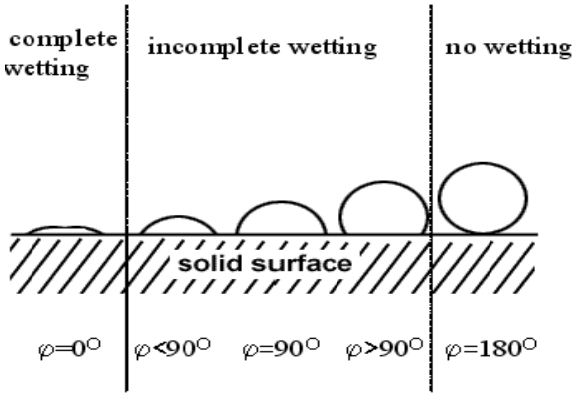

Figure 2.8 Various stages in the process of wetting.

In this process, an Al alloy is placed on the top of a preform of refractory material and the whole assembly is heated to a certain temperature well above the melting point of

the alloy. Under suitable conditions of atmosphere like N_2, the molten metal wets the ceramic preform and infiltration is initiated. The various stages involved in wetting are shown schematically in the Figure 2.8, which could be achieved by adopting appropriate thermo-dynamical conditions.

Among vapour phase methods, ***Osprey Process*** enabled building up of bulk material of SiC_p/Al composite by atomizing a molten stream of metal with jets of cold gas [17]. Injection of ceramic powder into the spray was recognized at an early stage and has been developed by many workers. Very high melt feed rates, reaching the $Kg.s^{-1}$ range, can be developed allowing ingots measured in tones to be produced during relatively brief runs. The ceramic particulate is normally injected into the gas stream, rather than the melt stream, and does not become significantly heated in flight. However, the process has a great limitation on the maximum ceramic content that can be injected into the melt stream. The process is very much suitable for bulk production of fine particle reinforced composites with low volume fraction of reinforcement and a schematic is shown in Figure 2.9.

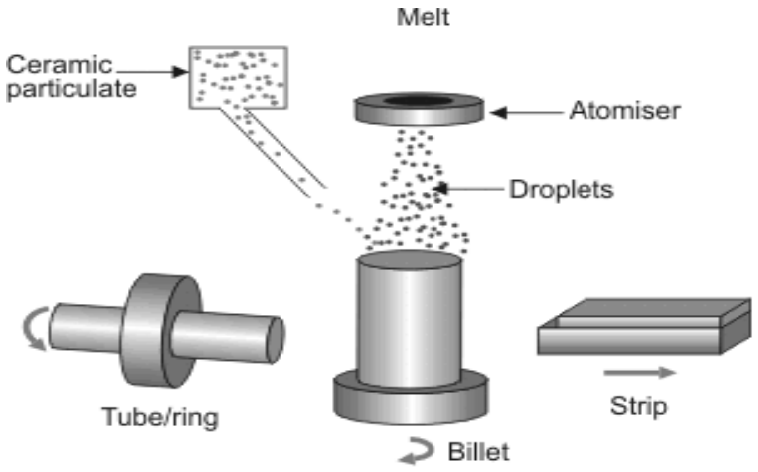

Figure 2. 9 A schematic view of the Osprey Process [17].

From a brief survey of various processes that can be used for the fabrication of Aluminum matrix composites, it is observed that metal matrix composites developed by methods such as powder metallurgy, stir casting, spray deposition etc. there is a limitation on the maximum volume fraction of reinforcement that can be achieved. Also the processes are prone to generate porosity in the interstices of powder particles or in melt during casting operation. The probability of developing a good metallurgical bond between the reinforcement and the matrix is also less. Other processes such as gas pressure infiltration, squeeze infiltration, pressure die infiltration which have the potential to deliver Al matrix composites with high volume fraction of reinforcement require specialized equipment and stringent safety measures for the process to be carried out. In comparison, the process of pressureless infiltration is a relatively cheaper technique for the fabrication of Al matrix composites with minimal or no defects at high volume fraction of reinforcement. Other advantages of pressureless infiltration include near-net shape forming and reasonable control over microstructure. Apart from these, the process also has potential to deliver composites with large dimensions and varied volume fractions of reinforcement. This is an essential feature that enables measurement of various physical properties which would in turn enable the development of a good understanding of the behavior of two phase composite systems.

b) Phase & Microstructure:

The process of pressureless infiltration has been used for fabrication of Al matrix composites reinforced with various ceramics such as SiC, Al_2O_3 and BN [18, 19]. Among these, SiC particulate reinforced Al matrix composites have received considerable interest owing to various applications. Aghajanian *et al.* [16] have developed the process

of pressureless infiltration to fabricate Al alloy matrix composites reinforced with various refractory materials by establishing suitable conditions of processing temperature, atmosphere etc. which have been patented. Subsequent to Aghajanian *et al*., many efforts were made to establish the conditions under which Al matrix composites can be prepared by pressureless infiltration [20 – 24]. Lee and Kwon have studied the age hardening behavior of SiC_p/Al composites fabricated by pressureless infiltration. Their studies on interfacial reactions in SiC_p/Al composite by XRD, SEM-EDS and TEM show that Al_4C_3 and $MgAl_2O_4$ were observed at the interface [20]. Pech-Canul and Makhlouf have paid attention to optimization of processing parameters such as concentration of Si and Mg in the alloy, surface condition of SiC, infiltration time, and particle size of reinforcing phase and height of SiC preform. They have also evaluated SiC_p/Al composites with a volume fraction of 0.40 and 0.50 for density, porosity by Archimedes principle, elastic modulus from ultrasonic pulse-echo technique and modulus of rupture by four point bend tests [21]. It was observed that the percentage porosity ranged between 2.1 and 7.5, elastic modulus varied between 162 GPa and 235 GPa and modulus of rupture varied between 183 MPa and 298 MPa for the two composites under different processing conditions. XRD and SEM-EDAX studies on SiC_p/Al composites indicated the absence of Al_4C_3 in the case of Al matrix composites reinforced with Si coated SiC particulates.

Luo *et al*. report XRD and TEM studies of SiC_p/Al composite prepared by pressureless infiltration method [22]. Their studies indicated formation of extra phases such as Mg_2Si and $MgAl_2O_4$. It was observed that by infiltrating an Al alloy that is rich in Si and Mg into a pre-oxidized preform of SiC, the formation of the hygroscopic and rather brittle phase of Al_4C_3 could be suppressed in the two phase composite system. Rao

and Jayaram have attempted to optimize growth conditions for the fabrication of Al_2O_{3p}/Al composites by pressureless infiltration [23]. They investigated the role of Mg as an alloying element and external getter in terms of initiation and continuation of the infiltration process from the studies of weight gain with time at different temperatures. It was observed that the depth of infiltration decreased with increasing temperature of infiltration. A maximum infiltration depth of 2-3 mm in the case of Al-Mg alloys and an infiltration depth of 6 mm in the case of Al-Mg-Si alloy were reported in the fabrication of Al_2O_{3p}/Al composite [22]. It was suggested that the termination of infiltration can be avoided/delayed either by using a preform cross-sectional area smaller than that of alloy billet or by placing an external getter in the pathway of incoming gas. Zulfia and Hand report the effect of Mg concentration and the dwell time for a temperature of infiltration of 900^oC under N_2 atmosphere [24]. A maximum infiltration volume of 9 cm^3 was reported with the use of Al-14Mg alloy. XRD studies indicated that Al_4C_3 phase increased with Mg concentration in the alloy and also the duration of infiltration at 900^oC. Further, the composites were found to possess porosity (7 – 9 %) and that the percentage porosity decreased with increase in the concentration of Mg in the alloy.

c) Physical Properties:

1. *Co-efficient of Thermal Expansion:*

The two phase composite system of SiC_p/Al is of interest as candidate material for electronic packaging applications, where it is required to minimize thermal mismatch stresses that develop at the semiconductor device and electronic package joint during thermal cycling of the device [25]. This is possible by making use of a material which has a low CTE that matches with semiconductor device materials like Si and GaAs. In this

context, Aluminum matrix composites with high volume fraction of SiC are considered for detailed investigations. Elomari *et al*. report their findings of CTE on high pressure infiltrated SiC_p/Al composites with a volume fraction ~0.56 [7]. They have observed that the average CTE is 12 x 10^{-6} K^{-1} and that particle size has a marginal effect on CTE at a constant volume fraction. In another work related to the evaluation of CTE of SiC_p/Al composites, Lemieux *et al*. reported the effect of reinforcement volume fraction on thermal expansion behavior of isotropic metal matrix composites within a volume fraction range of 0.10 to 0.40 [26]. A lowest CTE of 13 x 10^{-6} K^{-1} was reported in the temperature range of 25-350^{o}C. In the present context of CTE of SiC_p/Al composites, Arpon *et al*. have investigated the effect of reinforcement volume fraction on vacuum infiltrated SiC_p/Al composites in the higher volume fraction range of 0.52 – 0.74 [27]. They have made use of single particle size distribution up to a volume fraction of 0.59 and beyond which a bimodal particle size distribution was employed in order to improve the compactness of the preform and thereby increase the volume fraction. As a result, Arpon *et al*. have observed the average CTE to range between 14.9 – 7.8 x 10^{-6} K^{-1}. Lee and Hong have evaluated CTE of pressure infiltrated SiC_p/Al composites in volume fraction range between 0.50 and 0.70 [28], and found a good agreement with Turner's model for the effective coefficient of thermal expansion of a two phase composite system [29].

In order to predict the volume fraction of SiC in a composite to result in a CTE that is compatible with semiconductor device under consideration, it would be helpful to develop an understanding of the variation of coefficient of thermal expansion with relation to volume fraction. Earlier works on correlation of CTE of SiC_p/Al composites,

report a linear dependence on volume fraction of SiC [27]. Such relationships were found to hold good within a limited range of volume fraction. Much of CTE data over the entire volume fraction range is available in scattered form with differences in primary processing, secondary processing (if any), composition of the matrix, particle sizes involved, distribution of particle size or sizes (mono-modal, bi-modal or tri-modal), scheme of determination of volume fraction, test conditions etc. As a result, a clear understanding of the behavior of effective CTE of SiC_p/Al composites, over the entire volume fraction range is not present. Theoretical predictions are available in the literature in order to predict the effective CTE of a two phase composite system [29-33]. However, the agreement between the experimental results and theoretical predictions over the entire range of volume fraction of the reinforcement is to be validated.

2. Dynamic Elastic Modulus:

Refractory materials like SiC, B_4C, Al_2O_3 etc. possess high specific stiffness owing to its high modulus and low density which is a rarely observed feature in the case of metals. However, metals have the basic advantage of high fracture toughness and ductility. A composite of the two classes of materials is of considerable interest from design point of view as well as in understanding the behavior of effective properties of such materials under different conditions. Among several such combination of ceramic – metal, SiC and Al alloy have good potential to deliver features of high specific stiffness. It is of interest to deduce a relationship between effective elastic modulus of two phase composite systems and volume fraction of the reinforcing phase from application point of view as well as to notice any deviations from bounds predicted by Voigt [34] and Reuss [35]. It is known that the predictions of Voigt on effective elastic modulus of a two phase

composite, hold good on the condition that the Poisson's ratio of the two phases are equal [36]. Any difference in the Poisson's ratio between the two phases would result in a deviation of the effective elastic modulus of a composite system from the predictions of Voigt, at all volume fractions of the reinforcement other than for individual phases. In the present two phase composite system, the matrix and the reinforcement show large differences not only in Poisson's ratio but also other elastic properties. The effective elastic modulus of such a system would be of interest, in the context of Parallel [34] and Series [35] models. Evaluation of elastic modulus can be performed either by destructive methods such as a tensile test or non-destructive methods like ultrasonic testing. High volume fraction SiC_p/Al composites to be studied in the present work are rich in ceramic phase and have lower toughness owing to low concentration of ductile metallic phase. Tensile testing in such materials would be complex to perform and analyze. However, many such reports are available in literature where tensile testing is performed to evaluate the effective elastic modulus of SiC_p/Al composites [37-39]. More often such tests are limited to SiC_p/Al composites with lower volume fractions of SiC where the composites possess some amount of ductility. Because of the above reasons, it would be necessary to explore the possibility of non-destructive evaluation of high volume fraction SiC_p/Al composites for the determination of effective elastic modulus from sound wave velocity measurements in longitudinal and shear modes of vibration.

Many reports are available in the literature on non-destructive ultrasonic testing of various types of composite materials with different motivations [40-46]. Investigations of Gur were focused on relationship between microstructure – ultrasonic velocity in SiC_p/Al composites where the volume fraction ranged between 0.0 and 0.20 of SiC [40].

Fang *et al*. report the utility of ultrasonic testing in the fields of composite materials for the determination of volume fraction and its relevance in comparison with other methods [41]. Akimov and Evanov explored the applicability of ultrasonic testing on TiC-TiNi composites for the determination of elastic properties from the measurements of sound velocities in the material [42]. They have determined ultrasonic velocities in TiC reinforced TiNi matrix composites up to reinforcement volume fraction of 0.70. Gundtoft reported observations on ultrasonic attenuation and its variation with porosity in carbon fiber – epoxy, jute – polypropylene and other plant fiber composites and established a good agreement between ultrasonic attenuation and porosity, for different composite systems [43]. Shen *et al*. report investigations on ZrO_2/Al-Si composites using laser ultrasonic method and found that velocity and attenuation increased with increase in reinforcement content up to a maximum of 0.15 [44]. Djordjevic developed a remote ultrasonic inspection system using surface acoustic waves for subsurface inspection of in-line/in-process fiber reinforced composite materials [45]. Rokhlin *et al*. have focused their attention on the applicability of non-destructive ultrasonic testing in the characterization of fiber – matrix interphases owing to its importance in ensuring effective load transfer [46]. It is observed that very few studies are available in the literature on ultrasonic evaluation of SiC_p/Al composites. Further such studies were found to focus mostly on SiC_p/Al composites with low volume fraction [40] and use of ultrasonic velocity data for the determination of elastic properties of two phase composite systems has not been reported extensively. Irrespective of the method of evaluation of elastic modulus, in order to understand the variation in effective elastic modulus of a two phase composite system within the framework of existing theoretical models [34, 35, 36,

47, 48], a knowledge of the elastic moduli of the two phases and the corresponding volume fraction is required.

3. Electrical Resistivity:

It is a known fact that the effective physical properties of a two phase composite system greatly depend not only on the volume fraction but also on physical properties of individual phases. In SiC_p/Al composites, the two phases have marginal differences in their magnitudes for physical properties such as density, elastic modulus, tensile strength, fracture toughness, CTE, thermal conductivity etc. In contrast, a large difference is observed in the magnitudes of electrical properties of the two phases. Thus it is interesting to observe the variation in effective electrical resistivity of a two phase composite system and its variation with volume fraction, in a case where the magnitudes of physical properties of individual phases differ substantially. As a result, there was huge interest in the evaluation of effective electrical resistivity of metals reinforced with insulating inclusions [49-51]. Weber *et al*. studied the variation in normalized conductivity of gas pressure infiltrated Al_2O_3/Al composites in the volume fraction range of 0.40 to 0.67 of the reinforcement [49]. A nearly linear relationship was observed between the normalized conductivity and volume fraction of reinforcement. Whereas Chang *et al*. investigated the effective electrical conductivity of composites such as Mo_f/Al, SS_f/Al, C_{sf}/Ag, $Saffil_{sf}$/Ag, SiC_w/Cu, SiC_w/Ag and Al_2O_3/Ag for volume fraction ranging between 0.10 and 0.40 of the reinforcement [50]. In another work Weber reported a study of the influence of particle size on the relative electrical conductivity of gas pressure infiltrated Al_2O_3/Al composites at volume fractions of 0.45 and 0.60 [51]. It is of interest to determine the electrical resistivity of SiC_p/Al composites fabricated by

pressureless infiltration technique. Further, studies of variation in electrical resistivity as a function of volume fraction in comparison with theoretical predictions are of additional interest [34, 35, 52, 53].

4. Thermal Conductivity:

Thermal conductivity of SiC_p/Al composites is an important physical property from technological point of view and it enables us to understand the thermal response of the two phase composite material. In a two phase system such as ceramic – metal composite, the dominant mode of heat conduction in each phase is different. Theoretical studies have shown that the effective thermal conductivity of a two phase composite system is a function of volume fraction, the distribution and the thermal conductivity of the two phases [54]. Thermal conductivity of SiC_p/Al composites is of interest for electronic packaging applications where the heat generated during the operation of a device pass through packaging material onto which the device is mounted [25]. Reports on measurement of thermal conductivity of SiC_p/Al composites are available in literature [28, 55, 56]. Geiger *et al*. examined powder metallurgy based SiC_p/Al composites with volume fraction: 0.25 and 0.30, using Kohlrausch technique at sub-ambient temperatures [55]. Zhang *et al*. focused on the determination of effective thermal conductivity of squeeze cast SiC_p/Al composite with a volume fraction of 0.70 by measuring the difference in temperatures at either ends of a specimen [56]. Lee and Hong report thermal conductivity measurements on pressure infiltrated SiC_p/Al composites with volume fraction ranging between 0.50 and 0.70 [28]. They found a good agreement between experimental results and the predictions of Rule of Mixtures up to a volume fraction of 0.70, beyond which there was disagreement that is attributed to the presence of residual

pores at the particle matrix interface. In the present work, thermal conductivity of high volume fraction SiC_p/Al composites was evaluated from thermal diffusivity and specific heat measurements in order to assess the applicability of these composites for thermal management applications.

d) Mechanical Properties:

Above all, mechanical properties of SiC_p/Al metal matrix composites are of great interest for various technical applications. Despite being isotropic in nature, discontinuously reinforced Aluminum matrix composites possess many advantages such as high specific strength, ease of fabrication unlike polymer matrix composites and ceramic matrix composites, high fracture toughness and corrosion resistance etc. As a result, lot of research was carried out in the field of fabrication and evaluation of mechanical properties of SiC_p/Al composites. Some of the early techniques such as those based on powder metallurgy [9], stir-casting [10], rheo-casting [11] etc. were widely employed for the fabrication of SiC_p/Al composites in order to evaluate their mechanical properties. Though these processing techniques are simpler, they pose a great challenge on the quality of the composite material developed. This was evidenced from detailed investigation of mechanical, physical properties and microstructural features of the composite material developed using different processing techniques and under different processing conditions. Some of the limitations encountered were porosity, in-homogeneous distribution of reinforcement, undesired phases etc. For example, insufficient degassing of compacted preforms in the case of P/M processed composites, entrapment of gases during inclusion of particulates into Al melt in the case of stir casting

process etc. would result in voids, agglomeration, inhomogeneity in the distribution of reinforcement and other defects.

Use of superior techniques such as Gas-pressure infiltration [12], Squeeze casting [13], Osprey process [17] developed exclusively for the fabrication of SiC_p/Al composites were found to improve the situation with respect to microscopic issues such as porosity (open or closed), distribution of SiC particulates and undesired extra phases. However, macroscopic limitations such as dimensions of the composite material and maximum volume fraction of reinforcement have remained despite the use of sophisticated equipment in techniques like vacuum infiltration, squeeze casting, gas pressure infiltration etc. As discussed earlier, the process of pressureless infiltration possesses the potential to generate discontinuously reinforced Aluminum matrix composite with large dimensions, high volume fraction etc. [16]. This fact provides scope for evaluation of mechanical properties of SiC_p/Al composites prepared by the process of pressureless infiltration.

From a detailed literature survey, it is observed that there is a great necessity to generate systematic data on physical and mechanical properties of two phase composites, especially on the higher end of volume fraction. Further it is essential that the composite test materials are large enough for dependable characterization and free of defects/voids. Bulk specimens provide reasonable scope to obtain a statistically reliable data, whereas specimens that are not free from defects/voids would often mislead and result in erroneous understanding. The process of pressureless infiltration is very much suitable for the fabrication of SiC – Al system of composites with large dimensions, high volume

fraction of reinforcement and without many defects [16]. However, except the inventor of the process, its potential has not been realized to the best extent to obtain good quality specimens. Thus it is necessary to understand the process of pressureless infiltration that enables fabrication of SiC_p/Al composites. In order to understand the behavior of two phase composites as function of volume fraction in the high volume fraction range, it is essential to fabricate SiC_p/Al composites with different volume fractions. It is also necessary to ensure that the data corresponding to physical and mechanical properties of these materials is obtained under identical conditions of fabrication and evaluation, the major parameter being volume fraction of reinforcement. This would enable to suppress or rule out any discrepancies that could arise due to differences in processing conditions.

e) Objectives:

The main objectives of the present work:

- To optimize the composition of Al alloy under which spontaneous infiltration would occur into SiC preforms and also prevent the formation of undesired deleterious phases.

- To characterize the constituent phases i.e. SiC and Al alloys for phase purity, particle size distribution, melting point etc. as applicable.

- To generate SiC_p/Al metal matrix composites with different volume fraction of SiC in the high volume fraction range using bimodal and trimodal particle size distributions.

- To characterize SiC_p/Al metal matrix composites for complete phase composition and evaluate the volume fraction of SiC.

- To evaluate various physical and mechanical properties of SiC_p/Al composites fabricated by pressureless infiltration.

- To analyze the results obtained for phase composition, physical and mechanical properties in light of experimental and theoretical knowledge available in literature.

- To deduce relationship between physical and mechanical properties as a function of volume fraction that is valid over the entire range of volume fraction.

A detailed outline of the present thesis work is presented here.

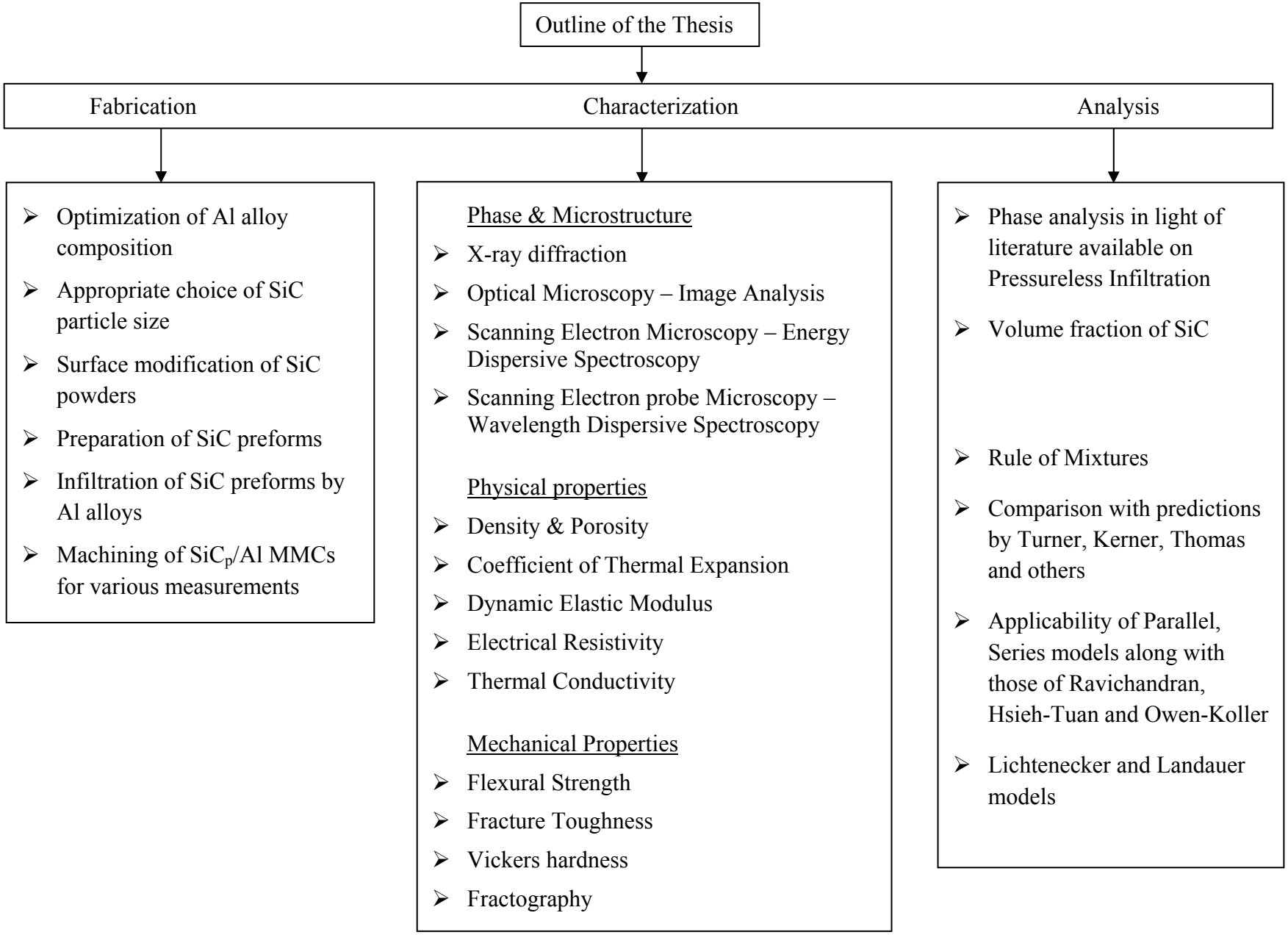
Outline of the Thesis
Fabrication
Characterization
Analysis
Optimization of Al alloy composition
Appropriate choice of SiC particle size
Surface modification of SiC powders
Preparation of SiC preforms
Infiltration of SiC preforms by Al alloys
Machining of SiCp/Al MMCs for various measurements
Phase & Microstructure
X-ray diffraction
Optical Microscopy – Image Analysis
Scanning Electron Microscopy – Energy Dispersive Spectroscopy
Scanning Electron probe Microscopy – Wavelength Dispersive Spectroscopy
Physical properties
Density & Porosity
Coefficient of Thermal Expansion
Dynamic Elastic Modulus
Electrical Resistivity
Thermal Conductivity
Mechanical Properties
Flexural Strength
Fracture Toughness
Vickers hardness
Fractography
Phase analysis in light of literature available on Pressureless Infiltration
Volume fraction of SiC
Rule of Mixtures
Comparison with predictions by Turner, Kerner, Thomas and others
Applicability of Parallel, Series models along with those of Ravichandran, Hsieh-Tuan and Owen-Koller
Lichtenecker and Landauer models

References:-

1. D. J. Lloyd, *Int. Mater. Rev*. **39** (1994) 1.
2. S. Elomari, H. Richards, C. San Marchi, M. D. Skibo and G. Vukovich, in Proceedings of the 37th Israel Annual Conference on Aerospace Sciences", edited by Kenes Tel Aviv (Omanuth Press, Haifa) p. 287.
3. F. A. Girot, J. M. Quenisset and R. Naslain, *Compos. Sci. Technol*. **30** (1987) 155.
4. D. Bacon, J. Moffatt, L. Edwards, M.E. Fitzpatrick and A. D. Tarrant, *Proceedings of the 5th Conference on Engineering of Sport,* held at Davis – USA, September 13-16, 2004, p. 216
5. W. R. Hoover (1991), *Metal Matrix Composites – Processing, Microstructure and Properties*, Ris∅, N. Hansen, D. J. Jensen, T. Leffers, H. Lilholt, T. Lorentzen, a. S. Pedersen, O. B. Pedersen and B. Ralph (eds.), Ris∅ Nat. Lab., Denmark, p. 387
6. G. J. Howell and A. Ball, *Wear* **181-183** (1995) 379.
7. S. Elomari, M. D. Skibo, A. Sundarrajan and H. Richards, *Comp. Sci. & Tech*., **58** (1998) 369.
8. D. D. L. Chung and C. Zweben, *Comprehensive Composite Materials*, Kelly, A., and Zweben, C. Eds., Pergamon Press, Oxford, UK, **6** (2000) 701.
9. T. W. Clyne and P. J. Withers: An Introduction to Metal Matrix Composites, Cambridge University Press, Cambridge, UK (1993) 318.
10. J. Hashim, L. Looney and M. S. J. Hashmi, *J. Mater. Proc. Tech*., **92** (1999) 1.
11. S. Das, T. K. Dan, S. V. Prasad and P. K. Rohatgi, *J. Mater. Sci. Lett*., **5** (1986) 562.
12. E. Carreno-Morelli, T. Cutard, R. Schaller and C. Bonjour, *Mat. Sci. Eng. **A*** **252** [1-2] (1998) 48.
13. S. K. Verma and J. L. Dorcic, *Cast Reinforced Metal Composites*, Chicago, S. G. Fishman and A. K. Dhingra (eds.), ASM (1988) 115.
14. J. N. Fridlymander: *Metal Matrix Composites*, Chapman and Hall, Oxford.(1995)

15. Y. Sahin and M. Acilar, *Composites A* **34** (2003) 709.

16. M. K. Aghajanian, M. A. Rocazella, J. T. Burke and S. D. Keck, *J. Mater. Sci*., **26** (1991) 447.

17. T. C. Willis, *Metals & Materials*, **4** (1988) 485.

18. K. B. Lee, Y. S. Kim & H. Kwon, *Metall. Mater. Trans*. **A 29** (1998) 3087.

19. K. B. Lee, H.M. Sim, S. W. Hoe, H. R. Yoo, S. Y. Cho and H. Kwon, *Composites* **A 33** (2002) 709.

20. K. B. Lee and H. Kwon, *Scripta Mater*., **36** (1997) 847.

21. M. I. Pech-Canul and M. M. Makhlouf, *J. Mater. Synth. Process*, **8** (2000) 35.

22. Z. P. Luo, Y. G. Song and S. Q. Zhang, *Scripta Mater*., **45** (2001) 1183.

23. B. Srinivasa Rao and V. Jayaram, *Acta Mater*. **49** (2001) 2372.

24. A. Zulfia and R. J. Hand, *J. Mater. Sci*., **37** (2002) 955.

25. C. Zweben, Power Electronics Technology, **2** (2006) 40.

26. S. Lemieux, S. Elomari, J. A. Nemes and M. D. Skibo, J. Mater. Sci. **33** (1998) 4381.

27. R. Arpon, J. M. Molina, R. A. Saravanan, C. Garcia-Cordovilla, E. Louis and J. Narciso, *Acta Mater*. **51** (2003) 3145.

28. H.S. Lee and S. H. Hong, *Mat. Sci. Tech*. **19** (2003) 1057.

29. P. S. Turner, *J. Res. Natl. Bur. Stand.,* **37** (1946) 239.

30. E. H. Kerner, *Proc. Phys. Soc.,* B **69** (1956) 808.

31. J. P. Thomas: *General Dynamics Report AD* 287-826 AQ4 (1960)

32. R. A. Schapery, *J. Compos. Mater.* **2** (1968) 380.

33. A. A. Fahmy and A. N. Ragai, *J. Appl. Phys.* **41** (1970) 5108.

34. W. Voigt, *Lehrbuch der Kristallphysik*, Leipzig. (1928)

35. A. Reuss, *Z. Angew Math*. **9** (1929) 49.

36. C.-L. Hsieh and W.-H. Tuan, *Mat. Sci. and Eng*, **A 425** (2006) 349.

37. D. L. Mc Daniels, *Metall. Trans*., **16A** (1985) 1005.

38. W. H. Hunt, *Comprehensive Composite Materials: Metal Matrix Composites*, T. W. Clyne (ed.), Pergamon, Oxford, UK, (2000) 701.

39. S. M. Seyed Reihani, *Mater. & Des*. **27** (2006) 216.

40. C. H. Gur, *Mat. Sci. and Eng*, **A361** (2003) 29.

41. C. K. Fang, R. L. Fang, W. P. Weng and T. H. Chuang, *Mater. Char*., **43** (1999) 217.

42. V. V. Akimov and N. A. Evanov, *J. Appl. Mech. And Tech. Phys*. **43** [2] (2002) 341.

43. Hans Erik Gundtoft, Proceedings of 15th *World Conference on Non Destructive Testing*, Roma (Italy), October 15-21, 2000.

44. Zhong-hua Shen, Xiao-rong Zhang, Shu-yi Zhang, fei-fei Zhang and Ming Zhou, *Anal. Sci*., **17** (2001) 301.

45. B. Boro Djordjevic, Proceedings of 15th *World Conference on Non Destructive Testing*, Roma (Italy), October 15-21, 2000.

46. S. I. Rokhlin, W. Huang and Y. C. Chu, *Ultrasonics*, **33** (1995) [5] 351.

47. K.S. Ravichandran, *J. Am. Ceram. Soc*. **77** [5] (1994) 1178.

48. A. J. Owen and I. Koller, *Polymer*, **37** [3] (1996) 527.

49. L. Weber, J. Dorn and A. Mortensen, *Acta Mater*. **51** (2003) 3199.

50. Shou-yi Chang, Chi-Fang Chen, Su-Jien Lin and Theo Z. Kattamis, *Acta Mater*., **51** (2003) 6291.

51. L. Weber, *Acta Mater*. **53** (2005) 1945.

52. K. Lichtenecker, *Physik. Z*. **25** (1924) 225.

53. Rolf Landauer, *J. Appl. Phys*., **23** [7] (1952) 779.

54. J. C. Maxwell: *A Treatise on Electricity and Magnetism*, **1**, 3rd Edn. Oxford University Press, Oxford. (1904)

55. A. L. Geiger, D. P. H. Hasselman and P. Welch, *Acta Mater*. **45** [9] (1997) 3911.

56. Qiang Zhang, Gaohui Wu, Dongli Sun, Guoqin Chen and Longtao Jiang, *J. Mater. Sci*. **39** (2004) 303.

3. Fabrication of SiC_p/Al Two Phase Composites

The physical properties of a two phase composite greatly depend on the physical properties of individual phases and their volume fractions [1]. However, these are affected by several other factors such as composition of the phases under consideration, porosity (if any), undesired extra phases etc. As discussed in the literature survey, in order to develop a concrete understanding of a two phase composite system, it is necessary to nullify or isolate the effects of other factors. Thus, it is highly necessary to evaluate specific features of the raw material involved in the fabrication of two phase composite materials. Such an exercise would ensure phase purity of raw materials, their specifications such as reinforcement size, morphology, density etc. In order to understand the effective physical properties of a two phase composite material, it is chosen to investigate SiC particulate reinforced Al metal matrix composites on an experimental basis. The choice to investigate SiC_p/Al composite is also based on potential of the material for applications in various industries.

SiC_p/Al composites can be fabricated by any of the metallurgical techniques described in Chapter 2. It is learnt that among these processing methods available for the fabrication of composites, pressureless infiltration technique developed for fabrication of SiC_p/Al composites, has the potential to deliver composites that are relatively free from undesired defects/voids. Other advantages of pressureless infiltration include near-net shape forming, cost-effectiveness and reasonable control over microstructure. Apart from these, the process also has potential to deliver composites with large dimensions and varied volume fractions of reinforcement. This is an essential feature that enables

measurement of various physical properties which would in turn enable the development of a good understanding of the behavior of two phase composite systems.

a) Basics of Wetting Mechanism in Infiltration Processes

The use of an infiltration technique such as Pressureless infiltration calls for a detailed understanding of the behavior of molten Al and its alloys in the presence of ceramic reinforcements in various atmospheres. The driving force for infiltration of powder preforms is capillary action and gravitation. The process of capillary action is preceded by wetting phenomenon. The primary requirement for any sort of infiltration to occur is that the liquid phase should establish a wetting condition with the solid particles during the entire infiltration process. The term wetting is generally used to describe the areal distribution of liquid on a solid surface. Experimental measurements of wetting are performed by using a steady state drop of liquid on a flat solid surface. This drop of liquid used for wetting experiments is referred to as *sessile drop*. If the liquid drop is small enough so that the gravitational force is negligible relative to its surface tension, the drop will attempt to assume a spherical shape because it presents the smallest surface area and, thus, the lowest surface free energy. Cross sectional view of sessile drops under different conditions are shown in Figure 3.1. The angle between solid-liquid and liquid-vapour interfaces is defined as the contact angle, θ.

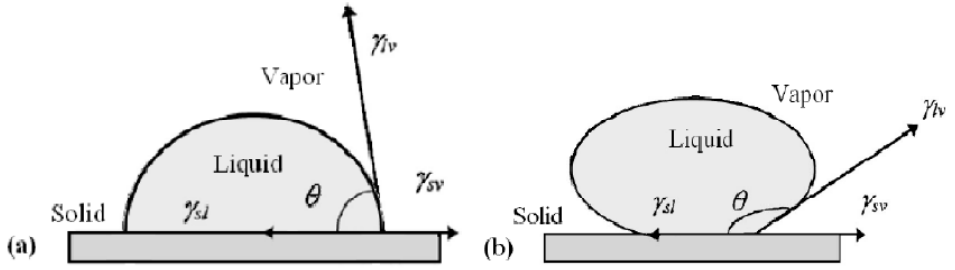

Figure 3.1 A schematic of a sessile drop in (a) wetting and (b) non-wetting conditions [2].

γ_{sl}, γ_{lv} and γ_{sv} depicted in Figure 3.1 represent the surface tension at the solid-liquid, liquid-vapour and solid-vapour interfaces respectively. If the free energy of the solid is lowered when in contact with a liquid, it will tend to be covered by the liquid and is thus wetted. On the other hand, if the surface tension of the solid is increased when in contact with liquid, it will tend to minimize the area covered by the liquid and is thus not wetted by the liquid.

The solid substrate determines the configuration of the sessile drop. When γ_{sv} is lowered by the presence of the liquid, then a driving force equal to $\gamma_{sv} - \gamma_{sl}$ will act on the periphery of the drop and will extend the liquid-solid interface. The situation is depicted in Figure 3.1a and exists when $\gamma_{sv} > \gamma_{lv}$ and $\gamma_{sv} > \gamma_{sl} > \gamma_{lv}$, and $\theta < 90^{o}$. A decrease in the contact angle causes an increase in the liquid's surface free energy. This is accompanied by a decrease in solid's surface free energy. A balance of these two forces results in a steady-state condition represented by an acute angle. Mathematically, this balance is expressed by Young-Dupre equation [2].

$$\gamma_{sv} - \gamma_{sl} = \gamma_{lv} \cos\theta \qquad (3.1)$$

The driving force for wetting is thus, $D_f = \gamma_{lv} \cos\theta$ (3.2)

When $\gamma_{sv} < \gamma_{lv}$ and $\gamma_{sv} < \gamma_{sl} < \gamma_{lv}$ (Figure 3.1b), a steady state condition arises with $\theta > 90^{o}$. An increase in the contact angle causes a decrease in the drop's surface area and, thus, an increase in the liquid's surface free energy. This is accompanied by an increase in the solid's surface free energy and a decrease in wetting of the solid by the liquid. From the above discussion, it is understood that the process of wetting can be initiated by

monitoring the liquid-vapour surface tension. This shall favor capillary action and thereby promote infiltration of liquids into powder preforms as shown in Figure 3.2.

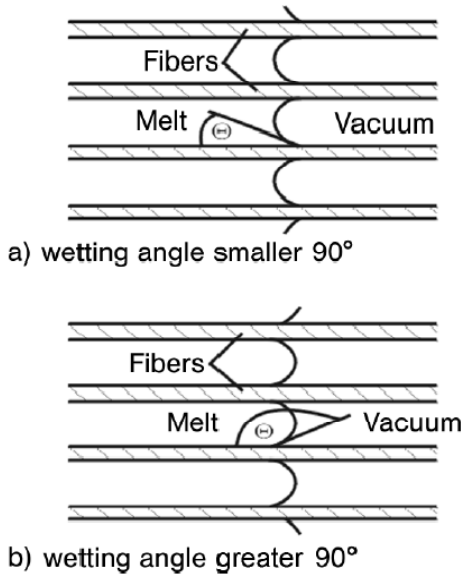

Figure 3.2 A schematic representation of an ideal melt infiltration of fiber preforms [3].

Thus it is necessary to establish conditions such that the molten metal possesses low surface tension and low viscosity. In the present case of fabrication of SiC_p/Al composites, it shall be ensured that the Al alloy possesses a wetting angle that is smaller than 90^o and thereby aid in wetting of SiC particulates. It is a known fact that both surface tension and viscosity of liquids decrease with increase in temperature. The process of pressureless infiltration occurs by reactive wetting of refractory materials by molten Al metal, resulting in a metal matrix composite upon solidification [4]. Fabrication of metal matrix composites by liquid metallurgical processes, usually employ temperatures that are well above the melting point of the alloy. In the event of contact between SiC and molten Al at a temperature above 650^oC, it is observed that, a chemical reaction occurs to form Aluminum Carbide (Al_4C_3), as per the following equation [5].

$$4Al_{(l)} + 3SiC_{(s)} \rightarrow Al_4C_{3(s)} + 3Si_{(s)} \quad (3.3)$$

Use of higher temperatures is beneficial in terms of reducing the viscosity of the melt, but on the other hand it is estimated that, also the rate of reaction is higher at temperatures above 700^{o}C resulting in accelerated dissolution of silicon carbide phase. Specific features of Al_4C_3 are that the phase is stable up to a temperature of 1400^{o}C with a hexagonal crystal structure [6]. However, this phase is susceptible to failure either by mechanical disintegration or by chemical disintegration. This phase is very brittle and hygroscopic in nature. Atmospheric attack on Al_4C_3 phase results in the formation of methane and Aluminum Hydroxide, as per the following chemical equation [7].

$$12H_2O_{(l)} + Al_4C_{3(s)} \rightarrow 3CH_{4(g)} + 4Al(OH)_{3(s)} \quad (3.4)$$

As a result of the above chemical reaction, the gaseous phase escapes into the atmosphere and leaves back porosity in the material during the service of the composite material. The release of methane from a material is also hazardous to the working environment. Porosity developed in this manner would affect several physical and mechanical properties of the composite in an unpredictable manner [8]. Keeping in view the performance of a component made out of a composite material it is very essential to avoid the formation of such a deleterious phase right in the beginning of the composite preparation. Thus there is a great necessity to inhibit the dissolution of silicon carbide phase in molten aluminum. Thus, merely increasing the temperature of infiltration does not serve the purpose of developing a SiC_p/Al metal matrix composite that shall be free from defects/voids etc.

However, use of temperatures ≥ 600^{o}C is necessary in the case of infiltration processes which pose a great demand to take steps for suppression of Al_4C_3 phase. The formation of Al_4C_3 can be prevented in several ways such as modifying the composition of the aluminum alloy, surface of the reinforcement, temperature of infiltration and dwell time at temperature etc. As a part of modification of alloy, silicon is much preferred among several of the combinations attempted by other researchers [9]. It is known that at temperatures above the eutectic point, silicon present in the alloy would be expelled from the melt outward. This phenomenon has been exploited to minimize the activity of aluminum at the interface thereby preventing the dissolution of silicon carbide. This is one of the primary reasons for using an aluminum alloy containing large amounts of silicon. Moreover, addition of silicon would also aid in reducing the melting point of the alloy substantially and enable good flow properties. It is observed that in order to aid wetting of ceramics by molten Al, Mg is used as alloying element. Addition of Mg to pure Aluminum reduces the surface tension of the melt and promotes wetting of a surface [10]. Fall in the surface tension of the aluminum alloy would enable proper wetting of the silicon carbide preforms.

Modifications to the processing schedule are yet another way of limiting the dissolution of SiC in molten Al and thus prevent the formation of Al_4C_3. The temperature and duration of infiltration can be optimized to evolve a sequence of operation that would result in metal matrix composites with zero or minimum amounts of aluminum carbide phase [11, 12]. Dissolution of silicon carbide can also be prevented by modifying its surface conditions [13]. These modifications are bound to be in such a way that any extra phase formed would not degrade the final properties of the composite in any manner.

Some of these are providing protective coatings of metals like nickel, silver, copper and sometimes even silicon [14, 15]. Apart from providing protective metallic coatings from external sources the surface of silicon carbide phase can also be modified by trivial heat treatment procedures. As received silicon carbide particulates would by themselves possess a native layer of amorphous silica developed on the surface. However the thickness of the silica layer can further be increased by controlled heat treatment either in air or oxygen atmosphere, if feasible.

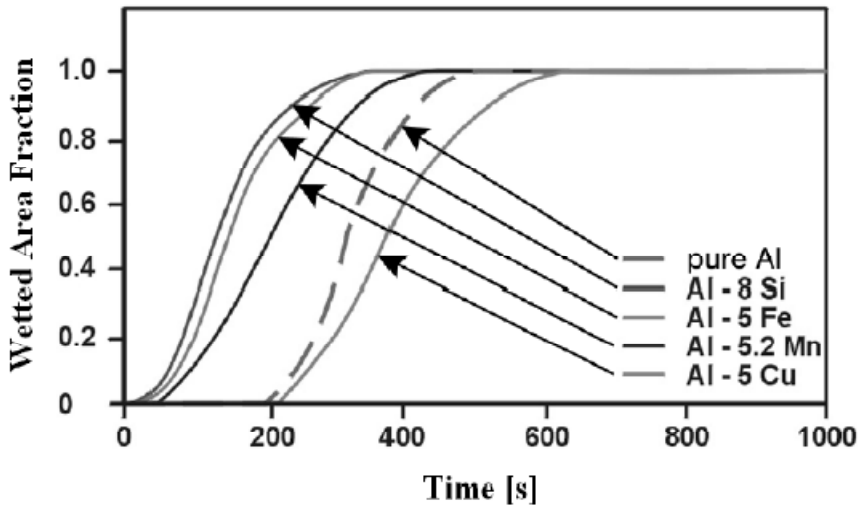

Figure 3.3 Degree of wetting of SiC plates by various Al alloys as a function of time [16].

Thus, in order to enable proper flow of the melt and wetting of the preform it is essential to use an aluminum alloy containing both silicon and magnesium. The choice of Si as an alloying element is also based on the work of Choh and Oki [16]. It is learnt from Figure 3.3, that Al-8Si alloy possesses a greater degree of wetting with SiC plates, when compared to other alloying additions such as Mn, Cu etc. From a detailed survey followed by variations in experimental conditions such as composition of the Al alloy, surface conditions of SiC reinforcement, atmosphere, temperature of infiltration and

duration of infiltration, a systematic schedule for pressureless infiltration was developed in the present work.

Apart from surface tension and viscosity of the melt, another parameter of paramount importance is the infiltration rate which has direct role in controlling the formation of Al_4C_3 and AlN phases that are not desired [5,17]. At low infiltration rates, the melt would be in contact with the reinforcement and atmosphere, both of which are to be minimized. High infiltration rates are favorable not only in terms of limiting the formation of undesired phases but also in reducing the effective processing time involved in the fabrication of SiC_p/Al composites. Martins *et al*. have developed an intrinsic parameter known as the infiltration rate which is directly governed by the surface tension and viscosity of the melt, apart from the pore radius [18].

$$\phi = \left(r\gamma_{LV}\cos\theta\right)/2\mu \qquad (3.5)$$

Ø: Infiltration rate parameter; $r\gamma_{LV}\cos\theta$: Surface tension force term and μ: Viscosity of the melt.

The Washburn equation, which is used to measure pore-size distributions by mercury porosimetry technique, provides the pressure P, required to infiltrate a pore of given radius and is expressed as follows [19].

$$P = \left(2\gamma_{LV}\cos\theta\right)/r \qquad (3.6)$$

Further McCoy *et al*. suggest that as the particle size decreases, an increased energy (pressure) is required for wetting to occur because the metal must deform to a smaller radius, thereby making infiltration difficult [10]. This is in coincidence with the

Washburn equation. As the particle size increases, the capillaries between the particles also increase which reduces the pressure required for infiltration to occur, thereby increasing the infiltration rate parameter. However, Aghajanian *et al*. report that under the conditions employed for pressureless infiltration, the results were contradictory to the aforementioned facts [17]. In their work, it was observed that fine fused alumina particles were easily wet and as the particle size increased, the tendency for infiltration was reduced. In the case of preforms with dual particle size distributions, the size of the pore is governed by finer particles because of the fact that the pore network generated by coarse particles would be occupied by the finer particles.

b) Optimization of Aluminum Alloy Composition

Commercially available Aluminum alloy LM-6 that is rich in Si was used to prepare alloys with varying concentrations of Mg such as 1, 3 and 5 wt %. These alloys were fabricated using a gas fired furnace to which LM-6 Al and Al-50Mg alloys were added according to necessary proportions in separate batches. The melt was degassed using suitable fluxes, before and after alloying with Mg. During the process of alloying some amount of Magnesium is likely to evaporate due to its high vapor pressure and low boiling point [20]. In order to arrive at the optimized composition for the alloy necessary corrections were made to the amount of magnesium to be added to the melt. It is estimated from routine foundry practices that a loss of up to 10% is observed in the case of Mg containing Al alloys. For example in order to arrive approximately at a composition of Al-9Si-5Mg, an additional 10 % Mg i.e., Al-9Si-5.5Mg was aimed at. Upon sufficient homogenizing of the molten aluminum alloy, the melt was cast into a

definite shape to obtain an ingot of Al-Si-Mg alloy intended for pressureless infiltration experiments.

Preliminary experiments were performed in a tubular furnace with nitrogen atmosphere and the thermal profile adopted is shown in Figure 3.4. Commercially available SiC belonging to the abrasive grade and Al-Si alloys with Mg: 1, 3 and 5 wt 5 were used for infiltration trials according to the aforementioned thermal profile.

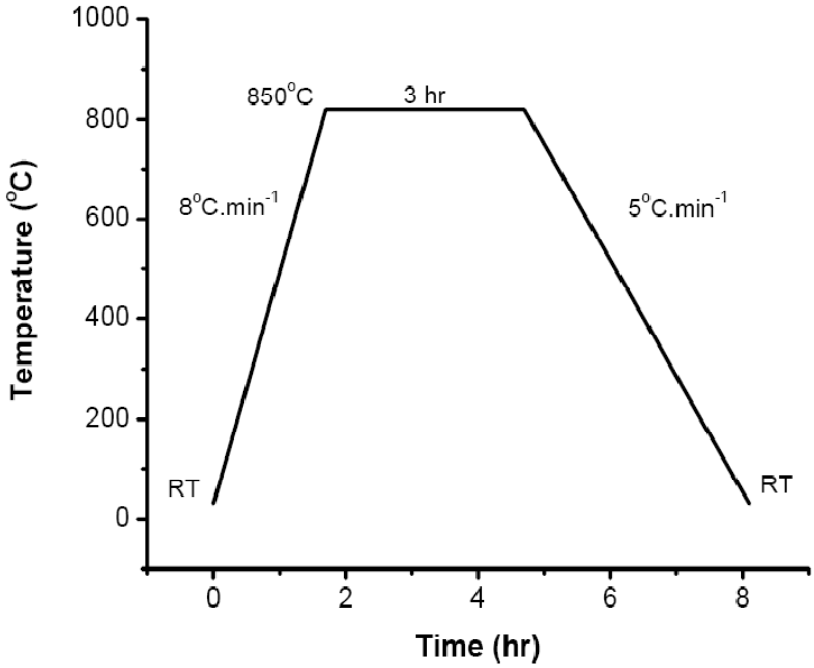

Figure 3.4 Thermal profile employed in the present work.

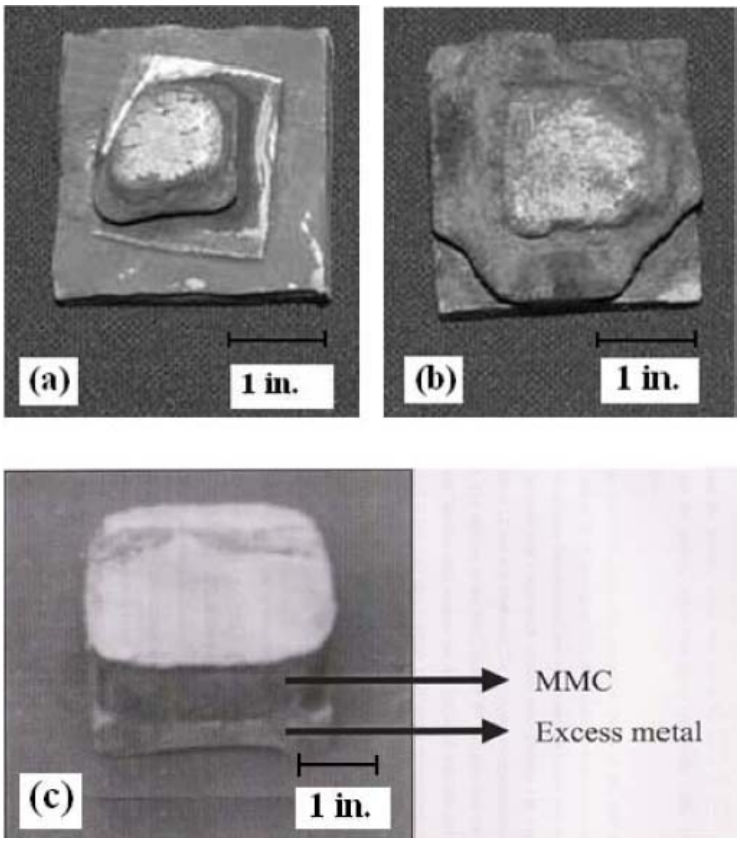

Figure 3.5 Photographs showing SiC_p/Al MMCs prepared using (a) 1 wt % Mg, (b) 3 wt % Mg and (c) 5 wt % Mg.

From a brief study, by varying the composition of Al alloy, it was found that by employing the thermal profile shown in Figure 3.4 in a nitrogenous atmosphere, Al-9Si-5Mg alloys are suitable for the growth of near net shape SiC_p/Al composites. By repeated small scale experiments of pressureless infiltration, it was ensured that the processing schedule developed above would yield metal matrix composite with complete infiltration on reproducible basis.

In order to ensure that the composites that shall be grown according to the experimental conditions that were optimized above are free from internal defects such as voids or undesired extra phases etc. further steps were taken to prevent the dissolution of

silicon carbide phase in molten aluminum. Apart from optimizing the composition of the matrix metal, surface modification of silicon carbide was considered as an important step. A protective layer between the melt and the reinforcement would prevent a reaction between molten aluminum and silicon carbide and thus suppress the formation of aluminum carbide [13, 14]. It is also essential that the protective layer is stable throughout and subsequent to the process of infiltration. Further it is necessary that the protective coating is adherent to the surface of the particulate in order to assure a firm bonding between the matrix and reinforcement. It is known from literature that silicon carbide that has been subjected for heat treatment in air develops a highly stable layer of silicon di-oxide on the surface of silicon carbide particulate [21].

$$2SiC + 3O_2 \rightarrow 2SiO_2 + 2CO \qquad (3.7)$$

The process of heat treatment of silicon carbide in air serves more than one purpose. The heat treatment schedule results in the development of a layer of amorphous silica that acts as a barrier between silicon carbide and molten aluminum. For having developed from the surface of silicon carbide as a native layer, the silica on the surface is expected to be much adherent than protective metallic coatings like nickel, silver, copper and other that are external in nature. Above all the surface silica layer is stable even at temperatures well above temperatures used for infiltration of aluminum into silicon carbide preforms. However an interfacial reaction cannot be inhibited and is a necessary criterion for a strong and stable bond between the reinforcement and the matrix. During the process of compositing it is expected that the molten aluminum gets in contact with amorphous silica layers present on silicon carbide powders. As a result of which molten

aluminum reacts with silica to form other phases according to the following chemical reaction [22].

$$3SiO_{2(s)} + 4Al_{(l)} \rightarrow 2Al_2O_{3(s)} + 3Si_{(s)} \qquad (3.8)$$

The result of the above reaction is again a refractory material at the interface. In either ways, heat treatment of silicon carbide powders would be beneficial not only by suppressing formation of aluminum carbide, a weak and deleterious interface but also developing a strong and stable interface. In order to determine the temperature at which the heat treatment of silicon carbide powders has to be carried out, a thermo-gravimetric analysis has to be performed. In this method the sample in the form of a powder is heated in air at a steady rate to a temperature of about 1500^{o}C. The gradual change in mass of the specimen as a result of change in temperature is recorded as a function of programmed temperature. A change in the slope of the mass versus temperature curve would give the temperature at which there is a rapid pick-up of oxygen to form silica on the surface of silicon carbide. It was observed from the literature that oxidation of SiC starts at a temperature above 800^{o}C and reaches a maximum at 1300^{o}C [23]. Subsequently reinforcement powders of commercial grade were heat treated in air at the temperature of 1200^{o}C. This heat treatment was carried out for duration of 8 hours, adopted arbitrarily and is expected to develop an amorphous layer of SiO_2 with an approximate thickness of 400 nm [23].

c) Characterization of Constituent Phases

The aluminum master alloy and surface modified silicon carbide powders were analyzed for phase purity prior to the process of fabricating SiC_p/Al metal matrix composites by pressureless infiltration technique. Knowledge of the phase composition of

a material is an essential feature that enables proper understanding of the properties of the material. It is also necessary to identify various phases present in the material in order to predict its behavior under different conditions and knowledge of its composition will be helpful at various stages of further evaluation. X-ray diffraction technique is a versatile technique in assessing the compositions of a material and involves only a small amount of work involved in sample preparation. Specimens are usually considered in powder form for being exposed to X-radiation and obtain reflections from the specimen. When a beam of parallel monochromatic X-rays of approximately 0.1 nm wavelength is incident on a crystalline substance, the material acts as a three-dimensional diffraction grating and produces an X-ray diffraction pattern. Constructive interference of such diffracted beams occurs according to Bragg's law, to result in a well resolved reflection pattern that corresponds to the material under investigation.

$$n\lambda = 2dSin\theta \qquad (3.9)$$

Where $\boldsymbol{n}$ is an integer representing the order of diffraction, $\boldsymbol{\lambda}$ is the wavelength of the incident X-rays, $\boldsymbol{d}$ is the distance between a lattice planes and $\boldsymbol{\theta}$ is the angle between the incident X-ray beam and the lattice planes. These lattice planes are represented by a set of integers in the form of (hkl), known as Miller indices that define the orientation of the plane with respect to crystallographic axes. The diffraction pattern of a powdered material is a collection of intensities corresponding to lattice spacings that are unique for each crystalline substance. As a part this procedure, X-ray diffraction analyses was carried out using an X-ray Diffractometer from Philips, with $CuK_{\alpha 1}$ radiation. The corresponding X-ray diffraction patterns were indexed according to the standard

diffraction patterns available in the form of a database PCPDFWIN version 2.02, May 1999 issued by ICDD. The corresponding diffraction patterns are shown in Figure 3.6 and Figure 3.7.

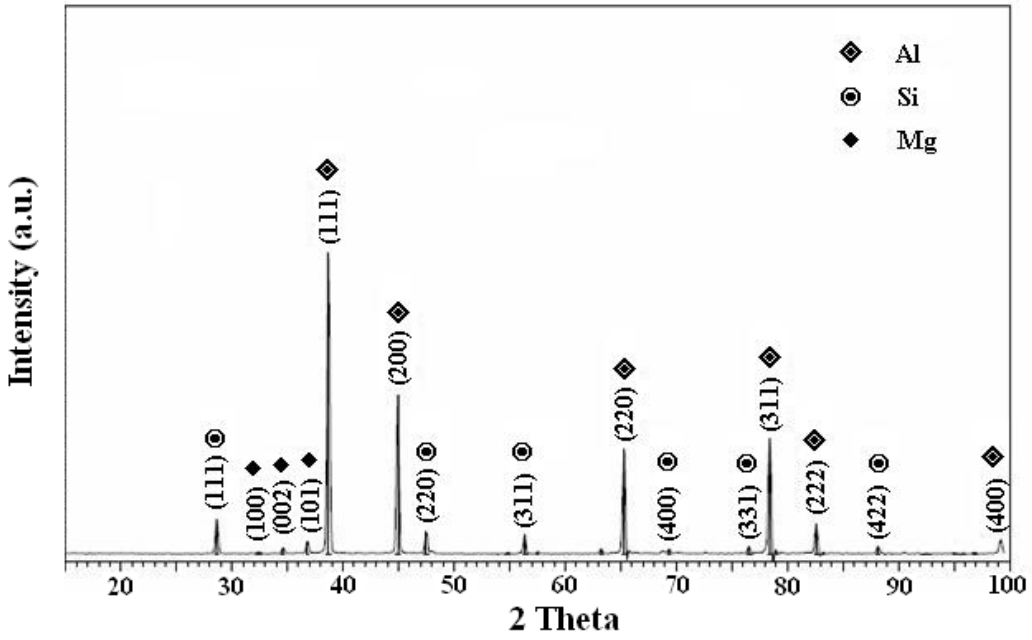

Figure 3.6 X-ray diffraction pattern of the Al-Si-Mg alloy.

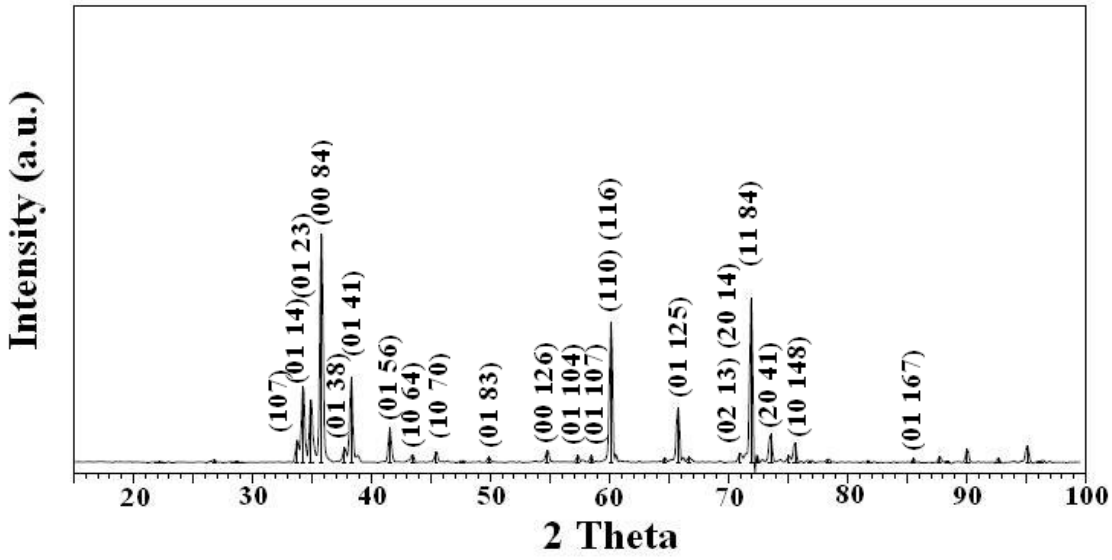

Figure 3.7 X-ray diffractogram SiC powder.

A TG - DT analyzer, TGA – 850 from METTLER TOLEDO was used for the determination of melting point. Melting transition can be observed at 564^{o}C from the thermogram shown in Figure 3.8. The aluminum alloys thus prepared were used for the infiltration of SiC preforms.

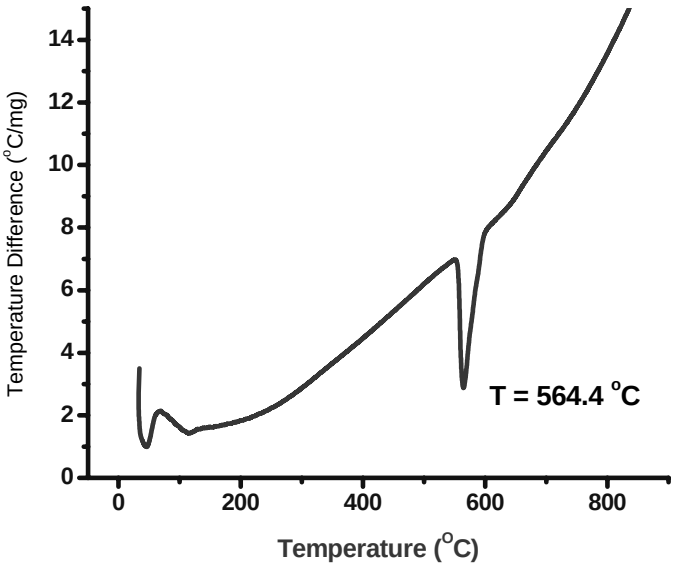

Figure 3.8 Differential Thermal Analyses of Al-Si-Mg alloy used for pressureless infiltration.

The binary phase diagrams corresponding Al-Si and Al-Mg are shown in Figure 3.9 (a) and (b) respectively. From the figure it can be observed that there is a eutectic point at Al-12Si with a temperature of 577^{o}C. Aluminum alloy used in the present work possesses a near eutectic composition with respect to the concentration of Si. The consequence of the same is the lower temperature of phase transition (solid→liquid) in the case of Al-Mg-Si alloy.

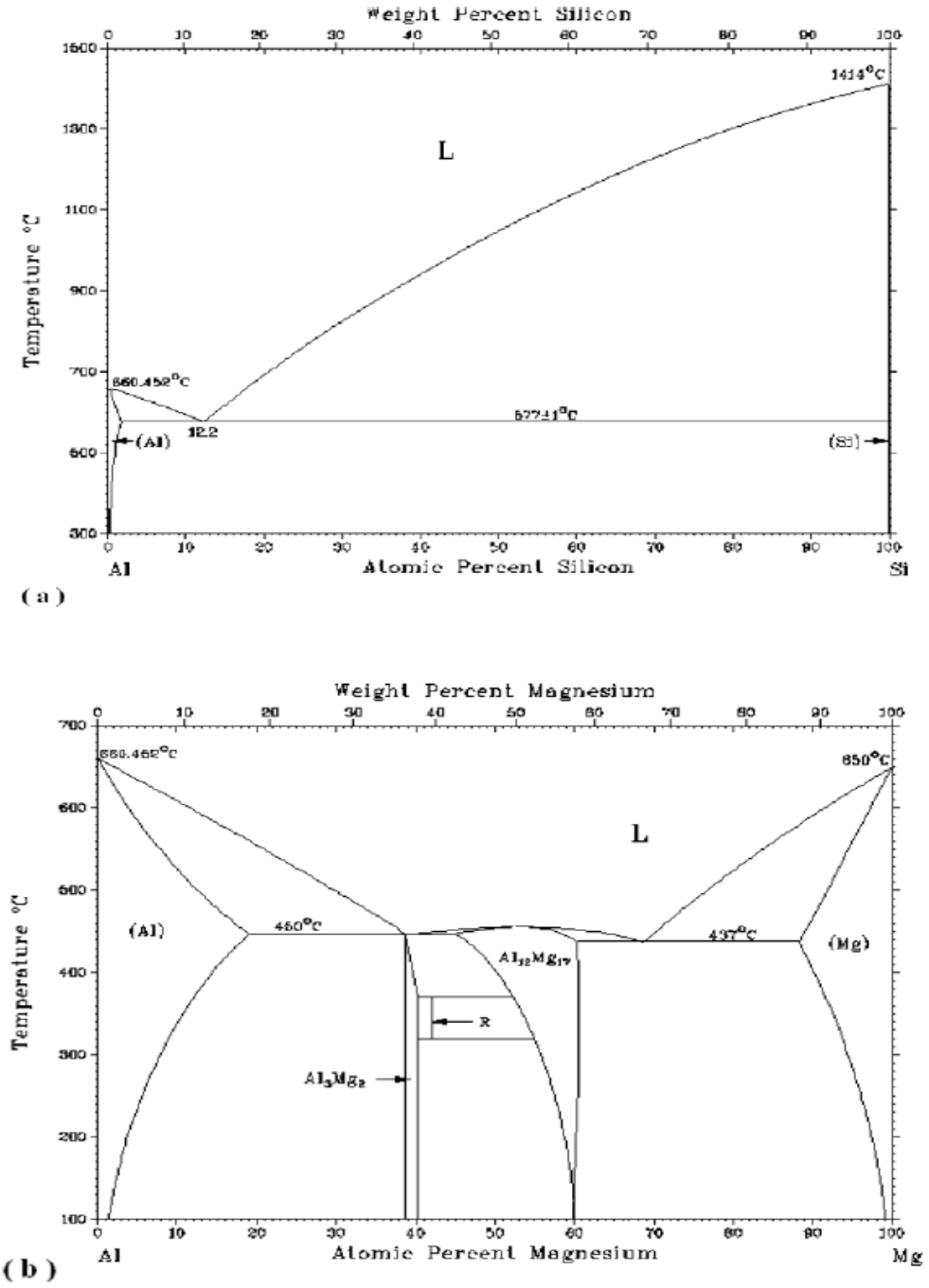

Figure 3. 9 Binary phase diagrams for Al alloys (a) Al-Si and (b) Al-Mg

Particulate preforms for metal matrix composites were prepared with different concentrations of reinforcement. A variation in the volume fraction i.e., reinforcement content was obtained by using a combination of particle sizes and optimized proportions.

As a result the preforms possessed either a bimodal or a trimodal distribution of the reinforcement. The silicon carbide powders subsequent to oxidation treatment were tested for their average particle sizes as measured using a particle size analyzer, Cilas Granulometer AS 920 which operates on the principle of dynamic light scattering. Particle size analysis was carried out by diffraction technique using a laser that operates at a wavelength of 830 nm and a photodiode sensor. A particle size distribution was obtained to determine the average particle size and is shown in Figure 3.10.

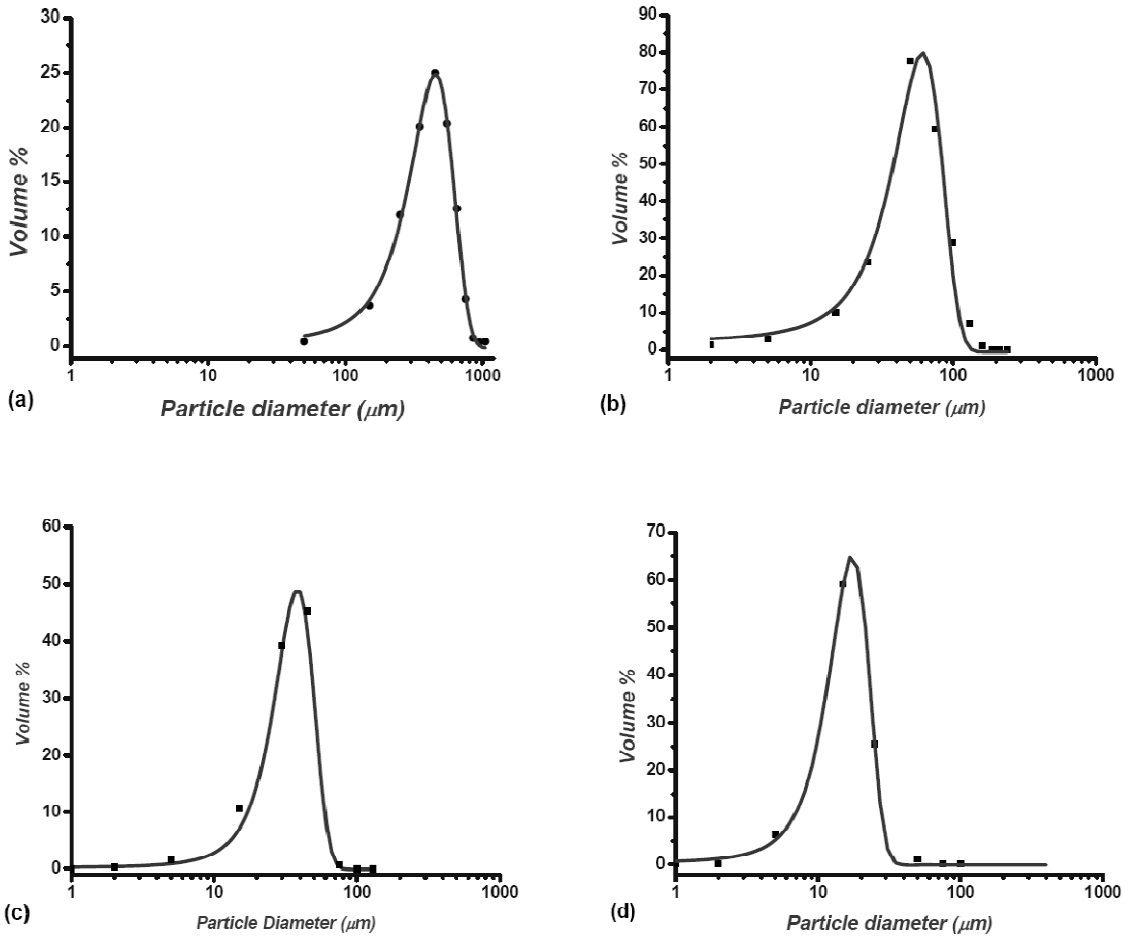

Figure 3.10 Particle size distributions for Silicon Carbide powders. (a) Grit 36, (b) Grit 220, (c) Grit 400 and (d) Grit 600

The powders were further examined under an optical microscope for the determination of average particle size and powder morphology, shown in Figure 3.11.

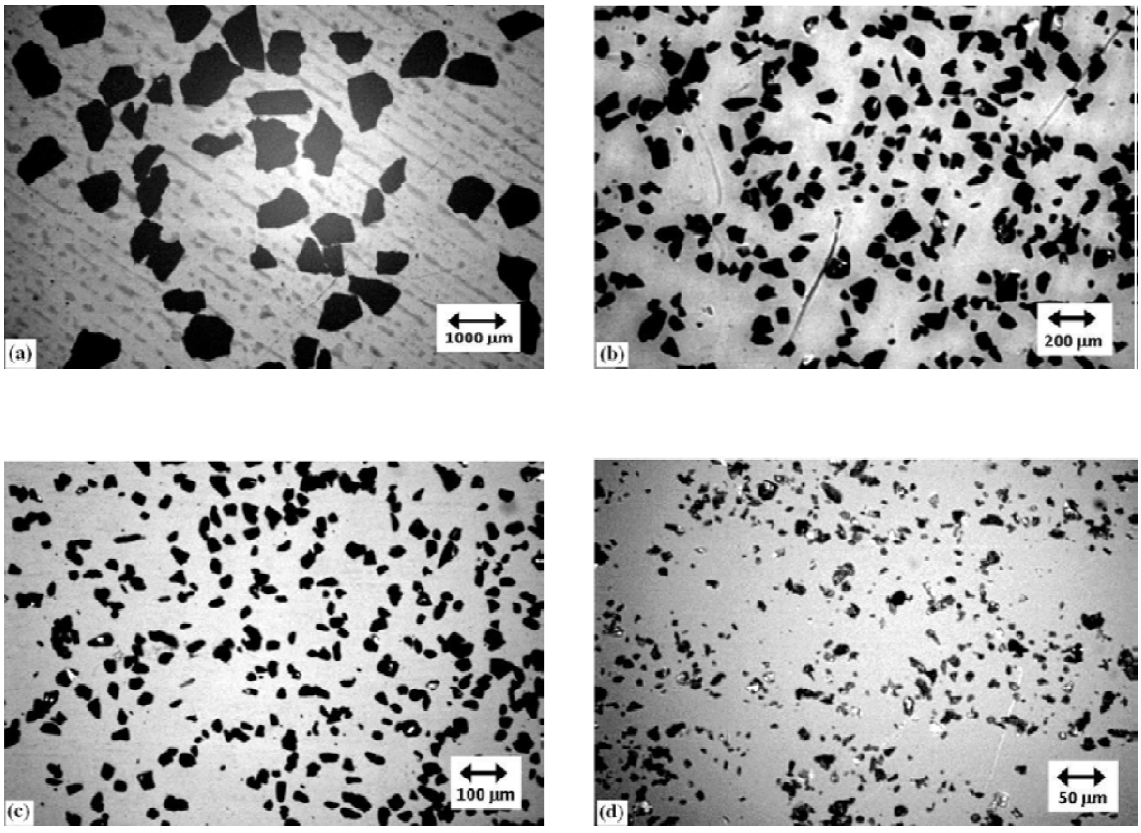

Figure 3.11 Optical micrographs of Silicon Carbide particulates. (a) Grit 36, (b) Grit 220, (c) Grit 400 and (d) Grit 600.

The true density of the powders was determined according to test procedures standardized by the American Society for Testing and Materials (1997). Among various available test methods, "Standard test method for specific gravity of soil solids by water pycnometer, D854-06" was employed for the determination of the density of the powder [24]. The method involves the application of a pycnometer, commonly known as specific gravity bottle and the technique is broadly known a pycnometry. There exist two types of

pycnometry namely liquid pycnometry and gas pycnometry. In normal cases liquid pycnometry is more feasible and the pycnometer in this a case is a glass vessel with a precisely known volume. A certain amount of pre-weighed dry powder sample is placed in a pycnometer and the rest of the volume is filled with double distilled water. The density of the powder was determined by measurement of the mass using a precise balance. The following relation gives the density of powder.

$$Density = \frac{x * density..of..liquid..(water)}{[y-(z-x)]} \qquad (3.10)$$

Where *x*: mass of the specimen, *y*: mass of water completely filled in the specific gravity bottle and *z*: mass of specimen along with water completely filled in the specific gravity bottle. The density determined in this manner was found to be 3.197 g/cc and the porosity present in the form of voids or cracks was estimated to be 0.53% in comparison to the density obtained from XRD measurements [25]. This data was further helpful in computing the absolute volume of silicon carbide powder in a preform from a measurement of its mass. The measurement of dimensions of the preform enabled to determine the volume of preform. The ratio of the absolute volume of silicon carbide in a preform to the volume of the preform is denoted as the volume fraction of silicon carbide in the respective preform or composite.

In the present study, it is intended to understand the behaviour of effective physical and mechanical properties of two phase SiC_p/Al composite systems as a function of reinforcement volume fraction. Different volume fractions of the reinforcement can be obtained in more than one ways. The most common method is compaction of powder of particular particle size and obtain desired volume fraction by varying pressures of

compaction. The process of compaction is an easy to use method for the preparation of powder preforms either for direct sintering or for infiltration experiments. However, the process of compaction has its own limitations. Some of these are requirement of a compaction unit, die of required dimensions, complexity of shapes etc. Apart from these, the volume fraction of reinforcement that can be obtained by compaction of powder of particular particle size is limited to a maximum of 0.55 of reinforcement [26]. A good way to overcome this limitation and obtain powder preforms with higher volume fractions is by compacting powder that is a mixture of two or more different particle sizes. However, this is not a straight forward method but involves careful choice of powder particle size ratios to be employed for mixing followed by successful compaction to obtain powder preforms with higher volume fractions. SiC powders with particle sizes suitable for high volume fraction were chosen to obtain preforms both loose and compact, with different volume fractions of SiC [27].

d) Fabrication of High Volume Fraction Composites

Silicon carbide powders with bimodal and trimodal distributions were obtained using optimized proportions of different sizes of SiC powders in order to obtain preforms with different loading levels of silicon carbide. The volume fraction of a preform is defined as the ratio of the absolute volume of reinforcement to the volume of the preform. Loose powder preforms and compacts of silicon carbide were used for the preparation of metal matrix composites. The absolute volume of reinforcement was determined from the measured mass for each preform and density of SiC. Further the volume of the preform is defined by the inner dimensions of the container and the height to which a powder bed could pack under substantially no-load conditions, for loose powder preforms. The

volume of a powder compact was determined by the external dimensions of the preform. Apart from having good control over the volume fraction of reinforcement that can be obtained in a composite, it is also essential to attain a homogeneous microstructure. The homogeneity of a microstructure in a composite can be controlled greatly by the distribution of reinforcement phase. Homogeneous powder mixtures of SiC were obtained by thorough mixing on a roller mill. Moreover, these mixtures when transferred into refractory crucibles would result in inhomogeneity along the height of the preform. Such inhomogeneities were eradicated by vibrating the crucibles containing SiC powder mixtures. Homogeneous distribution of SiC particulates in a preform ensures microstructural homogeneity in a composite material. Thus preforms with controlled volume fractions and homogeneous distribution of SiC reinforcement were prepared out of the master powder mix comprising of different particle sizes.

Subsequently, the preforms were dried in nitrogen containing atmosphere at a temperature ~100^{o}C for duration of 24 hours. This is essential in order to ensure removal of residual moisture from the preform and to develop handling strength in preforms prepared by compaction. The metal matrix composites have been prepared using a technique called the pressureless infiltration technique. In this process the molten aluminum alloy under suitable conditions of alloy composition and atmosphere spontaneously infiltrates a bed of refractory powder preform thereby generating a metal matrix composite upon solidification. The present technique for the preparation of metal matrix composites is different from other conventional methods of composite fabrication in that there is no application of any external force or vacuum to drive the molten metal into the capillaries of powder preform. The process can be carried out at a pressure

slightly above atmospheric pressure with a continuous stream of flowing nitrogen unlike the other techniques wherein extensive use of high precision equipment is made. In the case of pressureless infiltration, in order to prepare aluminum metal matrix composites it is sufficient to maintain a non-oxidizing atmosphere and proper alloying of the matrix metal. The absolute mass of the matrix metal required by the preforms was calculated and weighed out to an excess by ~50%. The aluminum alloys were then placed on the top of the preform that is contained in a refractory crucible as shown in Figure 3.12. The sample assemblies comprising of silicon carbide preform and corresponding aluminum alloy were placed in an Inconel muffle furnace.

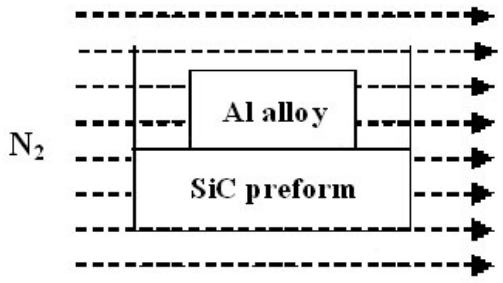

Figure 3.12 A schematic view of the pressureless infiltration process.

The furnace is heated up to a desired temperature in a controlled manner, using Kanthal A1 heating elements. A K-type thermocouple is located at the center of the furnace to read the input to a temperature controller, WEST 2054. The furnace was then flushed with high purity nitrogen gas for a period of 24 hours at room temperature. This was done in order to ensure that the atmosphere in the furnace is comprised of nitrogen and no other gas. The furnace was heated at a steady rate of $8^{o}C.min^{-1}$ from room temperature to a temperature of ~$850^{o}C$, well above the melting point of the master alloy, in an atmosphere of flowing nitrogen. The flow rate of nitrogen was maintained

throughout the process at a steady rate in order to prevent creep-in of any external gases. This would prevent surface oxidation of the molten metal. It is necessary to prevent surface oxidation of the melt because of the following reason. An event of surface oxidation would develop a thin layer of aluminum oxide which is very stable and cannot be disrupted at the temperature used for pressureless infiltration. As a result, the molten metal does not wet the preform and thus inhibits the process of infiltration in spite of maintaining optimized conditions for infiltration. Upon reaching the temperature of infiltration the furnace is held there for a period of 3 hours followed by cooling to room temperature at a steady rate of $5^{o}C.min^{-1}$. A dwell time of 3 hours was maintained in order to initiate spontaneous infiltration and complete infiltration of the preform. Silicon carbide particulate reinforced aluminum alloy matrix composites obtained in this manner were sectioned into requisite dimensions for further characterization. The microscopic features of the composites were evaluated with the help of standard techniques available. The bulk properties of the composites were determined and studied as a function of reinforcement volume fraction in as prepared condition without any further heat treatment.

References:-

1. L. Holliday: *Advances in Materials*, Pergamon Press. (1965)
2. F. Delanney, L. Froyen and A. Deruyttere, *J. Mater. Sci*. **22** (1987) 1.
3. G. A. Chadwick, *Mater. Sci. Eng*., **A 135** (1991) 23.
4. V. Laurent, C. Rado and N. Eustathopoulos, *Mater. Sci. Eng. A* **205** [1-2] (1996) 1.
5. T. Iseki, T. Kameda and T. Maruyama, *J. Mater. Sci*., **19** (1984) 1692.

6. Youngman Kim and Jae-Chul Lee, *Mater. Sci. Eng. A* **420** [1-2] (2006) 6.

7. T. Y. Kosolapova, "*Carbides Properties, production and Applications*", Plenum Press, New York, NY, 1971, p. 250.

8. F. P. Knudsen, *J. Amer. Cer. Soc*. **45** [2] (1962) 94.

9. J. C. Viala, P. Fortier and J. Bouix, *J. Mater. Sci*. **25** (1990) 1842.

10. J. W. McCoy, C. Jones and F. E. Warner, *SAMPE Q* **19** [2] (1988) 37.

11. J. C. Viala, F. Bosselet, V. Laurent and Y. Lepetitcorps, *J. Mater. Sci*. **28** (1993) 5301.

12. I. A. Ibrahim, F. A. Mohamed and E. J. Lavernia, *J. Mater. Sci.* **26** (1991) 1137.

13. Jae-Chul Lee, Sung-Bae Park, Hyun-Kwang Seok, Chang-Seok Oh and Ho-In Lee, Acta *Mater.* **46 (**1998) 2635

14. R. Y. Lin, R. J. Arsenault, G. P. Martins and S. G. Fishman, Interfaces in Metal-Ceramic Composites, The Minerals, Metals and Materials Society, Warrandale, PA, 1990.

15. M. I. Pech-Canul, R. N. Katz, M. M. Makhlouf and S. Pickard, *J. Mater. Sci.* **35** (2000) 2167.

16. T. Choh and T. Oki, *Mater. Sci. Technol*., **3** (1987) 378.

17. M. K. Aghajanian, M. A. Rocazella, J. T. Burke and S. D. Keck, *J. Mater. Sci*. **26** (1991) 447.

18. G. P. Martins, D. L. Olsen and G. R. Edwards, *Met. Trans*. **19B** (1988) 95.

19. A. Lane, N. Shah and W. C. Conner Jr., *J. Colloid. Interface Sci*. **109** (1986) 235.

20. M. I. Pech-Canul and M. M. Makhlouf, *J. Mater. Synth. Proc*. **8** [1] (2000) 35.

21. P. L. Rathnaparkhi and J. M. Howe, *Acta Metall. Mater*. **42** [3] (1994) 811.

22. Mingyuan Gu, Yangping Jin, Zhi Mei, Zengan Wu and Renjie Wu, *Mater. Sci. Eng. A* **252** (1998) 188.

23. Zhongliang Shi, Shojiro Ochai, Masali Hojo, Jaechul Lee, Mingyuan Gu, Hoin Lee and Renjie Wu, *J. Mater. Sci.* **36** (2001) 2441.

24. ASTM D854 – 06, ASTM International, 100 Barr Harbor Drive, PO Box C700, West Conshohocken, PA 19428-2959, United States.

25. A. H. Gomes de Mesquita, *Acta Crystallographica*, **23** (1967) 610.

26. R. Arpon, J. M. Molina, R. A. Saravanan, C. Garci-Cordovilla, E. Louis and J. Narciso, *Acta Mater*., **51** (2003) 3145.

27. Jong-Heon Lee, W. Jack Lackey and James F. Benzel *J. Mater. Res.* **11** [11] (1996) 2804.

4. Characterization of SiC_p/Al Composites

Two phase composites of SiC_p/Al system with different volume fractions have been generated and one of which is shown in Figure 4.1. It can be observed from the figure that the dimensions of the composite material fabricated by the pressureless infiltration schedule developed in the present work are large than those reported by others using similar pressureless infiltration approach [1]. Because of the large dimensions of SiC_p/Al composites it is possible to evaluate the material for many physical and mechanical properties.

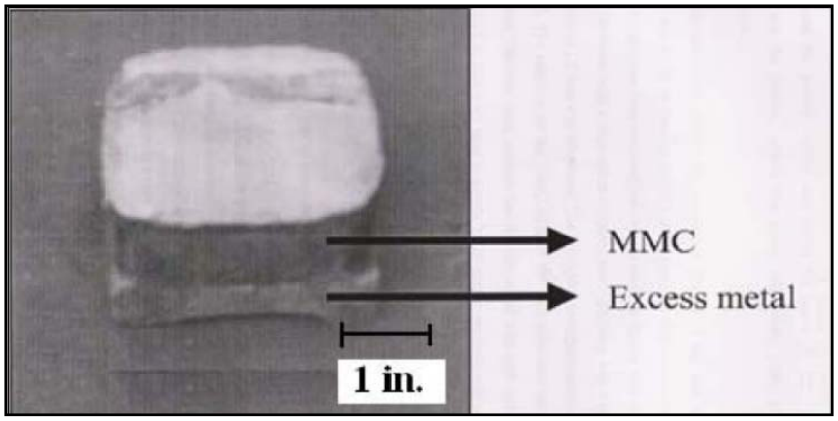

Figure 4.1 SiC_p/Al Metal Matrix Composite fabricated in the present work.

A systematic variation of volume fraction of SiC would enable a rigorous study of the effect of volume fraction, which is a significant parameter in the determination of effective properties of the two phase composite material. However, prior to evaluation of physical and mechanical properties of SiC_p/Al composites as a function of volume fraction, it is indeed necessary to ensure that the processing schedule of pressureless infiltration employed in the present work has not developed undesired features within the

composite material. It is to be recalled that in the SiC – Al system, the molten metal dissolves SiC and develop detrimental phases such as Al_4C_3, which would disintegrate in course of time. A detailed phase and microstructural analyses was conducted. This is further followed by various techniques employed in the evaluation of physical and mechanical properties of SiC_p/Al composites with different volume fraction of SiC.

a) Phase & Microstructure

1. X – Ray Diffraction Analyses

Small sections from various regions of the composite material were cut using a low speed diamond saw, ISOMET. These sections were then mixed up to form a collective representative of the feature of the composite material, developed under the present processing conditions. Powdered samples of SiC_p/Al composites were analyzed with the help of X-ray Diffraction technique. An X-ray diffractogram was obtained using a $CuK_{\alpha 1}$ radiation from a Philips X-ray diffractometer. Also presence of any extra phases formed within the composite as a result of processing schedule is detected with the help of standard diffraction patterns. The X-ray diffraction pattern was indexed and compared with the diffraction patterns of the starting materials i.e., master alloy, Al-9Si-5Mg and the reinforcement, SiC. Also X-ray diffraction pattern was obtained for the residual matrix metal that is left out upon complete infiltration of the preform. The extra metal in this case can be a real representative of the metallic phase existing in the composite as a three dimensional network. This portion of the metal is expected to possess a composition that is close to the matrix phase and has experienced similar thermal processing conditions. Finally the X- ray diffraction pattern of the composite material is compared with that of the starting materials and also the pattern for the residual matrix metal.

2. Optical Microscopy & Image Analyses

An optical microscope is an instrument that magnifies and resolves the structure of materials under examination and it is the most widely used instrument in the field of metallography [2]. The instrument consists of four components: A light source, condenser lens, objective lens and an eye piece. The condenser lens collects light rays from the source and focuses the beam onto the specimen. The reflected light is collected by the objective lens to form a real, magnified aerial image of the specimen. This real image is further magnified by the eyepiece to form the final image that represents the microstructure of the specimen. The quality of the image is greatly dependent on the surface roughness of the specimen. When the specimen has high surface roughness, the incident light beam gets reflected from local inclined planes and would result in a diffused image. In order to get rid of surface roughness and obtain a highly reflective surface, the specimen has to be polished according to standard metallographic techniques. The procedure of polishing involves the use of abrasive materials for gradual removal of material thereby developing a plane surface with high reflectivity.

A small representative section from a composite of each volume fraction is mounted and polished using diamond lapping compounds in order to obtain highly reflective surfaces. The metal matrix composites mounted onto bakelite using hot mounting technique were polished with some alterations in the standard metallographic procedures of polishing. Changes in the polishing procedures were necessary in order cope up with the surface relief arising as a result of a large difference in the hardness of the matrix and the reinforcement. In the present system of matrix/reinforcement the matrix is a soft metallic phase embedding hard ceramic particulates. The difference in the

hardness of the two phases being large, substantial amount of surface relief has been observed between the soft matrix and the hard reinforcement. The samples were polished using diamond lapping pastes starting from 9 μm, 3 μm, 1 μm and finally ¼ μm with distilled water as the lubricant and also coolant. The polished sections of the composites were ultrasonically cleaned while changing the size of abrasive being used and the evolution of microstructure was monitored. These sections were observed under a reflected light microscope from Leica for the examination of microstructural homogeneity and further quantitative analyses.

Optical microstructures also enable quantification of secondary phases, voids (if present), determination of grain size etc. Other methods of evaluation of phase/volume fraction like that of dissolution technique are quite tedious and are occasionally misleading [2]. Evaluation of phase/volume fraction by quantitative image analyses of microstructures is a rather simple and fast method. Image analysis is based on the principle of differential contrast that enables identification of various phases present as seen from the microstructure. A digital acquisition system attached to the microscope enabled to capture images of the microstructure. Sufficiently representative sections of the microstructure were captured and analyzed. These images were analyzed using image analysis software, Bio-Vis Materials Plus – version 1.5. This is later followed by the determination of phase/volume fraction of the dispersed phase, silicon carbide in this case. The basic principle employed here is that that the volume fraction of a phase is equal to the area fraction in a random planar section and is equal to the linear fraction over a random line through the three dimensional microstructure. The volume fraction of

a phase is also equal to the point fraction of randomly distributed points which lie within that particular phase [3].

$$V_f = \frac{V_d}{V} = A_f = \frac{A_d}{A} = L_f = \frac{L_d}{L} = P_f = \frac{P_d}{P} \qquad (4.1)$$

Where,

V_f **:** Volume fraction of dispersed phase.

V_d **:** Volume of dispersed phase in the specimen.

V **:** Total volume of the specimen.

A_f **:** Area fraction of dispersed phase in a random planar section.

A **:** Area of the random planar section.

L_f **:** Linear fraction of dispersed phase over a random line.

L_d **:** Total length of the dispersed phase along the random line.

L **:** Total length of the random line.

P_f **:** Point fraction of dispersed phase.

P_d **:** Number of points falling in the dispersed phase.

P **:** Total number of random points.

The measurement of volume fraction from image analysis is based on the principle of point counting with the help of an algorithm that would determine the area fraction of a particular phase and subsequently convert the area fraction in an area under observation to volume fraction of the corresponding phase. Several such areas were observed and evaluated for phase/volume fraction at different magnifications. An average of these was considered to represent the volume fraction of a composite.

3. Scanning Electron Microscopy

SEM is very much useful in analyzing the microstructural features, where the optical microscopes no longer provide adequate resolution, up to a magnification of the order of 10^5 X [4]. Another important feature of the SEM is the ability to observe in 3 dimensions, say a fractured surface. In the SEM an electron beam is focused into a fine probe and subsequently raster scanned over a small rectangular area. As the beam interacts with the sample it creates various signals (secondary electrons, internal currents, photon emission etc), all of which can be appropriately detected. These signals are highly localized to the area directly under the beam. By using these signals to modulate the brightness of a cathode ray tube, which is raster scanned synchronously with electron beam to form an image on the screen. This image is highly magnified and usually has the look of a traditional microscopic image but with much greater depth of field.

The composite materials, obtained using pressureless infiltration technique were further characterized for phase composition and distribution at the microscopic level. A scanning electron microscope – LEO 440i from Oxford Instruments that is coupled with EDS (Energy Dispersive Spectrometer) analyzer was used for this purpose. Exclusive analyses of the matrix portions of the microstructure were performed in order to assess the composition of the matrix phase after the pressureless infiltration process. The composition of the matrix phase obtained in this manner was further compared with the starting composition of Al alloy. Analysis was performed also at the interface of the particle and matrix to identify the phases present at the interface that have formed as a result of reaction between molten aluminum and the amorphous layer of silica developed

on the surface of SiC particles. This analysis would also enable identification of detrimental phases such as aluminum carbide, formation of which will be of a serious concern in assessing the final properties of the composites. The stability of an interfacial reaction product would decide the degree of bonding characteristics between the reinforcement and the matrix. An interfacial reaction product that is stable in operating environment would indicate good bonding characteristics between the matrix and the reinforcement. On the other hand an interfacial reaction product such as aluminum carbide would disintegrate in the presence of atmospheric moisture and leave porosity at the interface thereby degrading the quality of the composite material [5].

4. Scanning Electron Probe Microscopic Analyses

An electron probe microanalyzer is advancement over the electron microscope that has the ability to scan and is equipped with a more sensitive detector based on wavelength dispersion [6]. A scanning electron probe micro analyzer consists of an electron beam generated from a heated metal filament. The beam is then accelerated through an aperture and focused onto the surface of specimen using a set of magnetic lenses. As a result, emission of secondary, back scattered electrons, characteristic X-rays, photons of longer wavelength occur in the subsurface of the specimen. The characteristic X-rays emitted are specific to the atomic number of the emitting atoms. Qualitative analysis is accomplished by identification of emitting elements from calculations of wavelength pertaining to characteristic X-rays obtained. Upon relevant calculations, the intensities of the emitted lines enable to determine concentration of the emitting elements. Such quantitative analyses are carried out in an EPMA using a wavelength

dispersive spectrometer. The characteristic X-ray photon is absorbed by an atom with the subsequent ejection of one of the bound electrons of that atom. This photoelectron has a kinetic energy equal to the difference in photon energy and the binding energy of the electron to the atom. These photoelectrons scatter in-elastically in the detector to generate charge carriers which are used by the wavelength dispersive spectrometer.

The enhanced sensitivity of SEPMA as compared to SEM, prompted the use of this technique for the characterization of the two phase composite material developed in the present work. Among various other features to be characterized, it is of great importance to characterize the interface between SiC and Al phases. The interface between SiC particulate and Al alloy matrix plays a significant role in the performance of the composite. This acts as a medium for the transfer of load on to the stiffer inclusion. The ability to transfer an applied load on to the reinforcement phase helps in making efficient utilization of reinforcement properties. It is highly necessary that the interfacial bonding between the two phases is firm and free of deleterious phases. In this work, the particle-matrix interface has been characterized for its phase composition using a scanning electron probe micro analyzer, CAMECA SX-100. Overall phase analyses were carried out with the help of wavelength dispersive spectrometer. These include principal constituents like Al, SiC and alloying elements along with extra phases developed as a result of processing. Line scans were performed across several interfaces in order to identify the presence of Aluminum Carbide phase, a reaction product of dissolution of SiC in molten Al.

b) Physical Properties of SiC_p/Al Composites

1. Density and Porosity

The composite is primarily characterized for its density and porosity levels using the liquid displacement method i.e. Archimedes' principle. The density of an object is then given by the following relation.

$$\rho = \left(\frac{m_a}{m_a - m_l} \right) * \rho_l \qquad (4.2)$$

Where m_a, m_l are the masses of a particular specimen weighed out in air and displacing liquid respectively. The specimens meant for density measurements were heat treated in a ventilated oven at a temperature of ~ 150^{o}C for duration of atleast 24 hours. This is done in order to ensure that there shall not remain any moisture present in the specimens that would add to the mass of the specimen which can mislead the measurement. The heat treated samples intended for measurement were then cooled in a glass dessicator containing dried silica gel. Masses of the composite specimens for each volume fraction of reinforcement were measured using an electronic balance from Mettler that can measure the mass of an object to an accuracy of 0.1 mg. Measurements were carried out at room temperature with double distilled water as the liquid medium to displace. In order to obtain a representative figure for density and porosity of the metal matrix composite atleast 15 specimens from composites of each volume fraction were measured. An average of these measurements was projected as a representative figure for the density and porosity of corresponding composites. The term porosity as used here is referred to open porosity that can be accessed by a liquid in order to account for the true volume of the specimen under examination. However a measure of closed porosity could

not be obtained. Similar measurements were carried out on specimens of matrix metal that has been left out upon completion of pressureless infiltration process. The left out matrix metal would be a true representative element of the matrix material that is contained in the composite, in terms of composition and also the thermal processing history. Thus any measurement performed on the excess or left out metal would give a realistic picture of the microstructural, physical and mechanical properties of the matrix material that is contained in the metal matrix composite.

2. *Coefficient of Thermal Expansion*

The composite materials were characterized for the coefficient of linear thermal expansion in the temperature range: 50°C – 300°C. A schematic representation of the coefficient of linear thermal expansion is shown in Figure 4.2. The coefficient of linear thermal expansion of a material is defined as the relative change in the length of a specimen per unit temperature gradient or is expressed as the following relation [7].

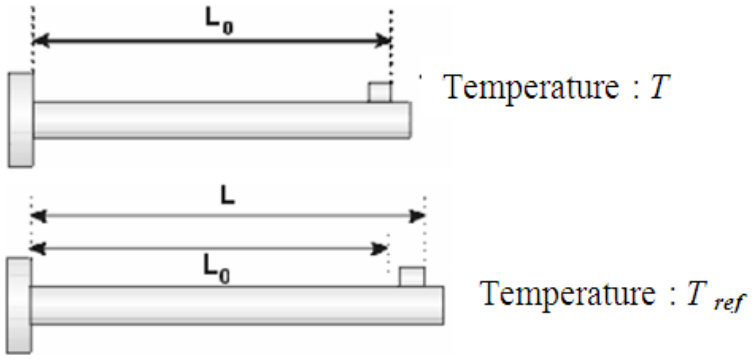

Figure 4.2 A schematic view of dilatation due to change in temperature

$$\alpha = \frac{1}{(T - T_{ref})}\left(\frac{\Delta L_{thermal}}{L_0}\right) \qquad (4.3)$$

where α is the coefficient of linear thermal expansion, $\Delta L_{thermal}$ is the change in length caused in a specimen of length L_o due to a change in temperature by ΔT. α, the coefficient of linear thermal expansion is measured in units of 10^{-6} /K, for all common purposes.

Measurements of coefficient of linear thermal expansion were carried out using a standard dilatometer from NETZSCH Instruments. A basic push-rod technique is involved in the operation of the instrument. The set-up consists of a long refractory tube with a stopper inside to arrest the movement of the specimen in one of the two directions, available along the length. A push-rod is located on the other side of the specimen in such a way that any changes in the dimensions of the specimen will be transmitted to the push-rod. The change in the position of the push-rod is indicated by a LVDT (Linear Variable Differential Transducer) the operation of which is based on the principle of a parallel plate capacitor. The output of the LVDT, in volt would be then transformed to represent the output of the dilatometer in units of length. The instrument is further interfaced to a personal computer through a general purpose interface bus in order to facilitate precise data acquisition. Thus the coefficient of linear thermal expansion is obtained as slope of a plot between relative change in length and temperature.

Thermal expansion tests were conducted under well specified conditions of a force of 30 cN applied by the push-rod on the sample and a steady flow of Ar/N_2 gas at a rate of 50 cc/min. SiC_p/Al composites with varied concentrations of SiC were cut into the following dimensions; 25 mm length, 6 mm width and 6 mm thickness. The specimens were heated to a temperature of 300^oC from ambient at a constant rate of 5$^oK.min^{-1}$,

along with simultaneous data acquisition. Specimens from composites of each volume fraction were tested for the coefficient of linear thermal expansion to understand the variation caused due to a change in volume fraction. In order to have a statistical representation of the data, a minimum of three specimens at each volume fraction were tested. The average of these measurements would represent the coefficient of linear thermal expansion of the metal matrix composite in the temperature range of measurement. Measurements of coefficient of linear thermal expansion were also performed on specimens from excess metal that is left out upon complete infiltration. The observed variation in the coefficient of thermal expansion was further compared with theoretical predictions and experimental results available in the literature.

3. Dynamic Elastic Modulus

The composites were characterized for sound wave velocity using ultrasonic pulse-echo technique. In this technique an ultrasonic pulse is transmitted through a material of known thickness and the back wall reflection was traced to measure the time delay between echoes [8]. A schematic of the experimental set-up for ultrasonic measurements is shown in Figure 4.3. All measurements were carried out at room temperature to determine the longitudinal and shear wave velocities in the metal matrix composites.

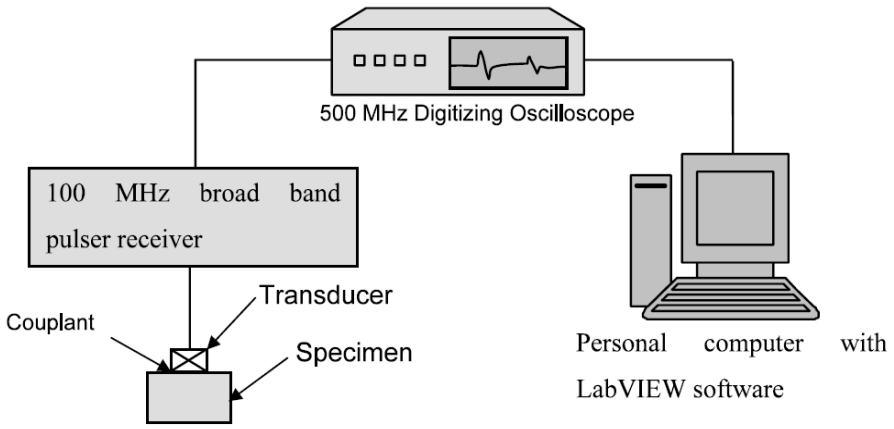

Figure 4.3 Schematic of the experimental set-up for ultrasonic measurements

Specimens measuring 25 mm x 25 mm x 5 mm were machined out of a block of metal matrix composite for ultrasonic velocity measurements. The specimens were ground to a good finish in order to minimize surface roughness that would enable efficient coupling between the specimen and the transducer. A 100MHz broad band pulser-receiver (M/s. Accutron, USA) was used to give the electrical pulse to the transducer for generating the ultrasonic waves. The transducers consist of piezoelectric crystals, which vibrate upon the application of electrical pulse across the thickness and generate the mechanical waves. For the longitudinal wave transducer, the piezoelectric crystal is cut perpendicular to the electric axis (X-cut crystals) and hence when the electrical pulse is applied in the thickness direction, the crystal vibrates in the thickness direction (i.e. perpendicular to the specimen surface) and generates the longitudinal wave in the specimen coupled to the transducer. Whereas for the shear wave transducer, piezoelectric crystal is cut perpendicular to the mechanical axis (Y-cut crystal) and hence when the electrical pulse is applied in the thickness direction, the crystal vibrates in the width (i.e. parallel to the specimen surface) direction and thus generates the shear wave in

the specimen coupled to the transducer. The schematic of the propagation of longitudinal and shear waves are as shown in Figure 4.4. In the case of longitudinal wave, the particle vibration is in the direction of wave motion, whereas, in the case of shear wave, the particle vibration is perpendicular to the direction of wave motion.

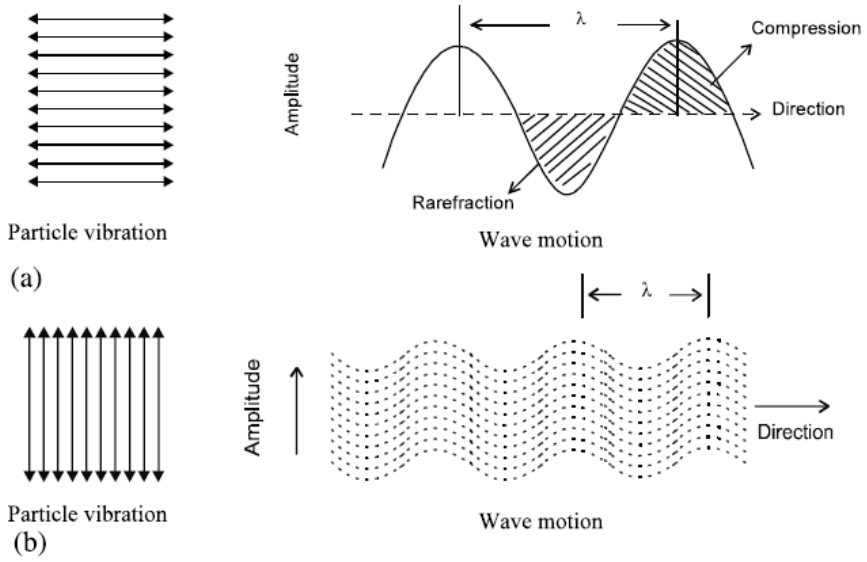

Figure 4.4 Schematic representation of ultrasonic wave propagation in (a) longitudinal and (b) shear modes of vibration

The incident pulse would travel through the material to reach its back wall and reflect to give echoes of the incident acoustic beam. During the course of its travel through a material such as a composite the ultrasonic pulse is expected to come across interfaces between matrix and reinforcement. The two phases in the composite possess different material properties like differences in velocity or even absorption coefficients which results in scattering at the interface. As a result, rapid attenuation of the reflected signal is observed.

In order to cope with the huge amount of interfacial scattering observed in composite material ultrasonic transducers with a broad frequency range were used to transmit and receive the pulses. A broadband ultrasonic transducer with 1 – 8 MHz frequency was used for longitudinal velocity measurements in the composites. Shear wave velocity measurements were carried out using a 5 MHz piezoelectric normal beam shear wave transducer (V155), supplied by M/s. Panametrics Inc, USA. For the measurement of longitudinal wave velocities, Glycerin was used as the couplant between the transducer and the specimen for an efficient transmission of the ultrasonic pulse into the material under investigation. The shear wave velocity measurements were carried out on specimens coupled to the respective transducer with the help of burnt honey (M/s. Panametrics, USA). The reflected ultrasonic waves from the back wall of the specimen were picked up by the same transducer and were converted to electrical signal. This electrical signal was acquired by the receiver at optimum gain and damping settings, and the RF signal was fed to the 500 MHz digitizing oscilloscope (Tektronix TDS524). The signal was digitized at 500 MHz and averaged for about 50 signals. The gated back-wall echoes (2048 ns duration) from the oscilloscope were transferred to the personal computer with the help of General Purpose Interface Bus (GPIB) interfacing and Lab-VIEW software. Specific program was developed in Lab-VIEW software version 3.1.1 for the calculation of transit time using cross-correlation technique. This was done to avoid the problem of near-field effect of the transducer. Measuring the cross-correlation function is especially useful in determining the exact time delay between similar but distorted noisy signals. In practice, cross-correlation is often used to eliminate jitter (random time uncertainty in the arrival of quasi-periodical signals). Cross correlation

technique has been used for the precise velocity measurements. Various steps involved in this methodology are as follows: (a) acquisition of two digitized echoes from the oscilloscope, (b) cross correlation of the echoes to find the approximate time delay, (c) application of an interpolation method for accurate time delay and (d) calculation of velocity measurement using time delay and thickness of the specimen along with the following equation.

$$Velocity = \frac{2 * Number..of..echoes. * thickness}{Time..delay} \qquad (4.4)$$

The accuracy in time of flight measurement is better than ± 0.3 ns and in turn the accuracies in the measurement of ultrasonic longitudinal and shear wave velocities for thickness of the specimens in range of 5.0 ± 0.002 mm are better than 4 m/s and 2 m/s, respectively. Ultrasonic measurements were performed at five different locations on each sample and the corresponding average is considered in the present investigation. The composites studied in the present work possess reinforcement in the form of a particulate and the fact that process of fabrication does not employ any form of external forces strengthens the concept of isotropic nature of the composites. Further to this, the distribution of the reinforcement in the matrix can be considered to be homogenous in the case of discontinuously reinforced metal matrix composite where the reinforcing phase is stationary. Measurement of sound wave velocities both longitudinal and shear would enable the determination of various elastic constants of a material. There exist a total number of 36 elastic constants defined for a material that is anisotropic. The number of elastic constants required for the description of a homogenous and an isotropic material would come down to 2. In the present case of a particulate reinforced metal matrix

composite it would be a well justified assumption that the composite is isotropic in nature. Standard equations valid for isotropic and homogenous material were used for the determination of Elastic, Shear and Bulk moduli of the two phase composite material from the ultrasonic velocity data.

4. Electrical Resistivity

The electrical resistivity measurements were performed using a home-made apparatus that is based on DC four probe technique. Electrical contacts between the specimen and the probes are made using conducting Silver paint. Out of the four in-line probes, the two outer probes are used to place the specimen in a uniform electric filed by passing a constant current through the specimen. The inner probes are used for the measurement of voltage drop across a particular section, along the length of the specimen and thus determine electrical resistance. A schematic of the experimental set-up for precise DC electrical resistivity measurements is shown in Figure 4.5. A Keithley 224 constant current source was used to supply a constant DC electrical current (*I*) to the specimen. A Keithley 181 nano-voltmeter was used to measure the voltage drop across the inner probes. In order to avoid thermo e.m.f. due to thermal gradient, if any, along the length of the specimen, the voltage drop across the inner probes was measured for both directions of a constant current (*I*). V_1 and V_2 being the voltage drops across the inner probes for forward and reverse directions of current (I), the electrical resistance (R) and electrical resistivity (ρ) were calculated as follows.

$$R = \frac{(V_1 - V_2)}{2I} \quad ; \qquad \rho = \frac{RA}{l}. \tag{4.5}$$

Where *A* is the area of cross section of the specimen normal to the direction of current, ***l*** is the distance between the inner probes used for measurement of voltage drop.

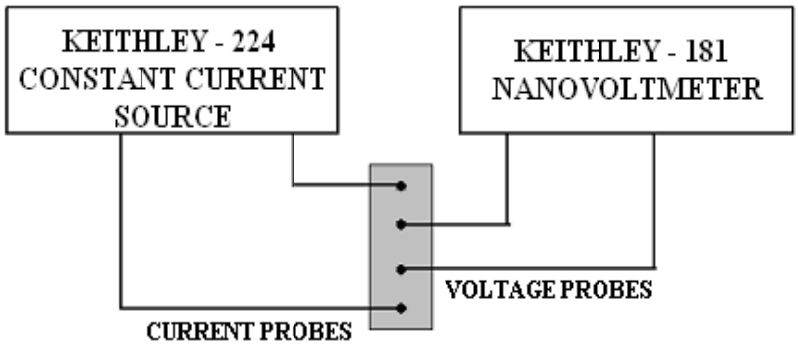

Figure 4.5 Schematic representation of dc electrical resistivity measurement

5. Thermal Conductivity

Thermal conductivity is a physical property of a substance and characterizes the ability of the substance to transfer heat. It determines the quantity of heat flowing per unit of time per unit area at a temperature drop of $1^{o}C$ per unit length. Thermal conductivity of materials can be determined from measurements of thermal diffusivity, specific heat capacity and density of the material. Thermal diffusivity measurements were performed using a Laser Flash Apparatus LFA 427 from NETZSCH. A schematic of the flash method is shown in Figure 4.6.

In this method the front face of a small disk shaped specimen is subjected to a very short burst of radiant energy [9]. The source of the radiant energy is usually a laser or a xenon flash lamp and irradiation times are of the order of milliseconds. The resulting temperature rise of the rear surface of the specimen is measured using an infrared sensor. The specimen holder is held in a refractory tube of an atmospheric furnace where a

specimen can be maintained at a constant temperature in a preferred atmosphere and the laser pulse is shot onto the specimen. The temperature at the other face of the specimen is recorded as a function of time. The temperature of the other face gradually increased with time and was stabilized. From the curve of temperature of the other face and time, at a particular temperature, the halftime $t_{1/2}$ was calculated. The half time thus calculated enabled the determination of thermal diffusivity of the specimen at the temperature of investigation.

$$\alpha = \frac{0.1388}{t_{1/2}} l^2 \qquad (4.6)$$

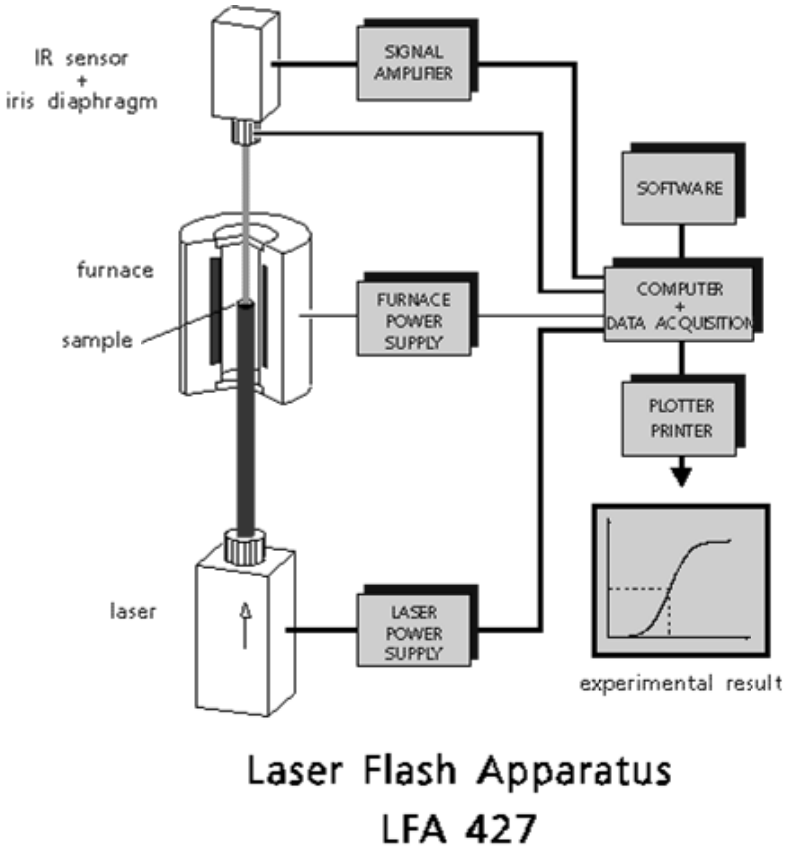

Figure 4.6 A schematic of the Laser Flash Apparatus LFA 427

The instrument is interfaced to a personal computer in order to execute operations faster and in an accurate manner. Thermal diffusivity of two phase composites SiC_p/Al was determined at different temperatures for different volume fractions of SiC. Measurements were performed at temperatures between RT – 300^{o}C in Argon atmosphere.

The DSC is a thermo-analytical method, which allows, by measuring the temperature difference between the sample and a reference, a quantitative measurement of the heat flow difference when the sample and the reference subjected to the same temperature program. The results are very important for many applications and provide information for the characterization of the materials. Measurements of specific heat can be performed in air, inert gas or under vacuum. C_p measurements up to 1500°C with an error ± 3% are possible.

Measurements of specific heat capacity were performed using a Differential Scanning Calorimeter. The temperature was varied between RT – 300^{0}C in Argon atmosphere. Thermal conductivity of the composite specimens was determined as a product of thermal diffusivity, specific heat capacity and density of the specimen. Measured values of density were used along with thermal diffusivity and specific heat capacity to determine the effective thermal conductivity of SiC_p/Al two phase composite samples.

$$\lambda = \alpha . C_p . d \qquad (4.7)$$

The Flash method for the determination of thermal conductivity of materials is a rather fast and reliable means of thermal analyses.

c) Mechanical Properties of SiC_p/Al Composites

1. Flexural Strength

Flexural strength is defined as the maximum stress in the outermost section of the test specimen loaded under bending. This is calculated at the surface of the specimen on the convex or tension side. The flexure test method measures behavior of materials subjected to simple beam loading. SiC_p/Al metal matrix composites fabricated by pressureless infiltration process were evaluated for flexural strength in accordance with ASTM standard C 1161-02b: "Standard Test Method for Flexural Strength of Advanced Ceramics at Ambient Temperature" [10]. In this method of flexural strength testing a specimen is loaded at a position midway between two support bearings as shown in Figure 4.7. Specimen is loaded at a constant loading rate till the specimen fractures. The maximum load at which a specimen fractures is recorded to compute flexural strength, σ_f as shown below.

$$\sigma_f = \frac{3PS}{2BW^2} \tag{4.8}$$

Where, P **:** Maximum load of fracture

S **:** Length of the span between bottom supports

B **:** Thickness of the specimen

W**:** Width of the specimen

Specimens with dimensions 50 mm x 8 mm x 8 mm were machined out of bulk SiC_p/Al metal matrix composites with different volume fractions of SiC. All the test specimens were chamfered uniformly at 45^o to a distance of 0.12 ± 0.03 mm as prescribed by the test method. Specimens were loaded at ambient temperature at a

constant loading rate of 0.5 mm/min in a universal testing machine, INSTRON-8500 with a maximum loading capacity of 100 kN. The samples were provided with a span length of 40 mm and the corresponding Load vs. Displacement curves were recorded with the help of inbuilt software, INSTRON Series IX Automated Materials Tester – version 8.12. About three specimens were tested for each SiC volume fraction in SiC_p/Al composites.

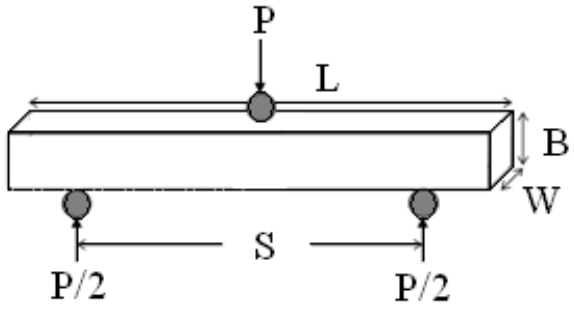

Figure 4.7 Schematic representation of three-point bend test set-up

2. Fracture Toughness

SiC_p/Al metal matrix composites with high volume fractions of reinforcement were evaluated for fracture toughness. ASTM standard E 399-90: "Standard Test Method for Plane Strain Fracture Toughness of Metallic Materials" was adopted for evaluation of fracture toughness of SiC_p/Al metal matrix composites [11]. In this test method single edge notched beam (SENB) specimens were loaded in a three point bend test set-up as shown in Figure 4.8. The specimens were provided with a pre-crack crack length '***a***' such that the ratio of pre-crack crack length to the width of the specimen lies between 0.45 and 0.55. Specimen was loaded at a constant loading rate till fracture and the load corresponding to a defined increment of crack length is used to determine fracture toughness as given below.

$$K_{IC} = \frac{P_Q S}{BW^{3/2}} f\left(a/W\right) \tag{4.9}$$

Where, P_Q : Load as determined from 9.1.1 of ASTM E 399-90

S : Length of span between supports

B : Thickness of the specimen

W: Width of the specimen

$f\left(a/W\right)$: Geometric factor

a : Length of the pre-crack

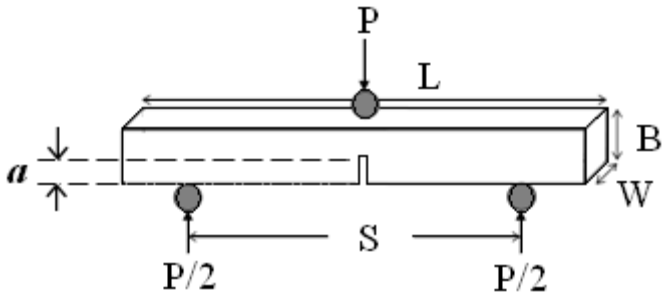

Figure 4.8 A schematic representation of three point bend test set-up for the evaluation of plane strain fracture toughness

Specimens measuring 50 mm x 8 mm x 8 mm were chamfered uniformly at 45^o to a distance of 0.12 ± 0.03 mm prior to loading under three point bend configuration. Samples were loaded at a constant crosshead speed of 0.5 mm/min on a universal testing machine, INSTRON-8500 with a maximum loading capacity of 100 kN. The samples were provided with a span length of 40 mm and the corresponding Load vs. Displacement curves were recorded with the help of inbuilt software, INSTRON Series IX Automated Materials Tester – version 8.12. Around three specimens were tested at room temperature, for each volume fraction of reinforcement in SiC_p/Al composites.

3. Hardness

SiC_p/Al composites with bimodal and trimodal particle size distribution of the reinforcement were evaluated for bulk hardness. Hardness is a property of a material that is a measure of its resistance to plastic deformation, usually by penetration. Principally, there exist three modes of evaluation of hardness of a material, namely Scratch Hardness, Indentation Hardness and Rebound Hardness. The present work deals with the determination of indentation hardness of SiC_p/Al metal matrix composites. Indentation Hardness is defined as the resistance to plastic deformation due to a constant load from a sharp object. Brinell Hardness (HB), Rockwell (HR) and Vickers (HV) are commonly used methods for the determination of indentation hardness of materials.

Vickers hardness measurements were performed on SiC_p/Al composites in accordance with ASTM E92-82(2003) e2**:** "Standard Test Method for Vickers Hardness of Metallic Materials" [12]. The Vickers hardness test method consists of indenting the test material with a diamond indenter, in the form of a right pyramid with a square base and an angle of 136^o between opposite faces subjected to a load of 1 to 100 kgf. The full load is normally applied for 10 to 15 seconds. A schematic of the indention process and the corresponding indentation is shown in Figure 4.9. The two diagonals of the indentation left in the surface of the material after withdrawal of the load are measured using a microscope and their average calculated. The area of the sloping surface of the indentation is calculated. The Vickers hardness is the quotient obtained by dividing the kgf load by the area of sloping surface in square mm.

$$HV = \frac{2F\sin\left(136^{o}/2\right)}{d^{2}} \approx 1.854\frac{F}{d^{2}} \tag{4.10}$$

Where, F **:** Load in kgf

d **:** Arithmetic mean of the two diagonals, d_1 and d_2 in mm

HV **:** Vickers hardness

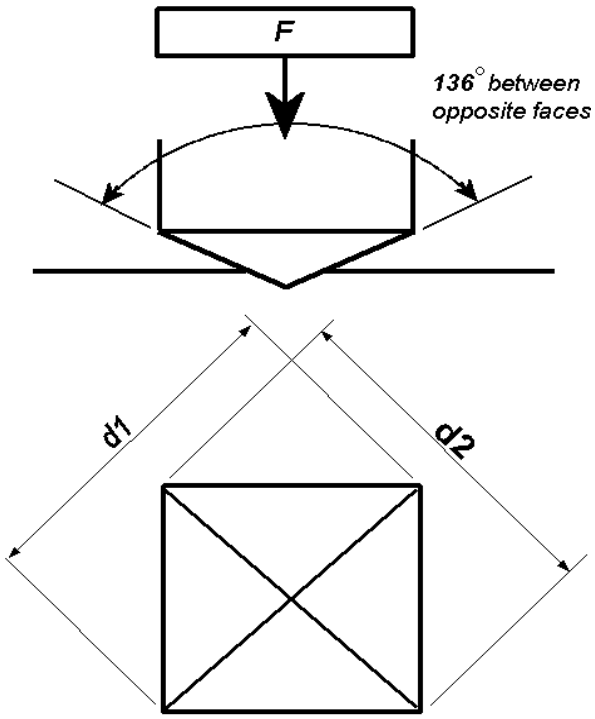

Figure 4.9 A schematic of Vickers indentation process

Hardness measurements were performed using Vicker's hardness indenter, Wolpert-Wilson. The test specimens were metallographically polished using diamond lapping compounds to a finish of 1 μm. Indentations were performed at 30 kgf load at three different locations. Diagonals of indentations were measured with the help of a reflected light microscope at a magnification of 140 **X**.

4. Fractography

Fractography is the interpretation of features observed on materials fracture surfaces using special analytical techniques. The term fractography was introduced by Carl A. Zapffe in 1944 upon discovery of a means of positioning the lens of a microscope close enough to a fracture surface in order to determine its features [13]. The aim of fractography is to analyze the fracture surface in order to gain some useful information about the material and its failure. Fractography is performed on a variety of levels depending on the specific purpose. Optical fractographic techniques include macrofractography which is used to describe visual fractal analysis whereas microfractography describes low magnification (≤ 25 **X**) analysis. Electron fractography uses an electron microscope for very high magnification and high resolution fractographs. The Scanning Electron Microscope (SEM) is a vital and essential tool for fracture research. The SEM has a broad range of magnification levels from 10 **X** to 30000 **X** with a large depth of focus compared to optical microscopy. Specimens are inspected directly and are prepared for the SEM easily and non-destructively. Fractographs produced by the SEM are unique and easy to analyze in that they have a 3D appearance.

Basically, brittle fracture is a rapid run of cracks through a stressed material. Brittle fractures have little or no plastic deformation and are usually characterized by a lack of necking. In brittle fracture, the cracks run close to perpendicular to the applied stress. This perpendicular fracture leaves a relatively flat surface at the break. Besides having a nearly flat fracture surface, brittle materials usually contain a pattern on their fracture surfaces. Some brittle materials have lines and ridges beginning at the origin of the crack and spreading out across the crack surface as shown in Figure 4.10 (a).

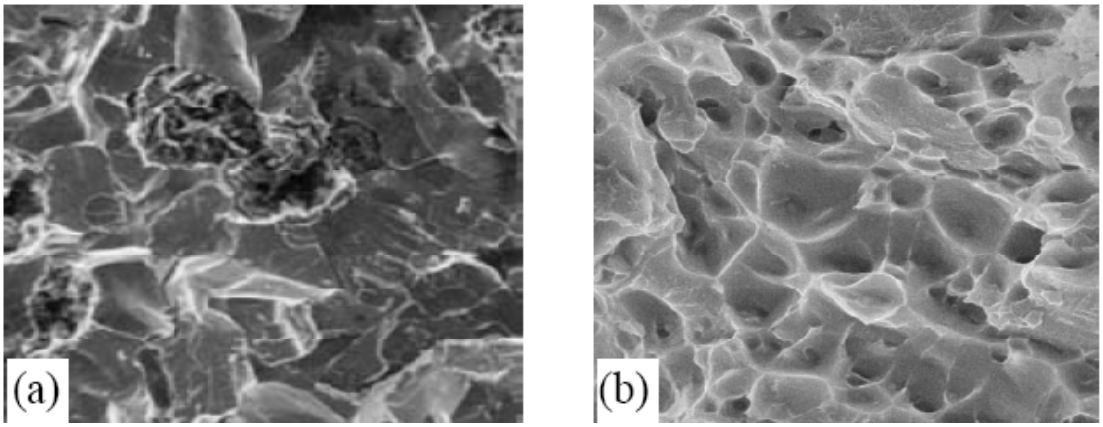

Figure 4.10 Fractographs showing (a) transgranular fracture and (b) ductile fracture.

Conversely ductile fractures can be characterized by necking of the material due to plastic deformation. A fibrous/rough and dull fracture surface can be observed associated with slow crack growth. Plastic deformation is produced by a ductile failure mode such as microvoid coalescence leading to dimple rupture which can be seen in Figure 4.10 (b), above. Failure at the edges of the sample occurs at 45º to the loading direction due to the maximum shear stress being at 45º to the loading stress. Ductile tensile failure begins with uniform plastic deformation leading to localized microvoid coalescence and then dimple rupture in the necked region which experiences a tri-axial stress state on formation of the neck. Dimple rupture leaves pits and holes on the surface structure. SiC_p/Al metal matrix composites that were tested for flexural strength and fracture toughness have been subsequently examined for fractographic analyses using SEM at different magnifications.

References:-

1. M. I. Pech-Canul and M. M. Makhlouf, *J. Mater. Synth. Proc*. **8** [1] (2000) 35.

2. Kay Geels, *Metallographic and Materialographic Specimen Preparation, Light Microscopy, Image Analysis and Hardness Testing*, in collaboration with Struers A/S, ASTM International (2006).

3. F. B. Pickering, *The Basis of Quantitative Metallography*, Institute of Metallurgical Technicians, Monograph No. **1**

4. G. I. Goldstein, D. E. Newbury, P. Echlin, D. C. Joy , C. Fiori and E. Lifshin, *Scanning Electron Microscopy and X-ray Microanalysis* (1981). Plenum Press, New York.

5. T. Iseki, T. Kameda and T. Maruyama, *J. Mater. Sci*., **19** (1984) 1692.

6. David B. Wittry, Electron Probe Microanalyzer, US Patent No. 2916621, Washington, DC: US Patent and Trademark Office.

7. ASTM E831, E228, ASTM International, 100 Barr Harbor Drive, PO Box C700, West Conshohocken, PA 19428-2959, United States.

8. R. Truell, C. Elbaum and B. B. Chick, Ultrasonic Methods in Solid State Physics, Academic Press, New York, (1969), 53-158, 183-186, 365-368

9. W. J. Parker, R. J. Jenkins, C. P. Butler and G. L. Abbott, *J. Appl. Phys.* **32** (1961) 1679.

10. Annual Book of ASTM Standards, **15** [1] (2003) ASTM International, West Conshohocken, PA, United States.

11. Annual Book of ASTM Standards, **3** [1] (2000) ASTM International, West Conshohocken, PA, United States.

12. Annual Book of ASTM Standards, **3** [1] (2003) ASTM International, West Conshohocken, PA, United States.

13. http://www.fract.ses.soton.ac.uk/bkgd.htm

5. Phase & Microstructural Analyses

SiC_p/Al composites have been prepared by the process of pressureless infiltration. In order to understand the behavior of various physical properties of a two phase composite such as SiC_p/Al metal matrix composite, it is necessary to identify any additional phases present in the composite that have developed as a result of processing schedule employed in the present work. It is essential to ensure that the processing schedule did not develop extra phases that are detrimental to the performance of the material or those which hinder the understanding of such a composite system. This chapter deals with characterization of the composite for phase composition and microstructure.

a) X-ray Diffraction (XRD)

X-ray diffraction analysis was performed on powdered specimen of Al-SiC composite and was indexed according to standard powder diffraction patterns. An indexed diffraction pattern of SiC_p/Al composite is shown in Figure 5.1. Extra phases formed as a result of processing schedule were identified from the diffractogram with the help of a database PCPDFWIN version 2.02, May 1999 issued by ICDD (International Council for Diffraction Data). Thereafter the diffraction pattern of SiC_p/Al composite was compared with those of starting materials and also the diffraction pattern of the matrix metal left over upon completion of the infiltration process.

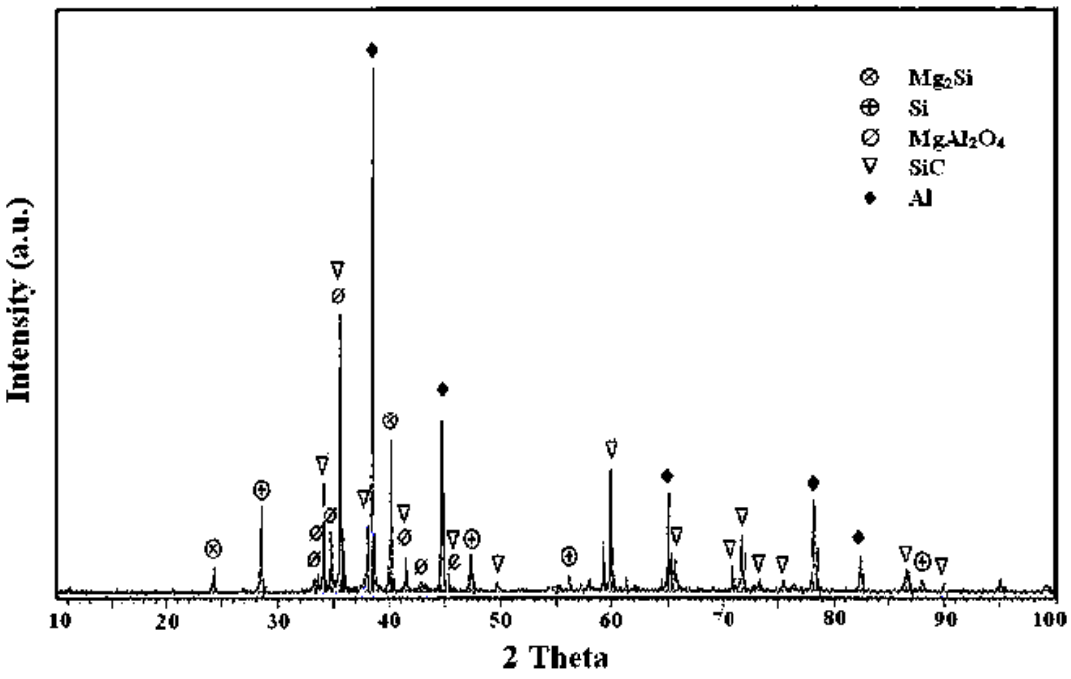

Figure 5.1 X- ray diffraction pattern of SiC_p/Al metal matrix composite.

The diffraction pattern shows presence of two extra phases as identified with the help of powder diffraction data base. These are Mg_2Si (Magnesium Silicide), an intermetallic compound and $MgAl_2O_4$ (Magnesium Aluminate), a spinel. However, no reflections pertaining to Al_4C_3 phase at significant peak positions of 2 theta equal to 31.74^o and 55.04^o were observed, JCPDF Card No: 35-0799 [1]. The diffraction pattern of a composite comprises of reflections from all phases together. In order to resolve the phases pertaining to matrix and interface, phase analyses was also performed on the matrix material that is left over upon completion of infiltration process. The residual matrix metal in this form is supposed to be a close representative of the matrix phase that is present within the metal matrix composite. The residual matrix metal as well as the matrix metal within the composite having undergone similar thermal processing, would have developed common extra phases. As a mark of measure the diffraction pattern

corresponding to the starting matrix material is also shown in Figure 5.2 followed by diffraction pattern for residual matrix metal and is shown in Figure 5.3.

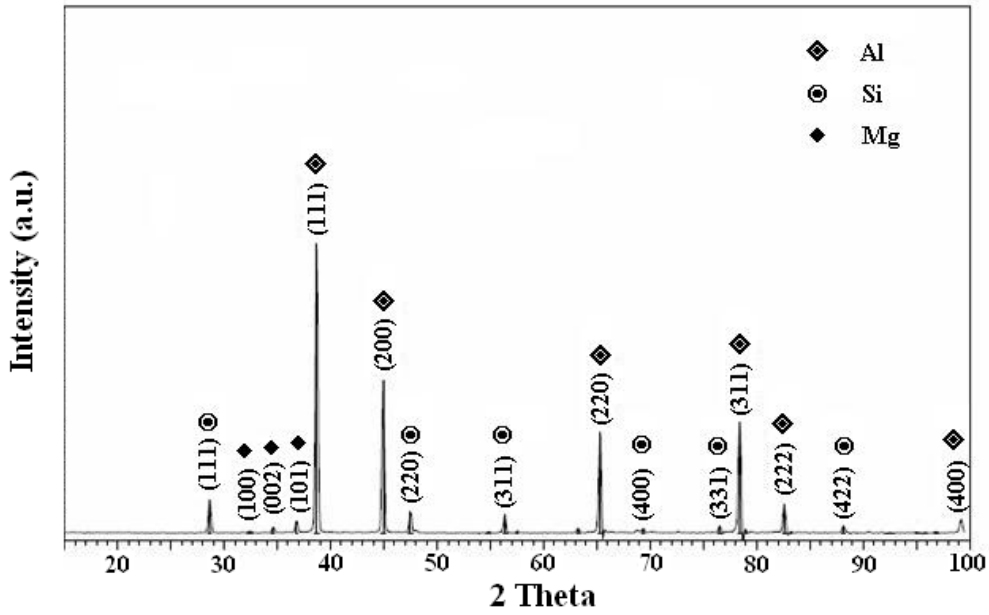

Figure 5.2 X-ray diffraction pattern of the Al-Si-Mg alloy.

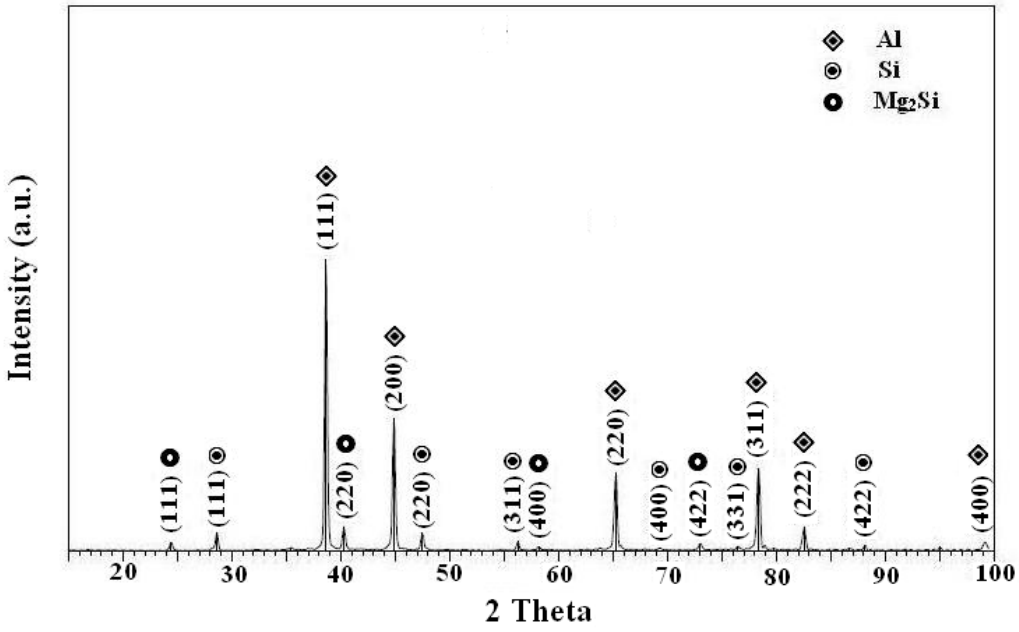

Figure 5.3 X- ray diffraction pattern of the residual matrix metal.

By comparing the diffraction patterns of SiC_p/Al composite, starting matrix metal and residual matrix metal, it can be concluded that the intermetallic phase Mg_2Si is a feature of matrix metal. Mg_2Si that is present in the matrix forms by a reaction between the alloying elements Mg and Si present in the alloy. The intermetallic phase would enable precipitation hardening of Al alloy. An X-ray diffraction pattern of SiC powder is shown below in Figure 5.4 for comparative studies with those of SiC_p/Al composite and residual matrix metal.

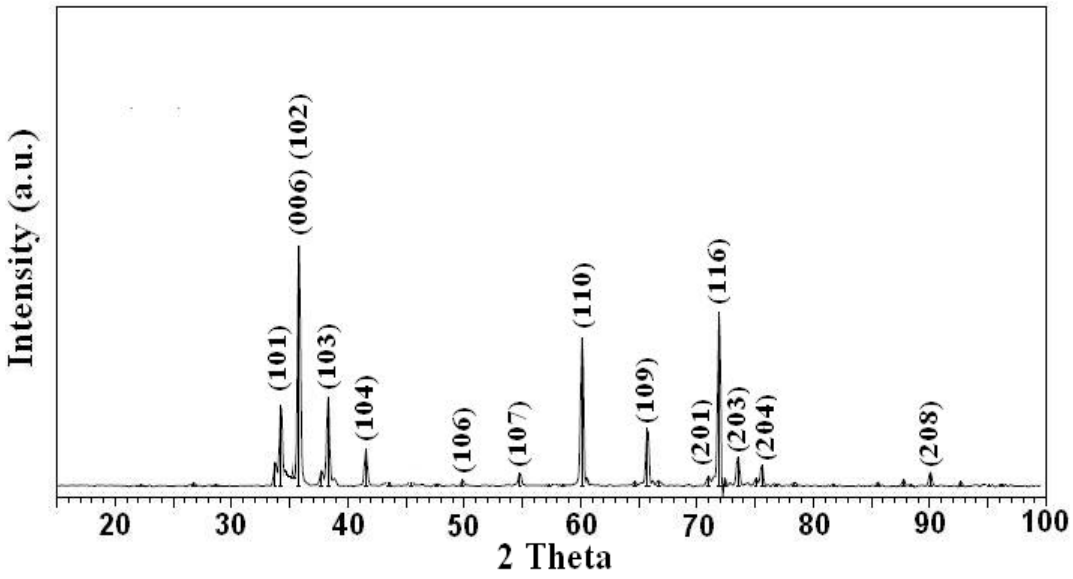

Figure 5.4 X-ray diffraction pattern of SiC powder.

The intermetallic compound, Mg_2Si is expected to have formed in any of the two ways listed below. Simplest of which could be a reaction between the alloying elements Mg and Si, as suggested below.

$$2Mg_{(l)} + Si_{(s)} \rightarrow Mg_2Si_{(s)} \qquad (5.1)$$

However a similar reaction is possible between Mg present in the Al alloy and Si that is precipitated at the interface of particle and matrix. The process of Si precipitation

at the interface is a consequence of a chemical interaction of Mg and SiO_2 present on the surface of SiC particles [2]. This free Si can react with Mg in the alloy to form Mg_2Si

$$2Mg_{(l)} + SiO_{2(s)} \rightarrow 2MgO_{(s)} + Si_{(s)} \qquad (5.2)$$

The precipitation of Si is further possible in the event of a reaction between Al and SiO_2 resulting in the formation of Al_2O_3 as shown below. Si precipitated in the manner indicated below would further react with Mg to yield Mg_2Si.

$$3SiO_{2(s)} + 4Al_{(l)} \rightarrow 2Al_2O_{3(s)} + 3Si_{(s)} \qquad (5.3)$$

Si precipitated in any of these ways can react with Mg in the Al alloy to form Mg_2Si precipitates. Thus Mg_2Si formed as a result of a reaction between alloying elements would reflect as a feature of matrix microstructure. Whereas the same intermetallic formed as a result of reaction between Mg from the alloy and Si precipitated at the interface would be a feature of interfacial reactions. This would further indicate that the affinity of Mg to react with Si would drag the melt towards the particle surface and thus aid in wetting.

The formation of the other extra phase i.e. $MgAl_2O_4$ can be explained in more than one ways. Dudek *et al*. propose that a reaction between SiO_2 present on the surface of SiC and Al-Mg-Si alloy where Al an Mg are in molten state at the temperature of processing [3]. The reaction occurs in a single step as given in (5.4).

$$Mg_{(l)} + 2Al_{(l)} + 2SiO_{2(s)} \rightarrow MgAl_2O_{4(l)} + 2Si_{(s)} \qquad (5.4)$$

However, another argument exists in literature to explain the formation of the spinel in more than one step. As discussed earlier, a reaction between Mg and SiO_2

present on the surface of SiC particles would result in the formation of MgO. MgO is a very stable compound in various atmospheres. But it is to be recalled that this interfacial reaction product, MgO is surrounded by a melt of Al alloy. Under these conditions MgO becomes unstable and would react with molten Al to result in formation of $MgAl_2O_4$ [4].

$$4Al_{(l)} + 2MgO_{(s)} + 3SiO_{2(s)} \rightarrow 2MgAl_2O_{4(s)} + 3Si_{(s)} \qquad (5.5)$$

Another equally possible mechanism by which the spinel could have formed is by a direct reaction between MgO & Al_2O_3. However, the diffraction pattern of SiC_p/Al composite does not indicate any traces of MgO and/or Al_2O_3 phases. These phases could have formed in the amorphous state upon interaction of Al alloy with SiO_2 on the surface of SiC particulates. The two intermediate phases could then react to form $MgAl_2O_4$ as indicated in (5.6). The possibility of such a reaction to occur between two solid phases is backed by the fact that ΔG, the Gibbs energy change was found to be negative as deduced by Luo *et al*. [18]

$$MgO_{(s)} + Al_2O_{3(s)} \rightarrow MgAl_2O_{4(s)} \qquad (5.6)$$

Thus it can be understood from such a comparative study that one of the reaction products i.e. the intermetallic compound, Mg_2Si is present both in the matrix and at the particle – matrix interface. The other reaction product was found at the interface of particle and matrix phases. McCoy *et al*. report that Mg is effective in reducing the surface tension of the melt and further induce interfacial reaction which would in turn favor reactive/spontaneous infiltration of Al [5]. Oh *et al*. also promote the argument that interfacial reactions are the dominant mechanism for enhancing the wetting of a solid ceramic surface with molten Al alloy [6]. Further to be noted is the fact that there is no

Mg present in the elemental form, indicating that all of which has actively participated in various chemical reactions with the reinforcement and promote pressureless infiltration. At the same time, there could also be losses due to evaporation. The interfacial reaction product of $MgAl_2O_4$ is a feature of all those metallurgical processes that combine Mg containing Al alloys and artificially oxidized SiC particles. This is clearly shown by Mingyuan *et al*. in the case of SiC particulate reinforced Al-2024 matrix composites by squeeze casting process [7]. However, the features observed so far like the absence of Al_4C_3, location of Mg_2Si: either in matrix or at the interface or both etc. are yet to be confirmed by means of more sensitive methods of phase composition analyses such as electron microscopy equipped with analyses of characteristic X-rays.

b) Optical Microscopy & Quantitative Image Analyses

In order to carry out detailed studies of phase composition based on electron microscopy, it is necessary to obtain a clear picture of distribution of various phases present in the composite. A rough estimate of the number of phases present in the composite can be obtained from optical microscopy studies. A representative section from each composite was polished and observed under a reflected light microscope. The results of optical microscopy performed on polished sections of SiC_p/Al composites are shown in Figure 5.5. A homogenous distribution of silicon carbide particulates can be observed from the micrographs captured at different magnifications. It is to be recalled that this is a result of the processing steps adopted in the preparation of powder preforms. A bimodal distribution of SiC particulates can be observed from each of the micrographs along with gradual increase in the dark phase indicating increase in volume fraction. Also shown in Figure 5.5(f) is the microstructure of residual matrix metal at a higher

magnification. A major alloying element of the matrix metal is Si which is stable unlike Mg present in the alloy. Figure 5.5(f) shows residual Si in darker contrast against a bright background of Al.

In a typical infiltration process, a liquid phase is allowed to permeate into a preform made up of discontinuous solid phase. This upon solidification at a temperature below the melting point of the liquid phase results in the formation of a composite material. The said preform is comprised of solid phase in discontinuous form wherein, each particulate has to rest on another particulate or an assembly of particulates. This results in developing a virtual continuity in the solid phase. At higher volume fractions, there exists a situation wherein, large numbers of particles are in contact with each other to a greater extent. This can be observed from optical micrographs of SiC_p/Al composites shown in Figure 5.5 (b) to (e). The microstructure at higher magnification depicts presence of extra phases other than that of matrix and reinforcement. Figure 5.6 shows micrographs where only a major extra phase could be identified and was learnt to be Si as hypo-eutectic phase. It is often observed that Si is located at the interface between particle and matrix [8].

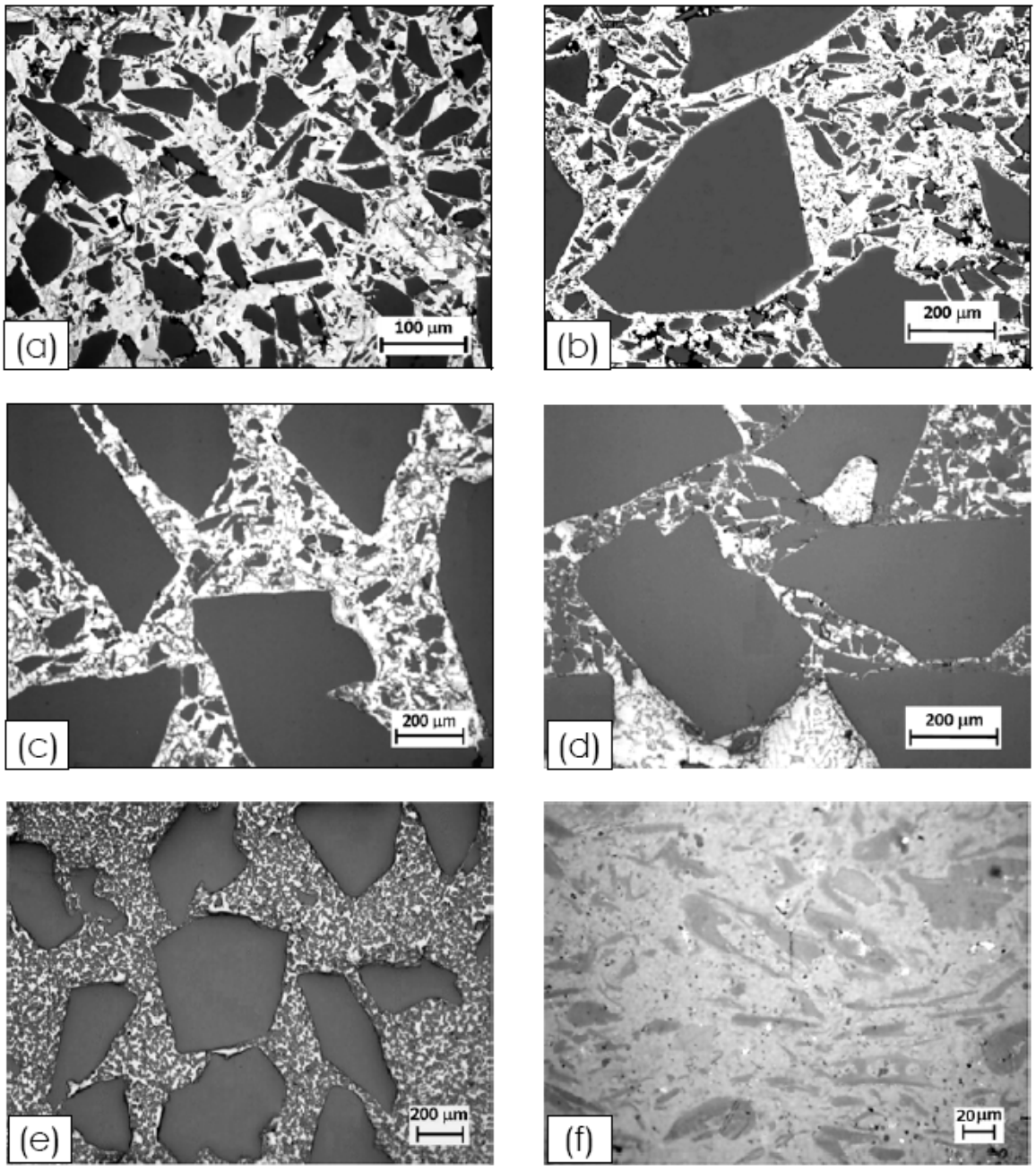

Figure 5.5 Microstructures of Al-SiC metal matrix composites with different volume fractions. (a) Al – 0.41SiC, (b) Al – 0.45SiC, (c) Al – 0.54SiC, (d) Al – 0.67SiC, (e) Al – 0.70SiC and (f) Al – residual matrix metal.

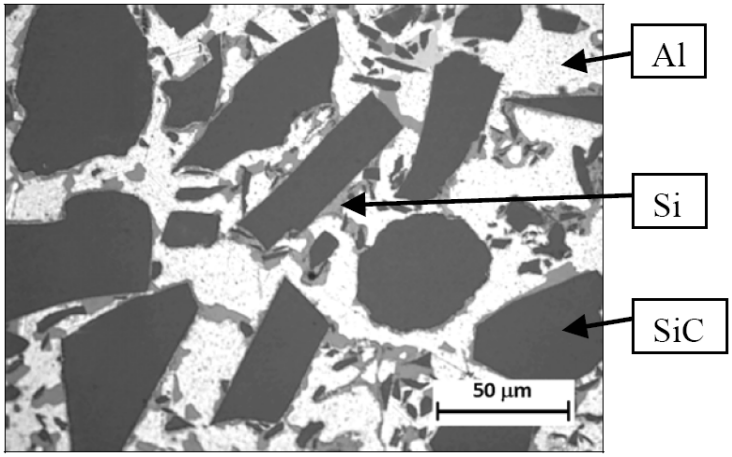

Figure 5.6 An optical micrograph showing the segregation of Si.

Presence of Si at the interface can be explained in more than one way. It is believed that Si present as the alloying element has a primary function to retard dissolution of SiC in molten Al. At temperatures above the melting point of Al-Si-Mg alloys, and under atmospheric pressure SiC becomes thermodynamically unstable and an invariant reaction occurs at 650 ± 3 ^{o}C, resulting in the formation of a detrimental phase – Al_4C_3 [9]. However, Si can also be precipitated out from the interfacial reactions between the melt and SiO_2 that was developed by artificial oxidation of SiC to prevent its dissolution [10].

$$4Al_{(l)} + 3SiC_{(s)} \rightarrow Al_4C_{3(s)} + 3Si_{(s)} \qquad (5.7)$$

Silicon carbide particulates used for reinforcement were provided in the form of a loose powder preform contained in a refractory crucible. The reinforcement phase is immobile during the entire course of the infiltration process, in contrast to other processes of composite fabrication like stir casting [11], rheo-casting [12] etc., where the reinforcement and the molten metal both are in motion and thereby develop complexities in the distribution of reinforcement. As a result of which the silicon carbide particulates

are distributed in the aluminum alloy matrix in an inhomogeneous manner. Whereas achieving good homogeneity in the distribution of reinforcement particles in the matrix phase is of crucial importance. The distribution of reinforcement has a great effect on the effective properties of a composite material at various stages of its evaluation and also application. There is a great necessity to achieve homogenous distribution of reinforcement in a matrix because it affects the final properties of a composite. Lack of homogeneity in the microstructure of a composite material, would result in local differences in the volume fraction and may mislead further interpretations that are based on volume fraction of reinforcement. The very fact that the local variations in the volume fraction of a composite affect the final properties, pose a great necessity to obtain composites with homogenous distribution of reinforcement. Therefore, it is very necessary that the reinforcement be quite homogenous in its distribution in the matrix phase. This can be confirmed from measurements of volume fraction of reinforcement and the statistical deviation associated with the result for each composite.

Measurements of volume fraction were performed directly on optical micrographs of SiC_p/Al composites using image analysis software. Results of phase/volume fraction by image analyses are listed in Table 5.1 against those determined manually from absolute and apparent volume measurements of the preforms.

Table 5.1 Measurements of volume fraction by Image Analyses of microstructures

Sl. No.	Manual method		Image Analysis	
	Volume fraction	Deviation from mean (%)	Volume fraction	Deviation from mean (%)
1.	0.41	5	0.40	10
2.	0.45	4	0.47	8
3.	0.54	3	0.56	8
4.	0.67	2	0.69	7
5.	0.70	2	0.73	5

A deviation of 2 – 5 % was observed in the measurements of volume fraction by manual method. Image analyses methods used in the determination of phase/volume fraction were found to have a larger deviation as compared to manual methods. This could be due to the difference in principle of measurement in the two methods of evaluation of volume fraction. Volume fractions of preforms measured by manual methods were found to be more reliable with lesser deviation from mean and hence were considered for representing SiC_p/Al composites prepared in the present work.

Specimens prepared for microscopy were further examined using electron microscopes for a detailed phase composition analyses.

c) Scanning Electron Microscopy (SEM)

As discussed earlier, in the present composite material system, the reinforcement is susceptible to dissolution in molten Al to form Al_4C_3. From the literature survey, it is understood that there is a great necessity to prevent the formation of Al_4C_3 phase that is

hygroscopic in nature. Necessary steps were taken to prevent formation of such phases. X-ray diffraction analyses of SiC_p/Al composites indicated absence of Al_4C_3 phase. Keeping in view the limitations of X-ray diffraction, more precise techniques such as electron microscopy need to be carried out.

Electron microscopy studies were performed on the composites prepared by using pressureless infiltration technique. Extra phases other than matrix and reinforcement could be observed clearly with the help of the high resolution offered by an electron microscope. Back scattered electron image of an Al-SiC metal matrix composite is shown in Figure 5.7. X–ray analyses (Energy Dispersive Spectroscopy - EDS) were carried out at different locations on the specimens to obtain the phase composition.

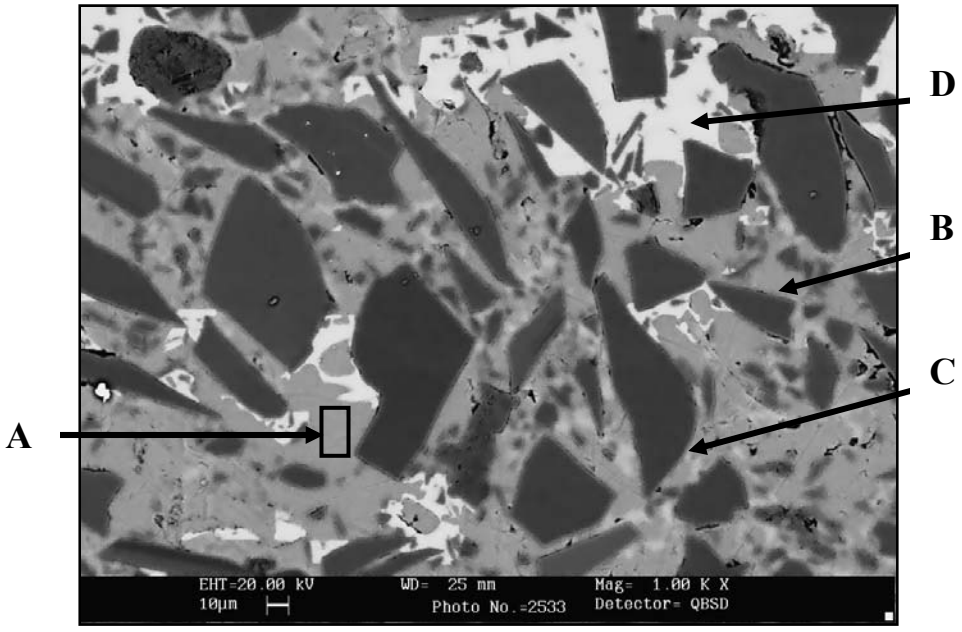

Figure 5.7 Back scattered electron image of Al-SiC composite.

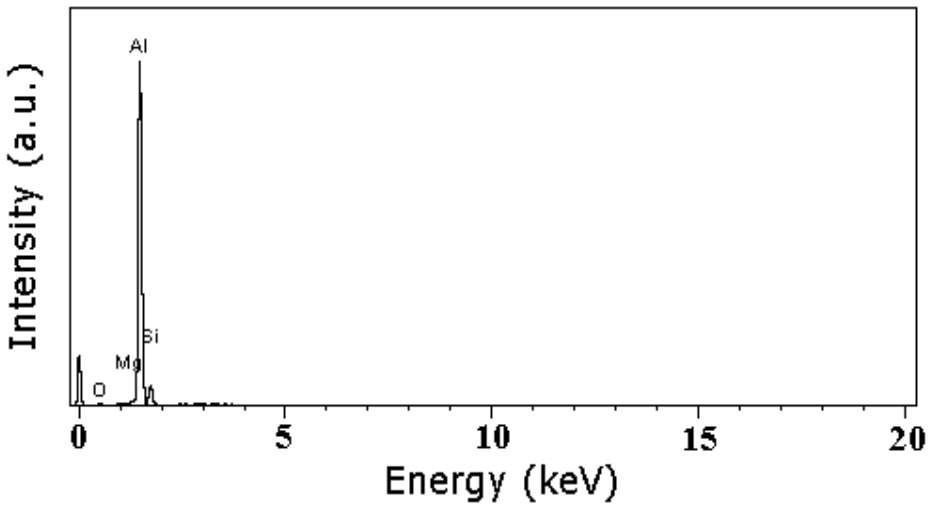

Figure 5.8 EDS of matrix phase **[A]** of Al-SiC composite.

Result of compositional analysis of the matrix phase is shown in Figure 5.8. Quantitative analyses of the matrix phase leads to a composition of Al-12.9Si by weight %. The matrix phase has a chemical composition close to that of LM-6 Al alloy used as the raw material for the preparation of the master alloy. As a whole the matrix phase is comprised of Al-12.9Si with an additional phase of Mg_2Si. It can be recalled that no elemental Mg was detected in the X-ray diffraction pattern. This shows that Mg alloyed with LM-6 Al alloy was completely used up in formation of compounds such as Mg2Si with some loss due to evaporation during fabrication process.

The particle-matrix interfaces as can be seen from the back scattered electron image in Figure 5.7, are clear with little or no inhomogeneity. The clear interface was analyzed by energy dispersive spectroscopy and the result is shown in Figure 5.9. The interface was found to comprise of elements Al, Si, O and Mg. This suggests that the molten metal had reacted with silica on the surface of the Silicon Carbide. The interface between particle and matrix is likely to be comprised of products of reaction among SiO_2,

Mg and Al. These include MgO, Mg_2Si and $MgAl_2O_4$ where MgO could be unstable in presence of molten Al [4]. As a result $MgAl_2O_4$ spinel is the likely product at the interface. These observations would strengthen the results obtained from X-ray diffraction analyses where reflections from spinel phase were observed. It may be recalled that MgO, Al_4C_3 and Al_2O_3 were not observed from X-ray diffraction analyses.

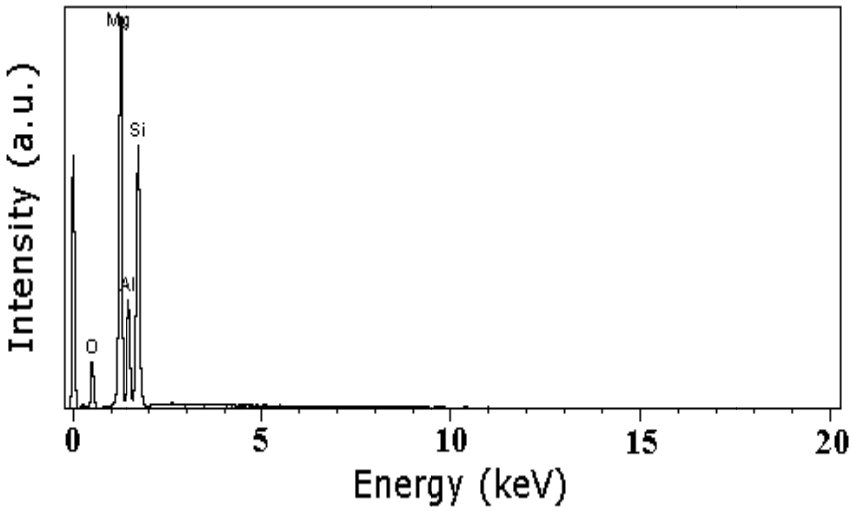

Figure 5.9 EDS of particle - matrix interface **[B]** in Al-SiC composite.

The microstructure shows presence of another interface material that is distinguished by contrast. This additional interface can be observed as a dark phase in the microstructure along the boundary of the particle, shown in Figure 5.7. Results of X-ray analyses (Energy Dispersive Analyses – EDS) carried out on additional interface material are shown in Figure 5.10.

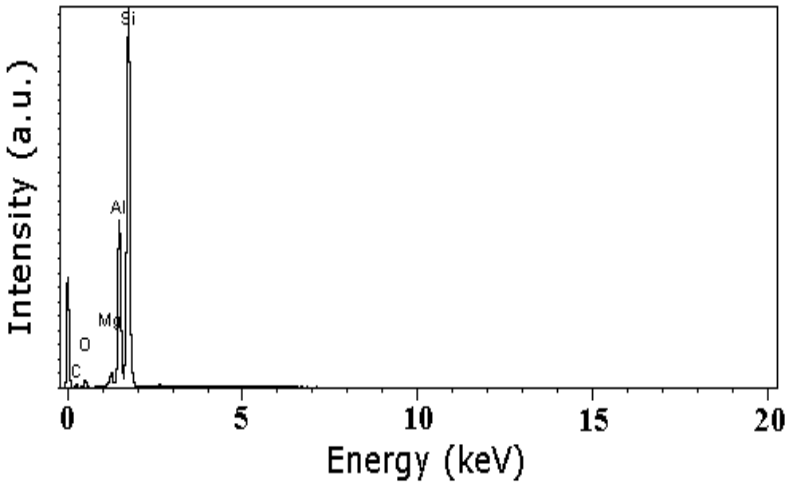

Figure 5.10 EDS of additional interface material **[C]** in Al-SiC composite.

The analysis of the additional interface material shows that it is comprised of C, O, Mg, Al and Si. The phase is reasonably rich in Si. Aluminum alloy containing Si and Mg has developed Mg_2Si to the stoichiometric ratio and leaving out excess Si thereafter. This excess amount of Si found at the interface indicates that it has migrated to the interface.

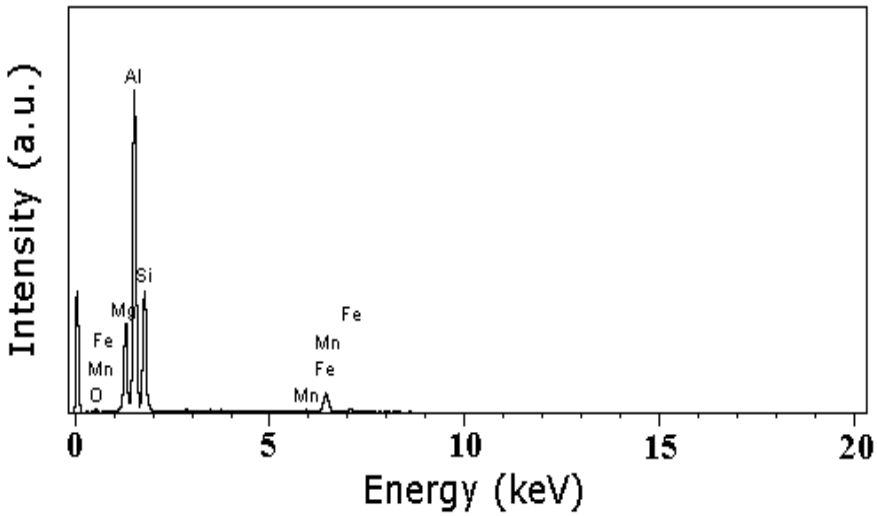

Figure 5.11 EDS of bright phase **[D]** in Al-SiC composite.

Energy dispersive spectroscopy of the bright phase in the matrix portion indicates that the region is rich in Mg and Si. However, it was also observed that the bright phase contains trace amounts of Mn and Fe. The corresponding spectrum is shown in Figure 5.11. X-ray diffraction pattern of Al-SiC composite indicate presence of Mg_2Si and no reflections from Mg were observed. These observations together conclude that the bright phase is comprised of Mg_2Si dispersed in Al matrix. The presence of extra phases of Fe and Mn could be traced back to the commercial Al alloy used to prepare Al-Si-Mg master alloy meant for infiltration experiments. The commercially available LM-6 series Al alloys contain Fe and Mn as impurity elements. As a consequence of the same, Fe and Mn were found in the matrix phase of the composite. Mg_2Si phase observed from X-ray diffraction studies was found to have formed within the matrix far from the interface, as a result of reaction between Mg and Si present in the alloy.

However, EDS studies did not indicate traces of nitrogen in the form of AlN which could have formed during the fabrication of SiC_p/Al composites by process of pressureless infiltration. This is indicative of the fact that AlN did not form in the composite material. Nevertheless, formation of AlN cannot be ruled out as evidenced by EDS analysis in the case of nitrogen which cannot be detected if present in very low concentrations. In order to explore the formation of AlN under the present experimental conditions, it was decided to investigate the periphery of the composite-metal duo i.e. residual matrix metal and its surface for presence of AlN. A Secondary electron image of a section of residual matrix metal is shown in Figure 5.12. The result of a full window analysis using EDS is shown in Figure 5.13. This analysis reflects the presence of elements O and Cl apart from Al, Mg and Si which are the principal constituents of the

matrix metal. The analysis does not indicate presence of nitrogen on a full window scale even in trace amounts. This may be due to the low temperature used for the infiltration process at which nitrogen shows limited reactivity compared to other elements such as oxygen.

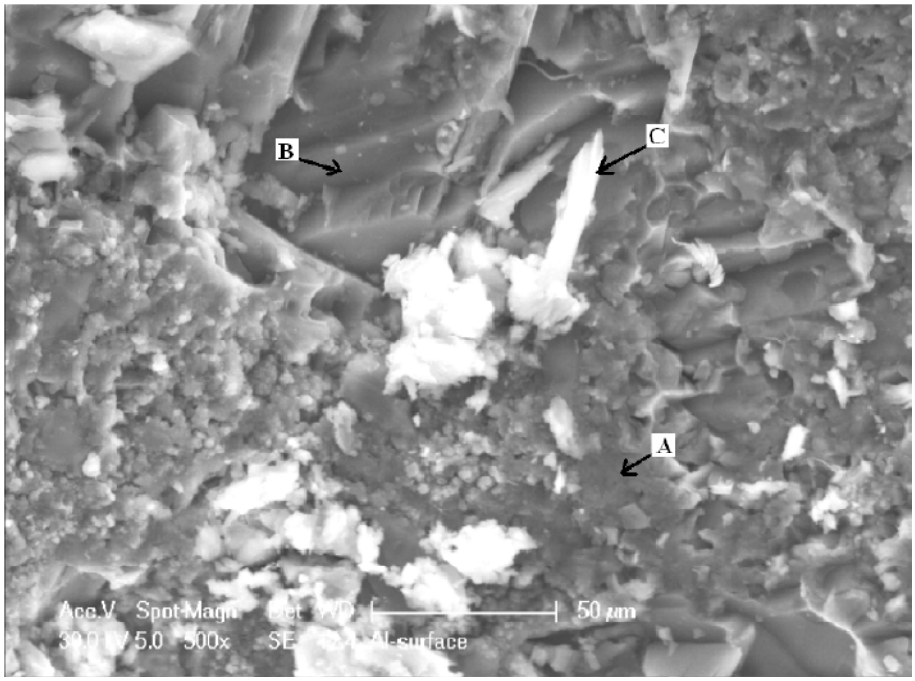

Figure 5.12 A SE image of residual Al matrix metal.

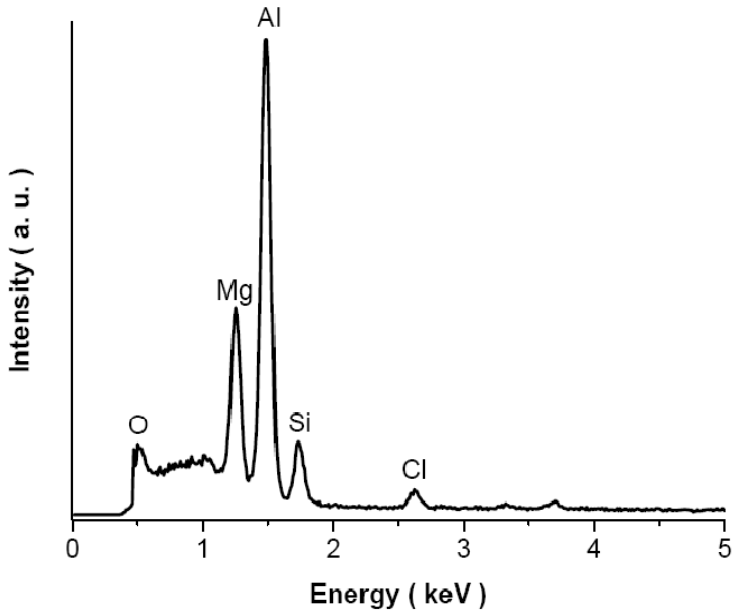

Figure 5.13 EDS of residual matrix metal in full window mode.

Energy Dispersive Spectroscopy was performed at locations A, B and C indicated in the secondary electron mage of the residual matrix metal and is shown in Figure 5.14, 5.15 and 5.16 respectively.

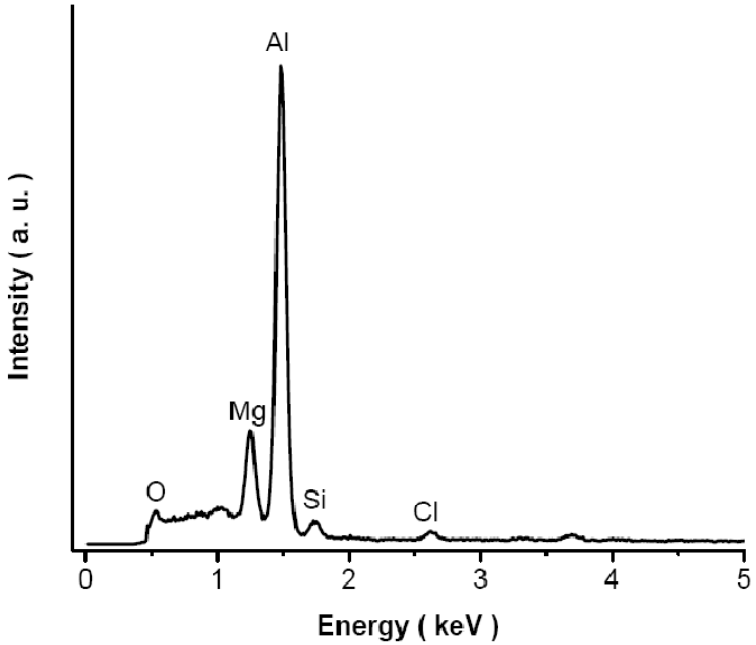

Figure 5.14 EDS at location **A** indicated in Figure 5.12

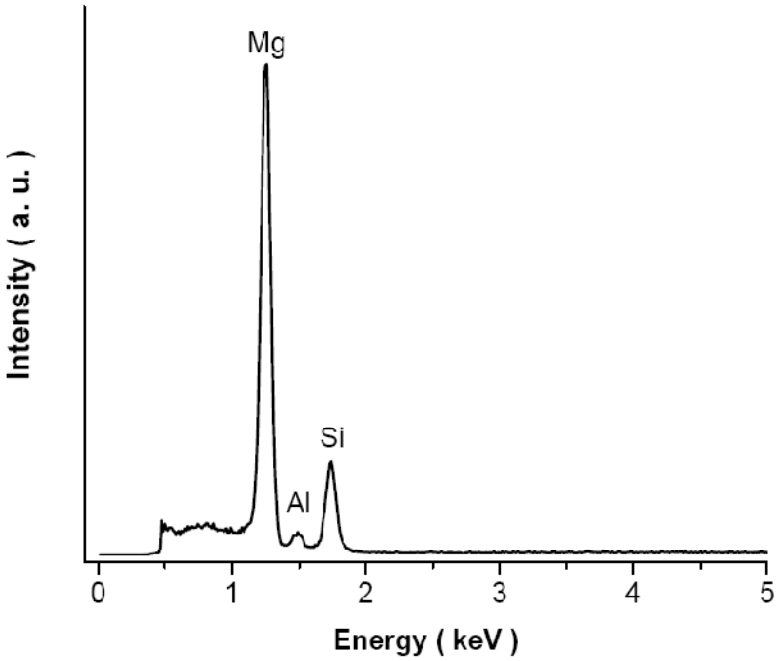

Figure 5.15 EDS at location **B** indicated in Figure 5.12

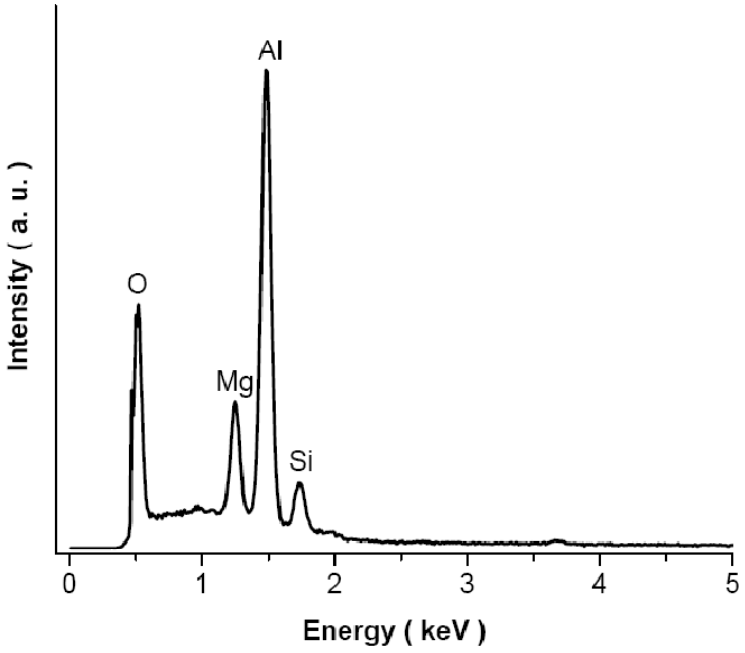

Figure 5.16 EDS at location **C** indicated in Figure 5.12

These studies indicate that even the much exposed matrix metal is comprised of Mg_2Si embedded within Al alloy along with trace amounts of oxygen and chlorine.

However, no traces of nitrogen were found in the present investigation which would confirm absence of nitride formation during the infiltration process according to the thermal profile adopted in the present work. Formation of AlN during the processing of aluminum matrix composites by liquid metallurgical techniques has been well documented in the literature. Creber *et al*. reported the growth of AlN-Al matrix on the surface of molten alloy and also into porous ceramic preforms containing Al_2O_3, TiB_2, AlN and B_4C by directed melt nitridation of Al-Mg based alloys in the temperature range of 900-1200^oC [13]. LeHuy and Dallaire report that an activation energy of 110 kJ/mole is required for the nitridation of Al-5Si-3Mg alloy in the temperature range of 1000-1200^oC [14]. Aghajanian *et al*. developed the process of pressureless infiltration wherein an Al- 10%Mg alloy infiltrates spontaneously into a preform of alumina with a particle size of 66 μm [15]. It was reported that at a temperature of 800^oC, for a soak time of 4 hours, complete infiltration occurred under an atmosphere of 100% N_2. Whereas, under similar conditions except that the atmosphere comprised of 10% N_2- 90% Ar, partial/incomplete infiltration was recorded. The latter experimental configuration has shown significant amount of AlN formed at the particle-matrix interface, which is supposed to be due to the reduced rate of infiltration that provided greater time for pick up of N_2 by the melt.

Pech-Canul *et al*. have demonstrated formation SiC_p/Al composites by pressureless infiltration at a temperature of 1235^oC in an atmosphere of Argon followed by N_2 [16]. In this study it was found that, irrespective of the nature of the surface of reinforcement, AlN has formed during the process of infiltration. In another study by Rao and Jayaram, it was observed that Al_2O_3/Al composites fabricated by pressureless infiltration at temperature between 900-1100^oC and a soak period of 3 hour have shown pronounced formation of AlN at the particle-matrix interfaces [17]. From all of the above studies, it can be observed that formation of AlN during

infiltration processing of aluminum matrix composites is basically governed by the temperature and concentration of N_2 in the infiltrating atmosphere. However, in the present work, the process temperature is fairly below the temperatures employed in the aforesaid studies and also the atmosphere is unfavorable for the growth AlN as found by Aghajanian *et al*. [15]. As a result of the thermal profile and atmospheric conditions employed in the present work, it was found that AlN did not form and if formed, the concentration is much below the nitrogen detection limits of EDS.

Detailed analyses using SEM-EDS has led to the understanding that the intermetallic phase of Mg_2Si was present both in the matrix as well as at the particle matrix interface. The particle-matrix interface was found to be made up of $MgAl_2O_4$. However, absence of Al_4C_3 phase could not be checked for the limitations of EDS on the lowest atomic number element at Z=7. As a result, it is difficult to say whether the detrimental phase of Al_4C_3 has been prevented by employing the processing conditions developed in the present work. Moreover, coexistence of Mg and Si suggests a probable presence of Mg_2Si. Thus, in order to confirm formation of Mg_2Si and detect Al_4C_3, it is necessary to investigate the phase composition of the composite material by sophisticated techniques such as Electron Probe Micro Analyzer (EPMA) – WDS.

d) Scanning Electron Probe Micro Analysis (SEPMA)

With the help of phase characterization techniques such as XRD and SEM-EDS, it was possible to understand the composition of the composite material to a great extent. However, due to the limitations with such characterization techniques, it was not possible to comment upon the presence or absence of Al_4C_3 phase. A versatile technique such as

Electron Probe Micro Analyzer equipped with a Wavelength Dispersive Spectrometer (WDS) is more sensitive than SEM-EDS.

SiC_p/Al composites prepared by pressureless infiltration were investigated for phase composition using a scanning electron probe microscopy. The main aim behind the use of EPMA-WDS is to analyze the particle-matrix interface for its composition and ensure that the process of pressureless infiltration did not develop undesired phases at the interface. A line scan was carried out across an interface between the Al alloy matrix and the SiC particle in the region as indicated in Figure 5.17. The result of the line scan across the interface is shown in Figure 5.18. From the figure it can be observed that there is a small peak corresponding to Mg at the interface. This is an indication of the presence of Mg_2Si at the interface.

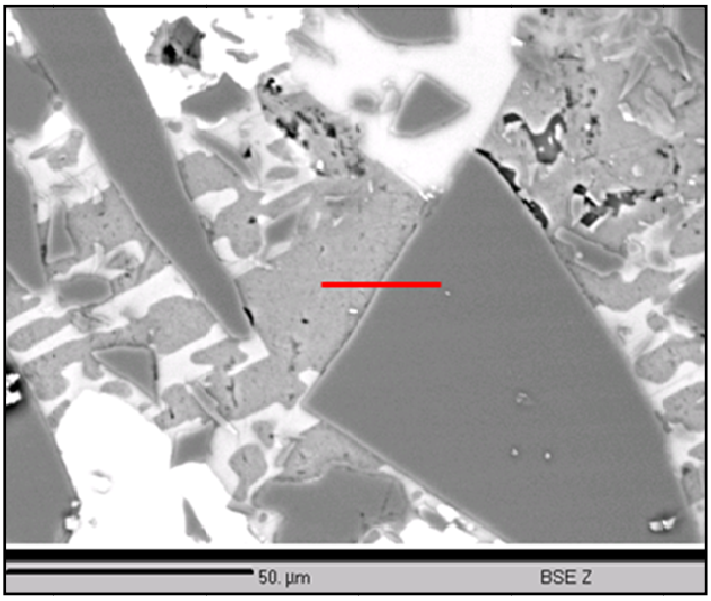

Figure 5.17 BSE image showing SiC-Al interface to be examined by WDS.

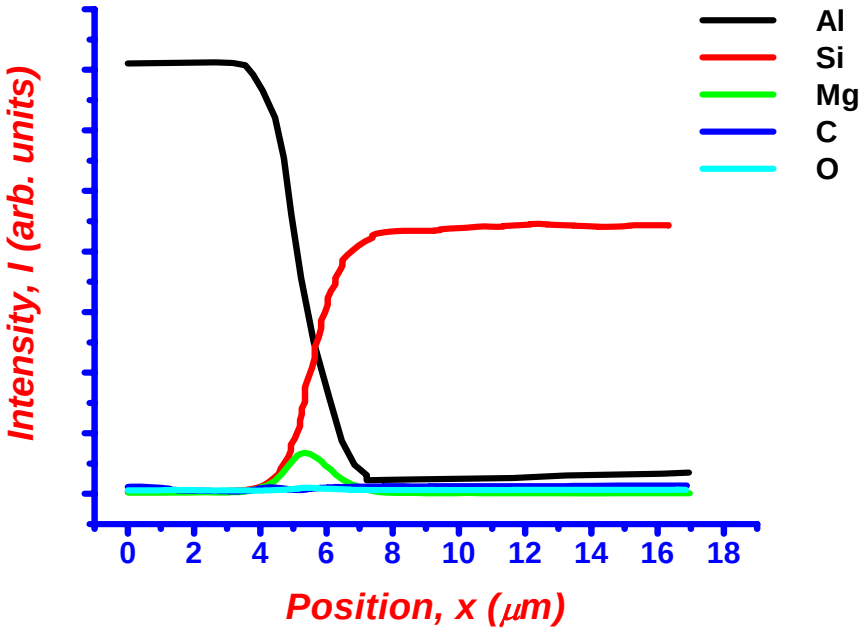

Figure 5.18 WDS line profile across SiC-Al interface shown in Figure 5.17.

A comparative study of the intensities across the same interface as in Figure 5.17 is shown in Figure 5.19, by separating the results where it can be observed that O coexists with Mg and Al at the interface. This is indicative of the interfacial reaction product $MgAl_2O_4$. A comparison of the intensities of O, Mg, Al and Si, it was understood that certain amount of Mg_2Si is also present in a region close to the interface.

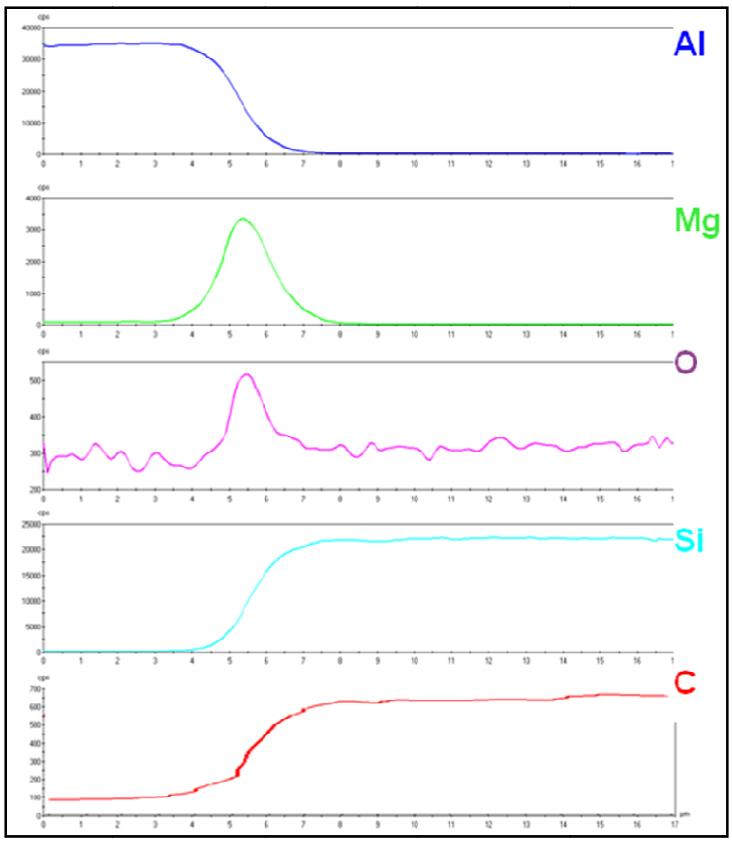

Figure 5.19 A split view of WDS line profile of interface shown in Figure 5.17.

Results from X-ray diffraction, show the formation of $MgAl_2O_4$ in the SiC_p/Al composite. It is to be recalled that this is a product of reaction between molten Al alloy and SiO_2, which was artificially developed on the surface of SiC. It can be seen from Figure 5.17 that the interface material is developed at the interface of all SiC particles. Presence of this reaction product all over the surface of SiC particulates is a rough indication to the absence of Al_4C_3. This observation supports the view in the literature that the process of wetting SiC by molten Al is promoted by the formation of $MgAl_2O_4$ phase at the particle – matrix interface [18]. This confirms that $MgAl_2O_4$ is formed at the interface of SiC and the Al alloy matrix. However, this needs to be confirmed from more of such interfacial studies and rule out the formation of Al_4C_3. Often, high intensities

from principal elements would tend to subjugate the response from minor phases such as alloying elements or interfacial reaction products. A similar situation arises in the present case where the intensity from Al dominates over that from Mg and O that are in relatively lower proportions in the material under investigation. Another back scattered electron image is shown in Figure 5.20 for further interfacial characterization.

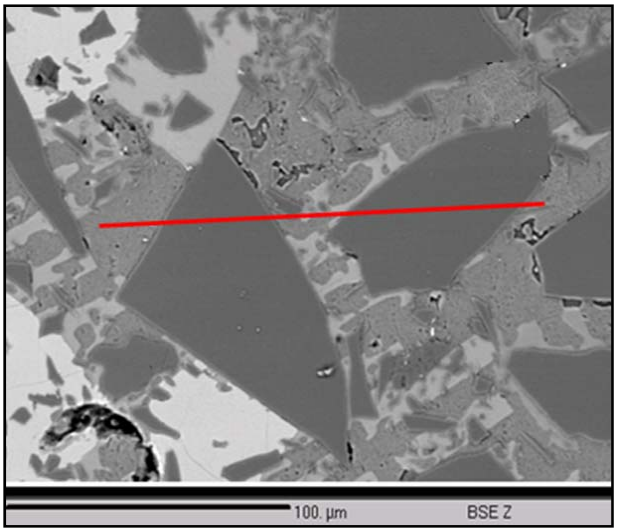

Figure 5.20 BSE image of few SiC - Al interfaces under investigation.

WDS Line scan for Mg, Si and O was performed across many interfaces as shown by the red line in Figure 5.20. The corresponding results are shown in Figure 5.21. Si was chosen for investigation so as to serve as a reference to indicate SiC particulate. From The profile shows presence of Mg and O simultaneously at each of the interfaces. Corresponding to every peak in the profile for O, a peak can be observed in the profile for Mg. However, one peak is left out in the profile for Mg, corresponding to which there is no peak in the profile for O. The profile for Si indicates that there are significant amounts of Si in the matrix. However, a closer look at the line profile for Si indicates a peak between the two SiC particulates that corresponds to the left out peak in the profile for

Mg. This co-existence of Mg and Si between SiC particulates indicates the formation of Mg_2Si in the matrix.

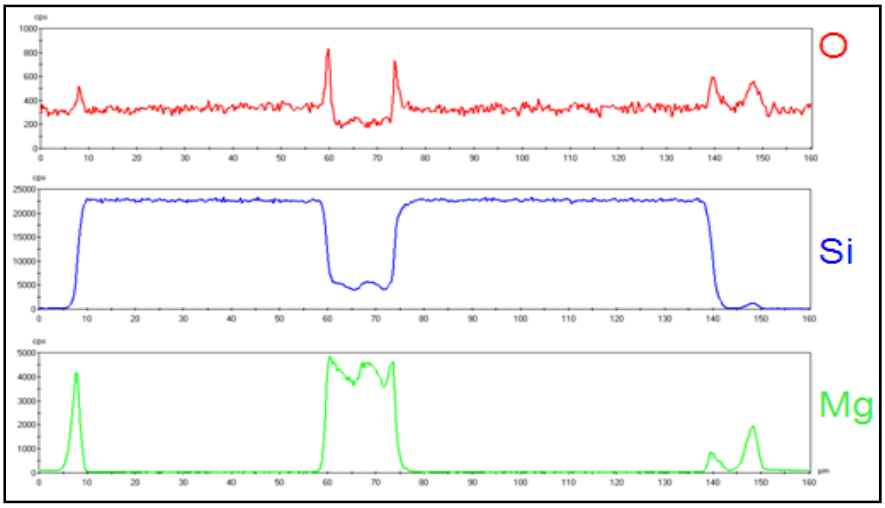

Figure 5.21 WDS line profile of SiC - Al interfaces, for Mg, Si and O.

The analysis was further extended to other locations of the composite microstructure in order to validate and strengthen earlier observations. Figure 5.22 shows another back scattered electron image of SiC – Al interfaces to be characterized.

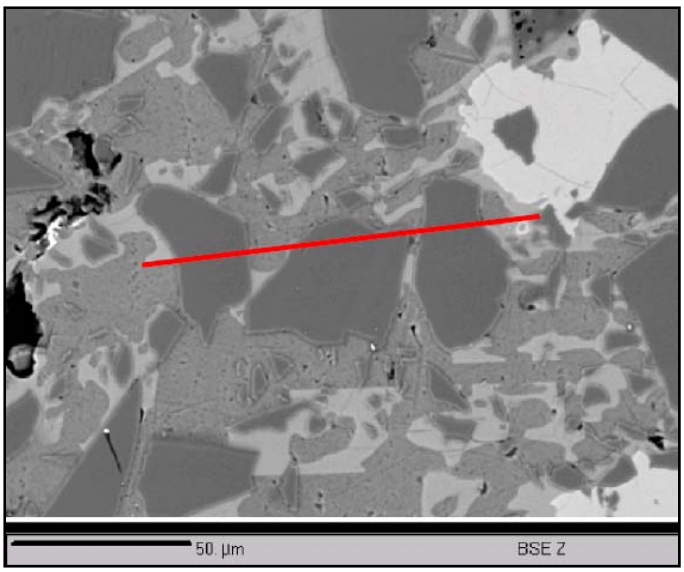

Figure 5.22 BSE image of SiC - Al composite for interfacial characterization.

WDS line profile corresponding to the above BSE image is shown in Figure 5.23. The results obtained here are in close correspondence with the previous results. Mg and O co-exist at almost all interfaces showing signs of reaction between them. These findings strongly reflect the formation of $MgAl_2O_4$ at the interface, as a reaction product between molten Al alloy and SiO_2. The formation of $MgAl_2O_4$ can be accompanied by the precipitation of Si liberated from SiO_2, present on the surface of SiC. This Si is susceptible to react further with Mg present as alloying element leading to the formation of Mg_2Si. This can causes the matrix beyond the interface to contain the intermetallic phase, Mg_2Si.

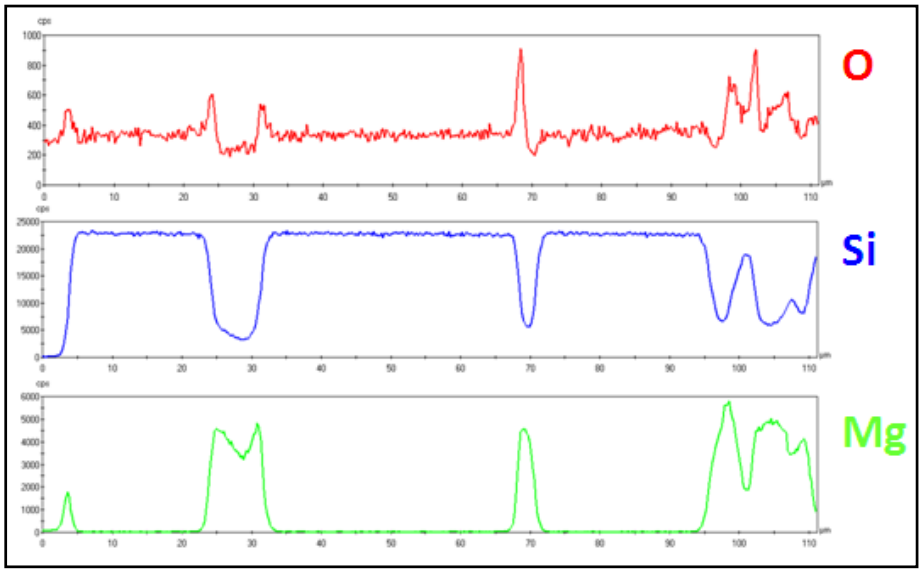

Figure 5.23 WDS line profile for SiC - Al interfaces shown in Figure 5.22.

Another back scattered electron image is shown in Figure 5.24 followed by the corresponding WDS line profile in Figure 5.25. It can be observed from Figures 5.23 and 5.25 that Mg_2Si forms in a region close to the interface. Free Si is also observed in a region close to the interface, which could be coming from the Al alloy.

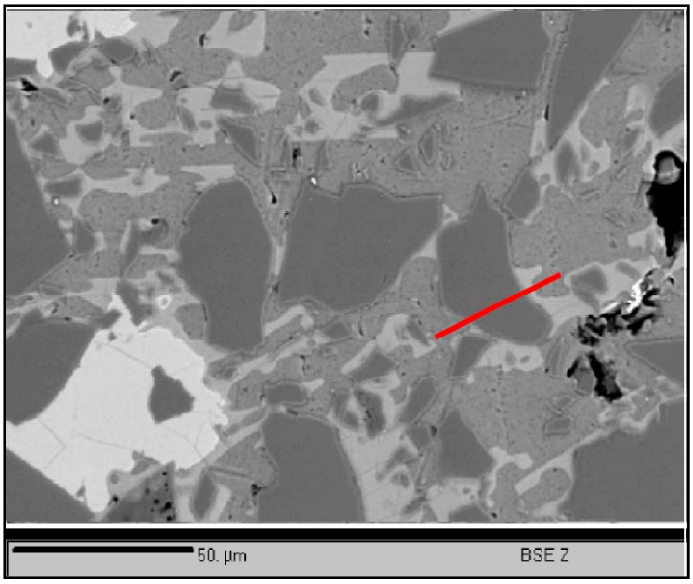

Figure 5.24 BSE image of SiC - Al interface.

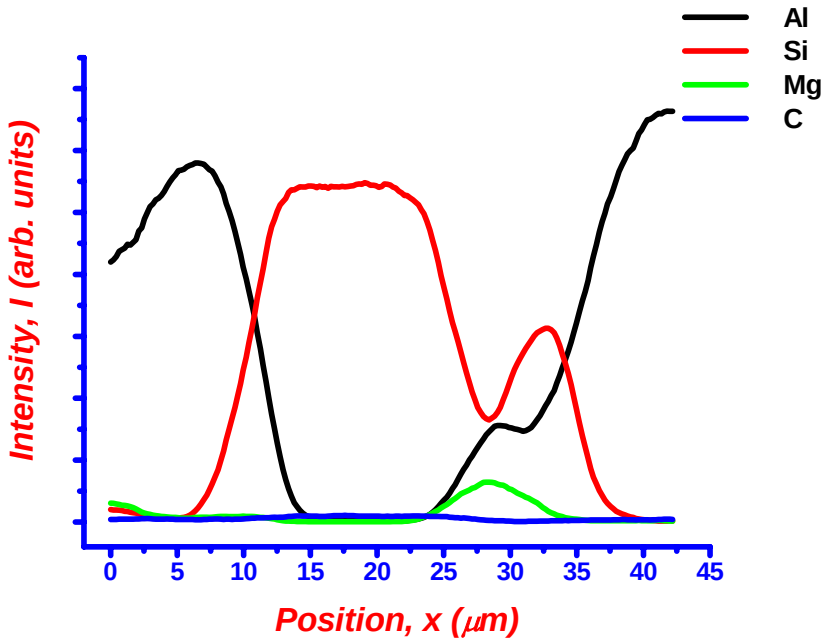

Figure 5.25 WDS line profile corresponding to SiC - Al interface shown in Figure 5.24.

Lee and Kwon report results from X-ray diffraction analyses and TEM studies on SiC_p/Al composites prepared by pressureless infiltration [19]. Formation of Al_4C_3 was observed in the composites for infiltration temperatures between 700°C and 1000°C in

nitrogen atmosphere. It was also reported that the Al_4C_3/SiC peak intensity ratio was insignificant for composites prepared at 700^oC. The ratio increased markedly with increase in temperature of infiltration up to 1000^oC. Further it is to be noted that the duration allowed for spontaneous infiltration has been limited to 30 minutes. In spite of small soaking time, formation of Al_4C_3 could not be arrested. Si liberated from the dissolution of SiC in molten Al was observed to react with Mg to form Mg_2Si and remain as precipitate at the interface. TEM studies reveal discontinuous presence of Al_4C_3 and $MgAl_2O_4$ along the particle – matrix interface. However, no traces of Al_4C_3 were observed from X-ray diffraction analyses and EPMA carried out in the present work.

Gu *et al*. report the effect of reinforcement oxidation on mechanical properties accompanied by TEM studies [7]. No traces of Al_4C_3 were observed from scanning & transmission electron microscopy studies. However these studies were found to identify $MgAl_2O_4$ at the particle – matrix interface. It was observed that the process of artificial oxidation of SiC powders would definitely benefit in terms of avoiding undesired reactions and enable proper interfacial bonding. Similar observations were made by Zhongliang Shi *et al.* [4] by SEM and TEM studies. In the case of oxidized SiC particulate reinforced Al alloy matrix composites, MgO forms at the interface which in turn transforms in to a more thermo-stable $MgAl_2O_4$ in the presence of molten Al.

Pech-Canul *et al.* reported the effect of Si coating on the SiC particulates to inhibit the formation of Al_4C_3 [20]. It was reported that SiC_p/Al composites did not possess any traces of Al_4C_3 as identified from X-ray diffraction analyses. Instead traces of AlN were observed in SiC_p/Al composites and show that the process of coating SiC

particulates with Si was beneficial in the suppression of Al_4C_3. In another work by Pech-Canul *et al*., high concentration of Si in Al alloy was found to suppress the formation of Al_4C_3 [21]. However, these composites are susceptible to lower levels of strength, as reported, because of relatively high concentrations of Si in the Al alloy matrix, up to 13.5 %. It was suggested that, irrespective of the manner in which Si is provided at the interface, either by coating or as an alloying element, the formation of Al_4C_3 can be arrested. However, the presence of Si at the interface has its merits and de-merits. The Si phase being rather brittle would have limited role in the event of load transfer. The concept of composites is very much based on ability to transfer load on to the reinforcement. SiC_p/Al composites with Si at the interface are susceptible to lower strength levels by initiating failure at the interface.

Zulfia *et al*. report in their work, findings from X-ray diffraction analyses of SiC_p/Al composites prepared by pressureless infiltration [22]. It was reported that XRD indicated presence of extra phases such as Mg_2Si, Al_4C_3 and minor traces of Al_2O_3. Also it was observed that the amount of the detrimental phase Al_4C_3 increased with increase in Mg content of Al alloy, which was supposed to aid in terms of initiation and continuation of pressureless infiltration. This increased with increase in dwell time. However, there was no evidence of AlN or Mg_3N_2 in the work reported by Zulfia *et al*. This fact illustrates the necessity to take prior steps in order to avoid the formation of Al_4C_3.

In the present work, prior care was taken to avoid the formation of Al_4C_3 phase at the particle-matrix interface. Both, the matrix and the reinforcement were modified as per the requirements and suggestions to obtain SiC_p/Al composites that are free from Al_4C_3.

As a part of this, the matrix was suitably alloyed with necessary alloying elements and the reinforcement was artificially oxidized in air at high temperature. Luo *et al*. have observed extra phases such as Mg_2Si and $MgAl_2O_4$ from X-ray diffraction and TEM studies [23]. A clear absence of phases like Al_4C_3, Al_2O_3 and MgO were recorded. The similarity in the phase constitution between the two works stems from the fact that the reinforcement powders were artificially oxidized and that the matrix is comprised of Mg and Si as alloying elements in reasonable proportions. However, Si and Mg concentrations as large as 14% and 8% respectively were employed by Luo *et al*. for the infiltration of artificially oxidized SiC. Similar results have been obtained in the present work despite having lower amounts of Si and Mg, 9% and 5% respectively. In the present work characterization of the particle – matrix interface was carried out using SEM-EDS and SEPMA-WDS. The results of interfacial characterization by SEM show that Mg_2Si is often present in a region close to the interface. SEPMA-WDS studies across the interface show presence of $MgAl_2O_4$ at the interface ruling out the presence of Al_4C_3. These studies show that the process of artificial oxidation is a necessary step in preventing the formation of Al_4C_3 phase and enable good interfacial bonding that would not disintegrate in due course.

References:-

1. PCPDFWIN version 2.02 from ICDD (International Council for Diffraction Data)
2. B. Hallstedt, Z. K. Liu and J. Agren, *Mater. Sci. Eng. A* **129** (1990) 135.
3. H. J. Dudek, A. Kleine, R. Borath and G. Neite, *Mater. Sci. Eng. A* **167** (1993) 129.
4. Zhongliang Shi, Shojiro Ochai, Masali Hojo, Jaechul Lee, Mingyuan Gu, Hoin Lee and Renjie Wu, *J. Mater. Sci.* **36** (2001) 2441.

5. J. W. McCoy, C. Jones and F. E. Warner, *SAMPE Q* **19** [2] (1988) 37.

6. S. Y. Oh, J. A. Cornie and K. C. Russell, *Ceram. Engg. Sci. Proc*. **8** [7-8] (1987) 912.

7. Mingyuan Gu, Yangping Jin, Zhi Mei, Zengan Wu and Renjie Wu, mater. Sci. eng. A **252** (1998) 188.

8. Jae-Chul Lee, Sung-Bae Park, Hyun-Kwang Seok, Chang-Seok Oh and Ho-In Lee, *Acta Mater*. **46** [8] (1998) 2635.

9. T. Iseki, T. Kameda and T. Maruyama, *J. Mater. Sci*., **19** (1984) 1692.

10. D. J. Lloyd, H. Lagace, McLeod and P. L. Morris, *Mater. Sci. Eng. A* **107** (1989) 73.

11. J. Hashim, L. Looney and M. S. J. Hashmi, *J. Mater. Proc. Tech*., **92** (1999) 1.

12. S. Das, T. K. Dan, S. V. Prasad and P. K. Rohatgi, *J. Mater. Sci. Lett*., **5** (1986) 562.

13. D. K. Creber, S. D. Poste, M. K. Aghajanian and T. D. Claar, *Ceram. Engg. Sci. Proc*., **9** (1988) 975.

14. H. LeHuy and S. Dallaire, *Proc. Int. Symp. On Advances in Ceramic and Metal Matrix Composites*, Hallifax, Canada. Pergamon Press, New York, 1989, 302.

15. M. K. Aghajanian, M. A. Rocazella, J. T. Burke and S. D. Keck, *J. Mater. Sci*. **26** (1991) 447.

16. M. I. Pech-Canul, R. N. Katz and M. M. Makhlouf, *J. Mater. Proc. Technol*. **108** (2000) 68.

17. B. Srinivasa Rao and V. Jayaram, *Acta Mater*. **49** (2001) 2373.

18. Y. D. Huang, N. Hort, H. Dieringa, K. U. Kainer and Y. L. Liu, *Acta Mater*. **53** [14] (2005) 3913

19. Kon Bae Lee and Hoon Kwon, *Scripta Mater*. **36** [8] (1997) 847.

20. M. I. Pech-Canul, R. N. Katz, M. M. Makhlouf and S. Pickard, *J. Mater. Sci.* **35** (2000) 2167.

21. M. I. Pech-Canul and M. M. Makhlouf, *J. Mater. Synth. Proc*. **8** [1] (2000) 35.

22. A. Zulfia and R. Hand, *J. Mater. Sci*. **37** (2002) 955.

23. Z. P. Luo, Y. G. Song and S. Q. Zhang, *Scripta Mater*. **45** (2001) 1183.

6. Physical Properties of SiC_p/Al Composites

In the present work, SiC_p/Al composites were fabricated by pressureless infiltration technique to obtain material with large dimensions and with varied levels of volume fraction in the range 0.41 and 0.70 of SiC. By employing appropriate methods it was ensured that the composite material developed in the present work did not contain undesired phases. Further, it was necessary to ensure that the material is free of defects/voids that might have formed as a consequence of processing technique. Before proceeding to evaluate various physical properties of SiC_p/Al composites such as Coefficient of Thermal Expansion (α), Ultrasonic Velocity (V), Thermal Conductivity (λ) and Electrical Resistivity (ρ), the material may be evaluated for its density and porosity.

a) Density and Porosity

A measure of the density and extent of porosity of any composite material is of crucial importance for the role it has in the determination of its final properties. The presence of porosity has a great effect towards the mechanical, ultrasonic and other properties of the material [1]. Finally a composite material with inhomogeneous porosity behaves in an unpredictable manner. The details of density measurements performed on several specimens from composites of each volume fraction are listed in Table 6.1, below. The corresponding mathematical relations are given below.

$$\text{Apparent density } (A) = \frac{x}{(x-y)} * \text{ density of liquid in g/cc.} \qquad (6.1)$$

$$\text{Bulk density } (B) = \frac{x}{(z-y)} * \text{ density of liquid in g/cc.} \qquad (6.2)$$

$$\text{Porosity } (P) = \frac{A - B}{A} * 100 \text{ in } \% \qquad (6.3)$$

Where, ***x***: mass of the dry specimen in air,

y: mass of specimen suspended in liquid, usually distilled water and

z: mass of specimen saturated with liquid (distilled water).

Table 6.1 Density and porosity data for SiC_p/Al composites

Sl. No.	Volume fraction	Density, d (g/cc)	Porosity (%)
1.	0.41	2.86	0.08
2.	0.45	2.88	0.11
3.	0.54	2.93	0.15
4.	0.67	3.01	0.14
5.	0.70	3.02	0.16

The uncertainty in the measurement of density and porosity were found to be 2.0% and 2.8% respectively. The variation in density was studied as a function of volume fraction and was observed to be linear in the volume fraction range of 0.41 to 0.70 of silicon carbide in aluminum alloy matrix composites. A plot of the same is shown in Figure 6.1, below. Apart from the data on density of composites prepared in the present work, also included in the plot are the density data for the end points of volume fraction, 0.0 and 1.0 of SiC. Density of SiC_p/Al composites was found to vary linearly with volume fraction of SiC. This is indicated by a linear fit of experimental data for density of SiC_p/Al composites and the fit was found to possess a coefficient of square of regression, R^2: 0.999. Also shown in the figure is the variation in density of SiC_p/Al composites as calculated from the Rule of Mixtures. It can be observed from the figure

that the linear fit of experimental data matches well with the prediction of Rule of Mixtures. This is an indirect indication of absence of porosity on a macroscopic scale of observation, within the composite materials developed in the present work. However, complete absence of porosity can only be confirmed from density measurements to evaluate bulk density and finally arrive at percentage porosity.

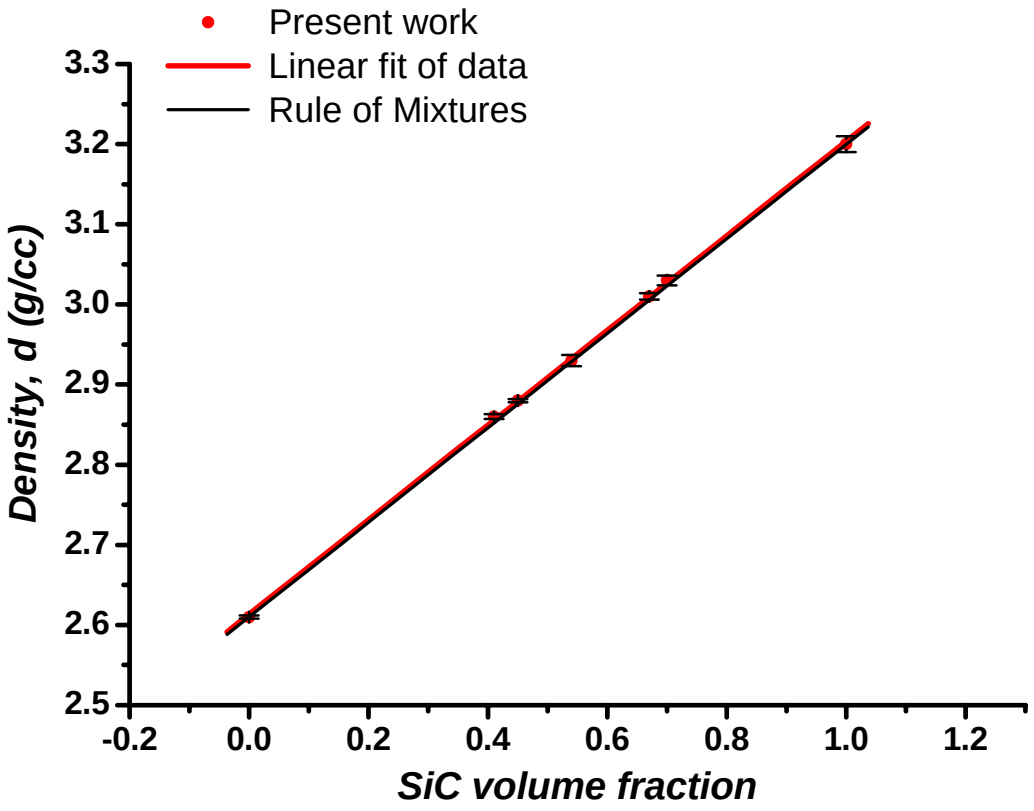

Figure 6.1 Density of SiC_p/Al composites as a function of volume fraction.

The experimental data for density was found to fit to a linear equation of the form given below.

$$\rho_c = 0.55 * V_f + 2.64 \qquad (6.4)$$

Where ρ_c denotes the density of the composite and V_f denotes the volume fraction of silicon carbide. Also shown in the graph is the variation in the density of the

composites as calculated using the rule of mixtures from knowledge of the densities of each phase and its volume fraction. A difference in the measured and calculated densities would give a measure of internal porosity i.e., closed porosity that cannot be measured by liquid displacement method for a two phase material. The porosity obtained from equation 6.3 is only a measure of pore volume that is accessible to a permeable liquid. The total porosity present in a material can then be obtained as follows.

$$\text{Total Porosity, } P_{total} = P_{open} + P_{closed} \qquad (6.5)$$

P_{open} refers to the porosity that is open or continuous in nature and can be measured using the liquid displacement method with suitable modifications. P_{closed} refers to that porosity which cannot be accessed and a direct measurement of which is possible in cases where in the material possesses a single phase. In case of a two phase material though a direct measurement of closed porosity is not possible but knowledge of measured density, open porosity and phase/volume fraction would enable estimation of closed porosity, if any.

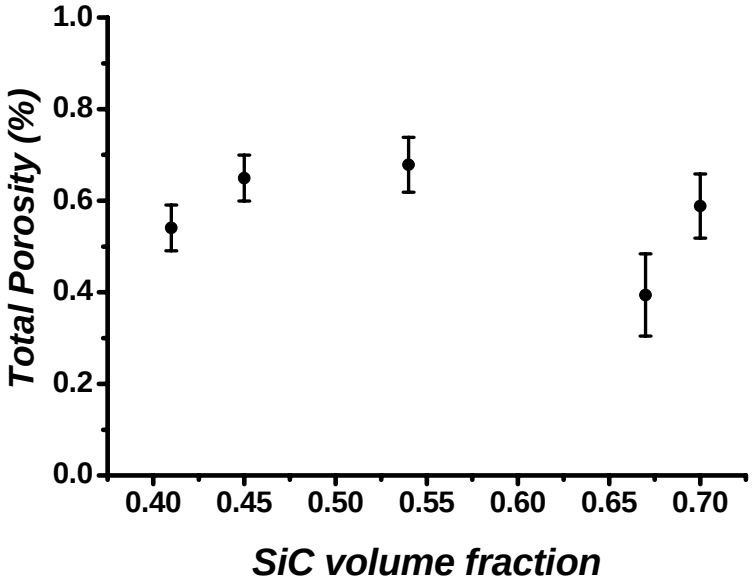

Figure 6.2 Variation in total porosity of SiC_p/Al MMC as a function of volume fraction

A plot of variation in the total porosity present in the composite as a function of volume fraction is shown in Figure 6.2. For SiC_p/Al composites with volume fraction ranging between 0.41 and 0.70, no regular trend could be observed in the variation of total porosity as a function of volume fraction. Nevertheless, porosity obtained in the present work is far less than those obtained in other works by pressureless infiltration, 2.1 – 7.5 % [2], 7 – 9 % [3]. Thus the two phase composite materials of SiC_p/Al system can be considered for further evaluation when compared to specimens that have higher levels of porosity. By employing the process of pressureless infiltration for the fabrication of SiC_p/Al composites, the role of porosity could be nullified for a dependable evaluation of physical and mechanical properties of two phase materials.

b) Coefficient of Thermal Expansion

Using the process of pressureless infiltration, SiC_p/Al composites with high volume fractions of SiC were prepared and tested for dimensional changes due to change in temperature. The results of relative change in length of test specimens of SiC_p/Al composites as a function of temperature for different volume fractions of SiC are presented in Figure 6.3. The resulting coefficients of linear thermal expansion in the temperature range of 50 – 300^oC, taken as the average of three measurements for each volume fraction of composite, are listed in Table 6.2. The uncertainty in the measurement of coefficient of thermal expansion was limited to 1.5 % by the use of a standard dilatometer such as DIL 402C.

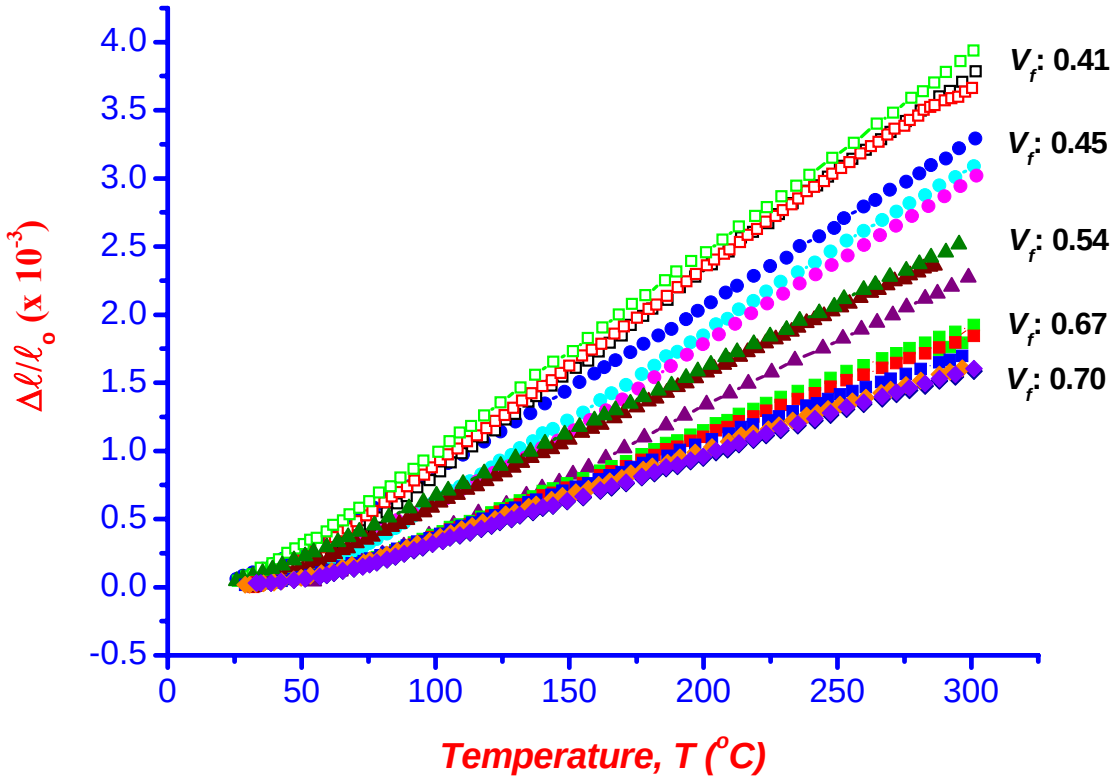

Figure 6.3 Plot of relative expansion vs. temperature for SiC_p/Al composites with different volume fractions.

Table 6.2 Average CTE of SiC_p/Al composites prepared by pressureless infiltration

Sl. No.	Volume fraction of SiC	CTE (x 10^{-6} /K)
1.	0.41	14.42
2.	045	12.33
3.	0.54	9.63
4.	0.67	7.06
5.	0.70	6.45

A variation in the coefficient of thermal expansion as a function of volume fraction is shown in Figure 6.4, for volume fractions ranging between 0.41 and 0.70 of SiC.

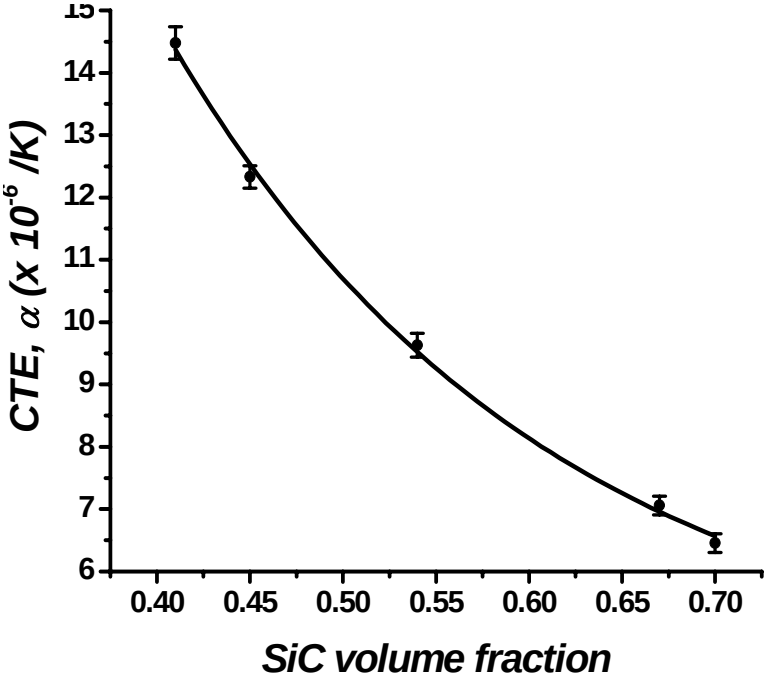

Figure 6.4 Variation in the measured values of CTE for SiC_p/Al composites.

The coefficient of thermal expansion was found to vary in a non-linear fashion with respect to the volume fraction. An empirical fit was obtained between coefficient of thermal expansion and volume fraction of SiC_p/Al composites. The thermal expansion coefficient was found to decrease in an exponential manner with volume fraction of SiC for the composites studied in the present work. The coefficient of square of regression was found to be 0.998.

The experimental data for coefficient of thermal expansion of individual phases of Al alloy and SiC was considered along with the data for coefficients of thermal expansion of SiC_p/Al composites prepared and evaluated in the present work. In this case it was observed that the coefficient of thermal expansion possesses a sigmoidal relationship with volume fraction. The experimental data was found to fit with a square of regression coefficient of 0.998. The corresponding plot is shown in Figure 6.5, below.

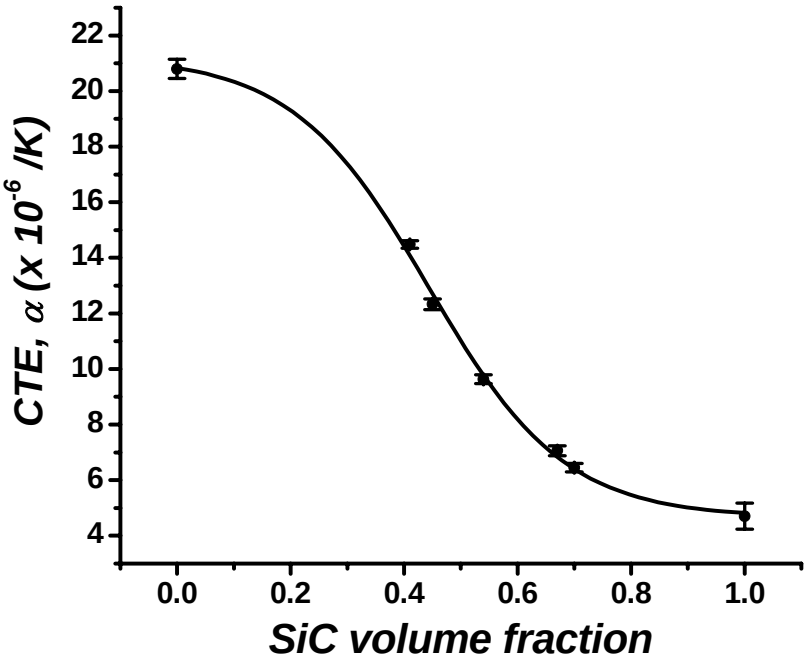

Figure 6.5 Sigmoidal relationship of CTE with volume fraction.

The observed variation in the coefficient of thermal expansion was then compared with experimental observations on SiC_p/Al composites fabricated by other methods of fabrication. Arpon *et al*. have performed measurements of coefficient of thermal expansion on SiC_p/Al composites prepared by vacuum infiltration technique [4]. It was reported that the average coefficient of thermal expansion for SiC_p/Al composites with volume fraction between 0.55 and 0.74 was linear with volume fraction of SiC and is given by the following relation.

$$\alpha = 31.3 - 32.0V_f \text{, in units of } 10^{-6} \text{ /K,} \qquad (6.6)$$

The same data was found to fit to an exponential decay in a manner similar to the present work. Apart from an exponential fit in the present range of volume fraction, the data when considered along with extreme cases of volume fraction, i.e., 0.0 and 1.0 of

SiC was found to have a sigmoidal relationship with volume fraction which is shown in Figure 6.6 (b).

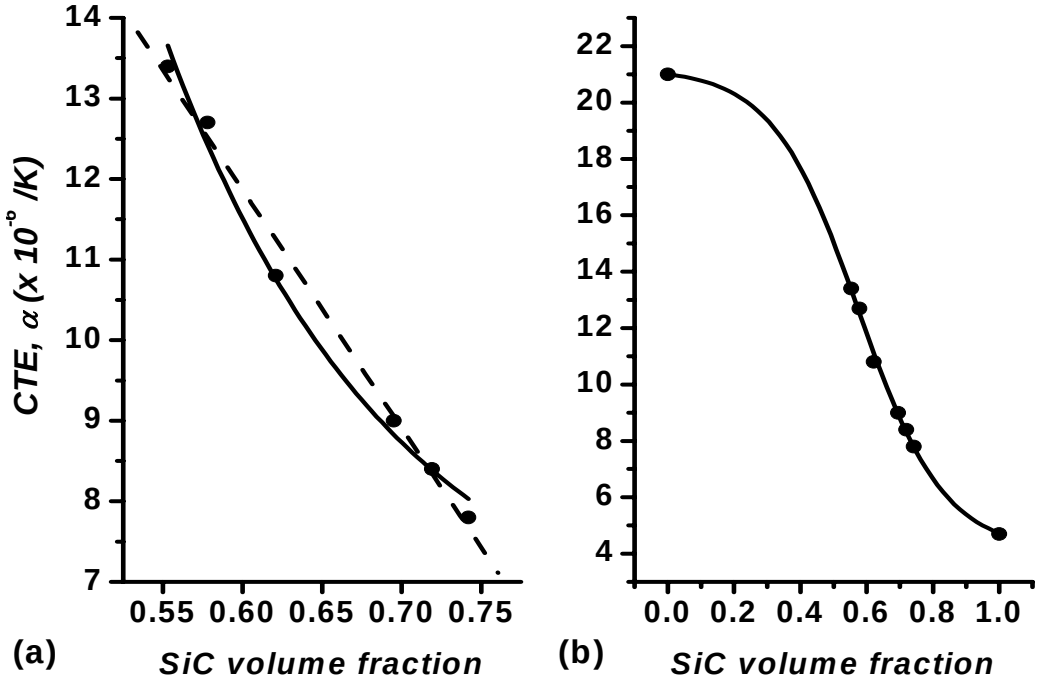

Figure 6.6 Variation of CTE with volume fraction of SiC in SiC_p/Al composites prepared by Arpon *et al*. [4] (a) Exponential decay and (b) Sigmoidal.

The Sigmoidal fit had a coefficient of square of regression, R^2: 0.999. Thus it is to be understood that the experimental data for the coefficient of thermal expansion of SiC_p/Al composites has a non linear dependence with volume fraction.

The experimental observations were further put to comparison with theoretical predictions available in the literature on composite materials. Several theoretical models are available for the prediction of effective properties of two phase composite material systems. As a rule of thumb the effective properties of an isotropic composite material could be deduced using a Rule-of-Mixtures (RoM). Prominent among the theoretical

models for variation of the coefficient of thermal expansion of a variety of two phase materials are those of P. S. Turner [5], E. H. Kerner [6] etc. and are listed in Table 6.3. Comparison of the present experimental results for the coefficient of thermal expansion of SiC_p/Al composites with various theoretical predictions is shown in Figure 6.7. From the figure it is obvious that the predictions of the theoretical models do not match with experimental results on the coefficient of thermal expansion of SiC_p/Al composites as a function of volume fraction of SiC.

Table 6.3 Model predictions for CTE of two phase materials

Model	Expression		Ref.
Mixture Rule	$\alpha_c = \alpha_m V_m + \alpha_d V_d$	(1)	-
Turner	$\alpha_c = \dfrac{\alpha_m V_m K_m + \alpha_d V_d K_d}{V_m K_m + V_d K_d}$	(2)	[5]
Kerner	$\alpha_c = \alpha_m V_m + \alpha_d V_d + \dfrac{(\alpha_d - \alpha_m)(K_d - K_m) V_m V_d}{V_m K_m + V_d K_d + 3K_m K_d / 4G_m}$	(3)	[6]
Thomas	$\alpha_c = \alpha_m^{Vm} * \alpha_d^{Vd}$	(4)	[7]
Schapery	$\alpha_c^{u} = \alpha_m V_m + \alpha_d V_d + \dfrac{4G_m (K_c - K_d)(\alpha_m - \alpha_d) V_d}{K_c (4G_m + 3K_d)}$ $\alpha_c^{l} = \alpha_m V_m + \alpha_d V_d + \dfrac{4G_d (K_c - K_m)(\alpha_d - \alpha_m) V_m}{K_c (4G_d + 3K_m)}$	(5)	[8]
Fahmy – Ragai	$\alpha_c = \alpha_m - \dfrac{3(\alpha_m - \alpha_d)(1 - \nu_m) V_d}{2(1 - 2\nu_d) V_m (E_m / E_d) + 2V_d (1 - 2\nu_m) + (1 + \nu_m)}$	(6)	[9]

Where, α refers to the Coefficient of Thermal Expansion, E refers to the Elastic Modulus, υ refers to Poisson's ratio and the subscripts c, m, d refer to the composite, matrix and dispersed phases respectively.

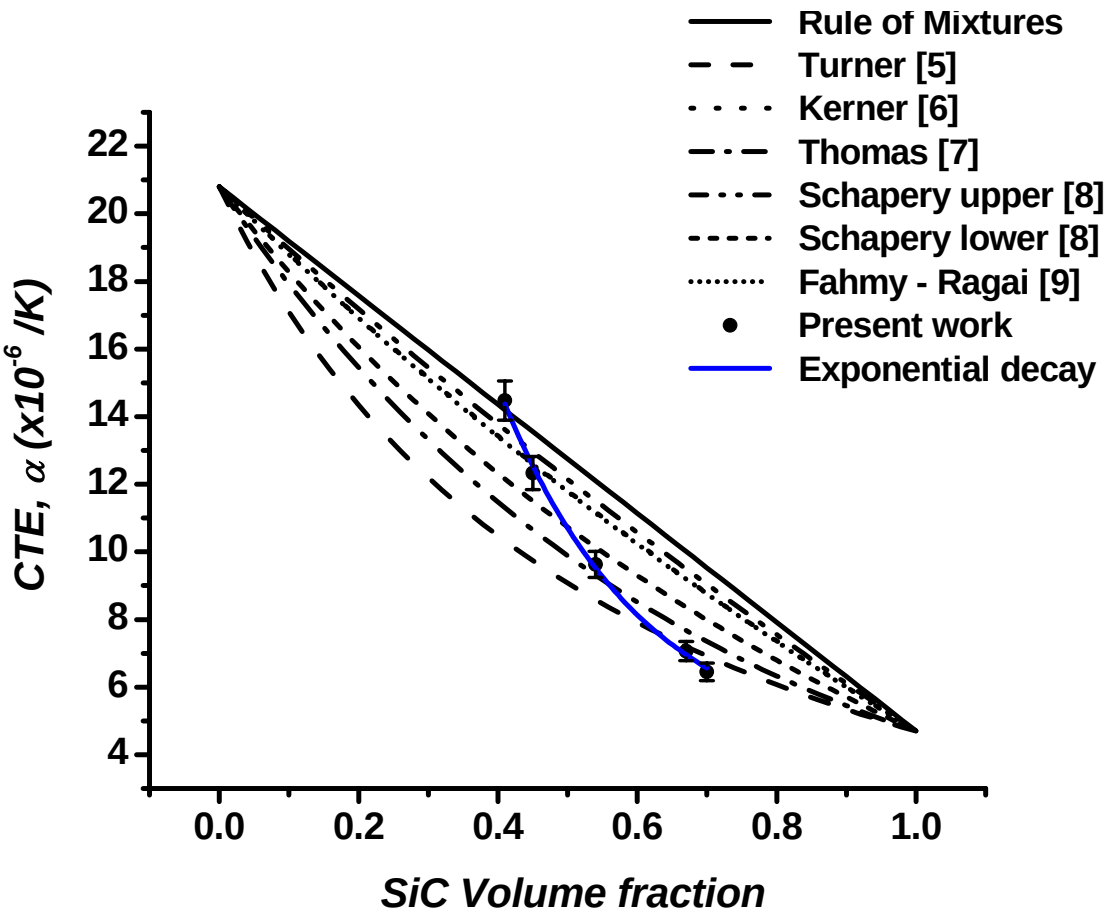

Figure 6.7 Comparison of the present experimental results with theoretical predictions.

The prediction by Rule-of-Mixtures served as an upper bound on the effective coefficient of thermal expansion of SiC_p/Al composites. It was observed that the behavior of the coefficient of thermal expansion with respect to volume fraction has a non-linear response. The observed lower values for the thermal expansion at each volume fraction were ascribed to the influence of huge mismatch in thermal expansion and elastic moduli of the individual phases, Al and SiC. It was postulated that due to these differences,

thermal mismatch stresses would develop at the interface and prevent the matrix phase near the interface from expanding in usual manner. Many theoretical models have considered the effect of matrix hardening as a result of thermal mismatch stresses and have proposed individual predictions that would enable determine the coefficient of thermal expansion. Results obtained by Arpon *et al*. have also been compared with theoretical predictions and the corresponding plot is shown in Figure 6.8.

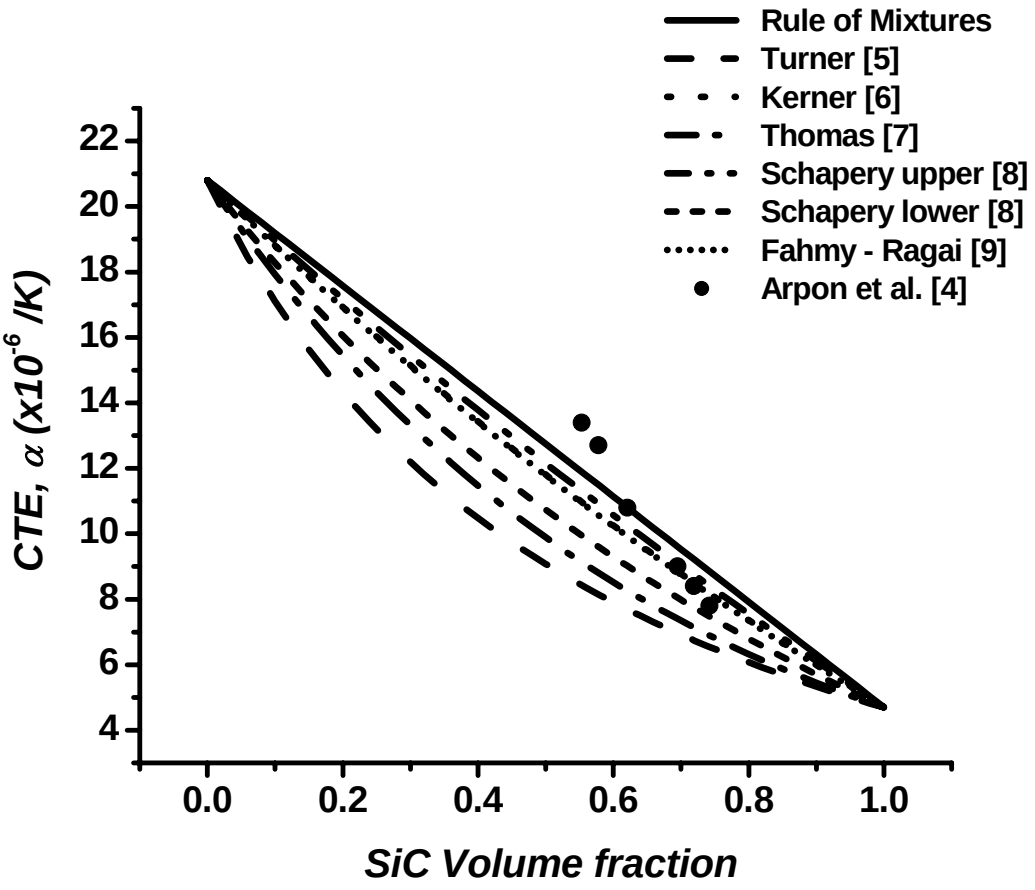

Figure 6.8 Comparison of experimental results of Arpon *et al*. and theoretical predictions.

From the above two comparative studies, it can be understood that the theoretical predictions are unable to predict the effective coefficient of thermal expansion for SiC_p/Al composites with high volume fractions of SiC. However, empirical fits for the

two sets of experimental results could be obtained that fall very much away from theoretical predictions for the effective coefficient of thermal expansion of SiC_p/Al composites. The disagreement between empirical fit and the theoretical predictions for the effective coefficient of thermal expansion can be seen in Figure 6.9.

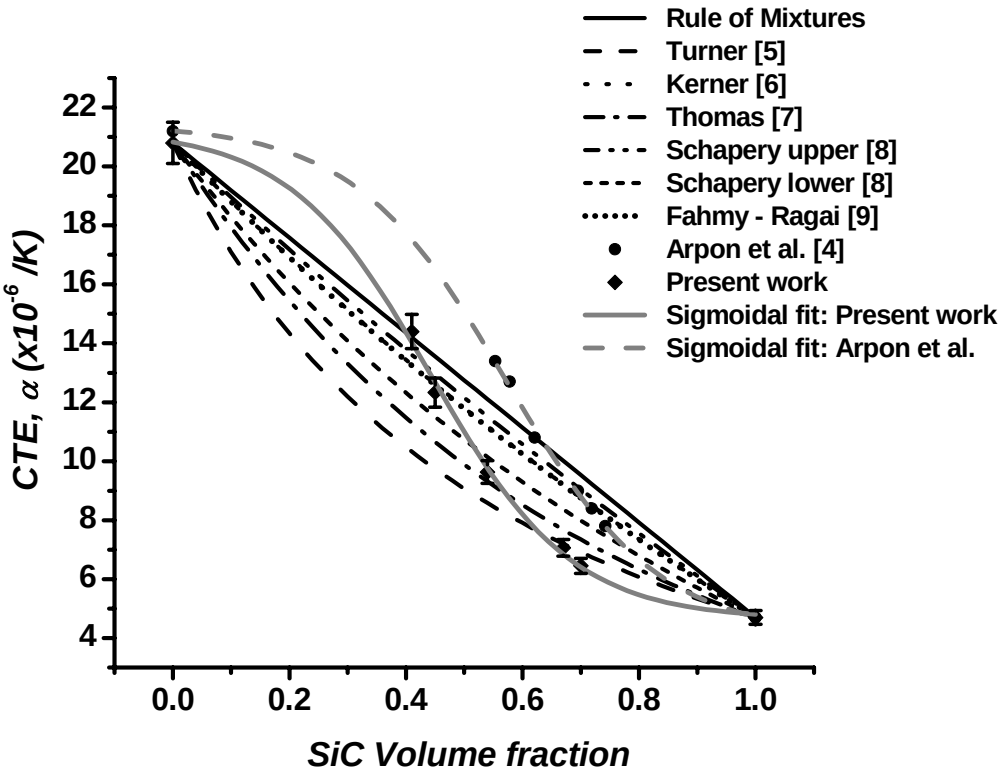

Figure 6.9 A comparison between Sigmoidal relationship and theoretical predictions

It can be observed from the Figure 6.9 that there is a good agreement between the experimental results from both the works with the sigmoidal relationship. At this stage it is worthy to note that the Rule-of-Mixtures (RoM) is an upper bound on the effective coefficient of thermal expansion for composite materials. In the present case, though the experimental results could not be predicted by the Rule-of-Mixtures yet the rule serves as an upper bound for composites with volume fraction ≥ 0.40 of SiC. Turner proposed an

expression for the effective coefficient of thermal expansion of a composite material, which is based on the relative compressibilities apart from individual coefficients of thermal expansion and their proportions [5]. The model assumes that each phase of the composite is constrained to change dimensions with temperature at the same rate as the aggregate and that shear deformation is negligible. The resultant expression governing the effective coefficient of thermal expansion is shown in Table 6.3. A good agreement between experimental values and prediction for lead – antimony and beryllium – aluminum mixtures was projected by Turner. However, large deviations were observed from Turner's prediction with experimental values of Lemieux *et al*. [10] and the present work in respect of SiC_p/Al metal matrix composites. The major reason for this deviation is supposed to be that the model assumes that shear deformation along the interface is negligible. In the present case, the two phases not only differ largely in coefficient of thermal expansion and elastic modulus but also shear modulus. This certainly invokes the necessity to consider the role of shear stresses in modulating the effective coefficient of thermal expansion of a two phase material that is intimately bonded at the interface.

Theoretical prediction of Kerner is shown in Figure 6.9. Kerner's model is based on the averaging procedure due to Bruggemann where it is assumed that the reinforcement is spherical and surrounded by a uniform layer of matrix [6]. The effective coefficient of thermal expansion of composite material is projected to be identical to a volume element that is comprised of a spherical reinforcement particle surrounded by a shell of matrix material, bearing respective volume fractions. It is stated that in such a suspended-grain composite, a small temperature change would change the state of stress in the composite. The net dilatation was calculated from knowledge of effects of uniform

hydrostatic compression and uniform tension. From the figure it can be observed that Kerner's prediction is more realistic as compared to prediction made by Turner in respect of coefficient of thermal expansion of SiC_p/Al composites from the present work. However, there is a marked deviation between Kerner's prediction and the experimental results obtained from the present work. A similar observation was made by Lemieux *et al*. in the case of SiC_p/Al composites prepared by gas pressure infiltration for SiC volume fractions between 0.10 and 0.40 of SiC. Similar is the observation with predictions of Thomas [7] which is somewhat closer to that of Turner. Schapery's bounds based on extremum principles of thermo-elasticity for the prediction of effective coefficient of thermal expansion were found to be of promise, but limited to a certain volume fraction of ~ 0.55 in the case of SiC_p/Al composites evaluated in the present work [8].

Predictions of effective coefficient of thermal expansion by Fahmy and Ragai are based on the assumption that the entire volume of the composite is an assemblage of composite spheres of various sizes filling up all space. Furthermore, it is assumed that the thermal mismatch stress falls off rapidly with distance from the interface. The resulting expression for the coefficient of thermal expansion is shown in Table 6.3. This prediction records significant deviations from the experimental results of the present work. It was projected to have a good agreement with experimental values for Al-Si system associated with investigations limited to volume fraction of 0.40. The prediction of Fahmy and Ragai fall entirely in line with that of Kerner as can be seen from the figure. This could be because of the fact that the basic construction of the composite and to some extent assumptions involved in the construction of the two models is similar.

However, an empirical relationship could be established between effective coefficient of thermal expansion and volume fraction of the dispersed phase. It is observed that the sigmoidal fit has a coefficient of square of regression that is near to 1; Present work: 0.998 and Arpon *et al.* [4]: 0.999. At the same time it is to be noted that the sigmoidal relation is an over estimate when compared with the Rule-of-Mixtures, at volume fraction ≤ 0.40 of SiC. This fact invokes the necessity to investigate further, the validity of the present sigmoidal relationship over the entire range of volume fraction of the reinforcement.

In order to accomplish this, experimental observations on the coefficient of thermal expansion of SiC_p/Al composites from various works have been considered [11]. The data is collected from sources which might have generated SiC_p / Al composites as a piecemeal for a variety of applications. As a result, these composites would have differences such as composition of the matrix, SiC particle size, its distribution, primary processing methods, secondary processing methods, determination of volume fraction, the test conditions for evaluation of co-efficient of thermal expansion and other physical properties. Due to which, only a part of the spectrum has been investigated by each of the groups working on SiC_p/Al composites: processing, characterization and development. Nevertheless, the data available so far can be a guideline towards understanding the behavior of coefficient of thermal expansion, which might undergo subsequent refinements depending on the availability of more systematic data. A plot of coefficient of thermal expansion as a function of volume fraction is shown in Figure 6.10.

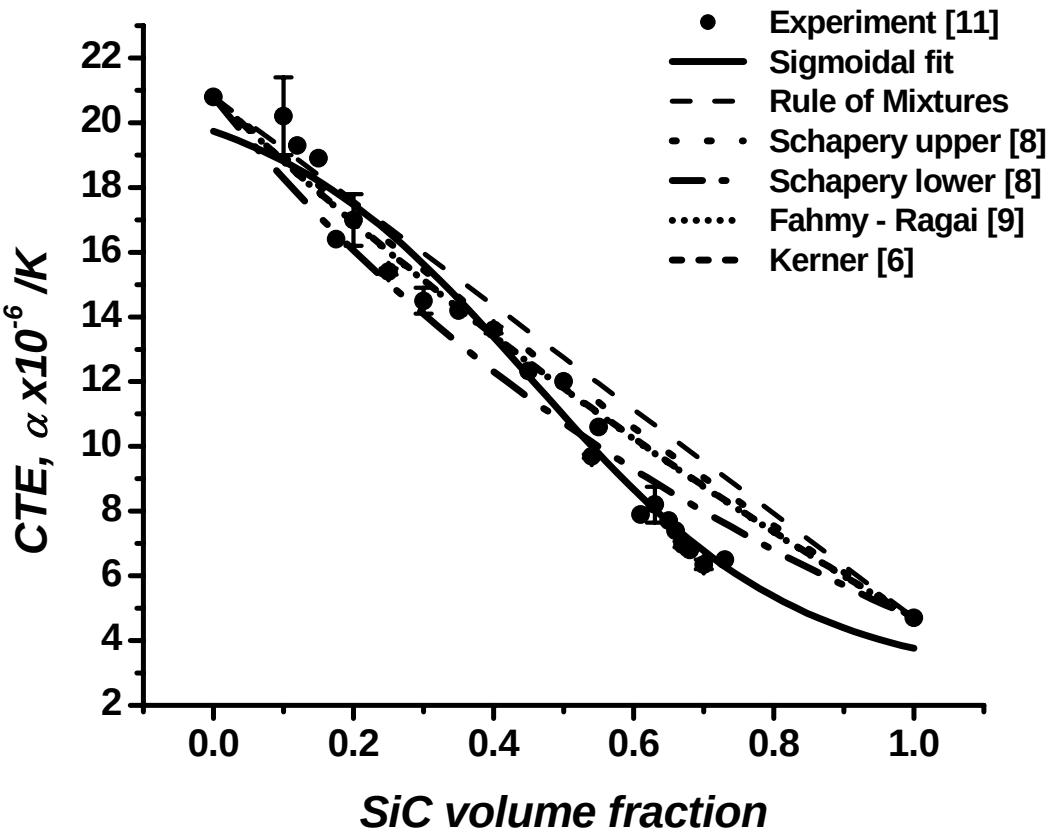

Figure 6.10 Experimental CTE data for various concentrations of SiC

From Figure 6.10, it can be observed that for SiC volume fractions up to ~0.55, there is a good agreement between experimental data from various works and earlier theoretical predictions for the effective coefficient of thermal expansion. The data agrees well with the predictions of Schapery (upper) [8], Fahmy-Ragai [9] and Kerner [6] up to a volume fraction of 0.55 of SiC. However, there is considerable amount of disagreement for composites with volume fraction beyond ~0.55 of SiC. From this point onwards, the coefficient of thermal expansion has a non linear decrease with volume fraction. A sigmoidal relationship between co-efficient of thermal expansion of SiC_p/Al composites and SiC volume fraction is shown in Figure 6.10. The reason for the drastic change in the behavior of the coefficient of thermal expansion beyond a certain volume fraction could

be any or all of the following: decrease in inter-particle spacing with volume fraction, number of particles that get interconnected by trapping Al in the interstitial sites and increasing ratio of reinforcement surface area to matrix volume [4]. Any or all of these factors could have affected the effective coefficient of thermal expansion of SiC_p/Al composites at high volume fractions.

However, a relatively simpler means for the estimation of effective coefficient of thermal expansion of SiC_p/Al metal matrix composites over the entire range of volume fraction is by the sigmoidal relationship shown in Figure 6.10. This empirical relationship clearly reflects a transition in the behavior of thermal expansion of SiC_p/Al composites from a semi-linear to non-linear with volume fraction of SiC. A transition is observed at a volume fraction ~0.55 of SiC, which is indicative of either a decrease in inter-particle spacing with volume fraction or number of particles that get interconnected or increasing ratio of reinforcement surface area-matrix volume (S_r/V_m) or all. Similar behaviors have been observed in the case of effective thermal conductivity of MgO – $MgSiO_4$ composites [12] and the relative dielectric constant of $BaTiO_3$ – BT gel composite thick films [13].

c) Dynamic Elastic Modulus

Velocity of sound was measured by ultrasonic pulse-echo technique in longitudinal and shear modes of vibration. Results of ultrasonic velocity measurements on SiC_p/Al metal matrix composites of different volume fraction are given in Table 6.4. An accuracy of ±0.3 ns in the time of flight measurements has limited the uncertainty in the measurement of longitudinal and shear wave velocities to 0.04 %.

Table 6.4 Ultrasonic wave velocities in SiC_p/Al metal matrix composites

Sl. No.	Volume fraction	Density, d (g/cc)	Longitudinal velocity, V_L (m/s)	Shear velocity, V_S(m/s)
1.	0.41	2.86	7570	4430
2.	0.45	2.88	8172	4748
3.	0.54	2.94	8560	5036
4.	0.67	3.01	8936	5262
5.	0.70	3.02	9285	5490

A plot of variation of longitudinal and shear wave velocity in SiC_p/Al composites as a function of volume fraction of SiC is shown in Figure 6.11.

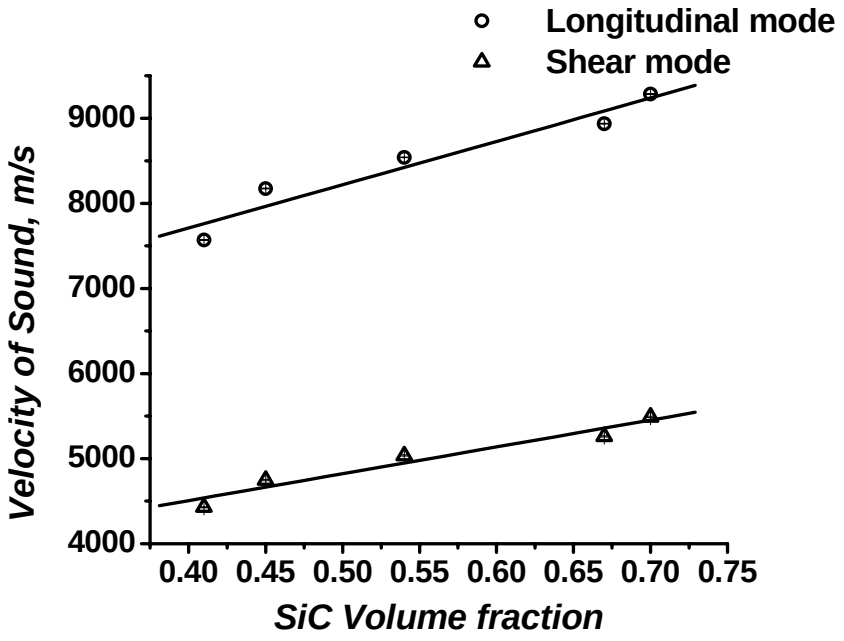

Figure 6.11 Sound velocities in SiC_p/Al MMCs as a function of volume fraction of SiC

From the figure, it can be seen that the velocity of the longitudinal sound wave increases with increase in volume fraction of silicon carbide, the reinforcing phase. The variation in shear wave velocity of SiC_p/Al metal matrix composites was found to be similar to that of longitudinal velocity in the volume fraction range of 0.41 to 0.70. Ultrasonic velocity measurements were also performed on remaining portions of the matrix material. An aluminum alloy containing Mg was used for infiltration experiments as discussed earlier and there was substantial loss of Mg during the process. Hence the matrix in the composite is better represented by the residual alloy than the starting matrix metal for the residual alloy has undergone metallurgical processes similar to the matrix material. Specimens from excess metal were machined to dimensions of 25 mm x 25 mm x 5 mm for ultrasonic velocity measurements in both modes of vibration. Ultrasonic velocity measurements were performed and the results are shown in Table 6.5, along with data for SiC taken from Munro [14].

Table 6.5 Ultrasonic properties of the residual matrix metal and sintered α-SiC

Sl. No.	Volume fraction	Density, *d* (g/cc)	Longitudinal velocity, V_L (m/s)	Shear velocity, V_S (m/s)
1.	0.00	2.61*	6643*	3326*
2.	1.00	3.19*	11820[@]	7520[@]

* Present work; [@] [14]

Figure 6.12 shows the variations in the velocity of sound in two modes of vibration i.e., longitudinal and shear wave modes, while considering extremes of volume fraction of SiC i.e., 0.0 and 1.0. The dotted lines in the figure show the expected sound wave

velocities for the composite at different volume fractions as per rule of mixtures. The deviation of the measured velocities from those expected according to rule of mixtures can be noticed for both longitudinal and shear velocities.

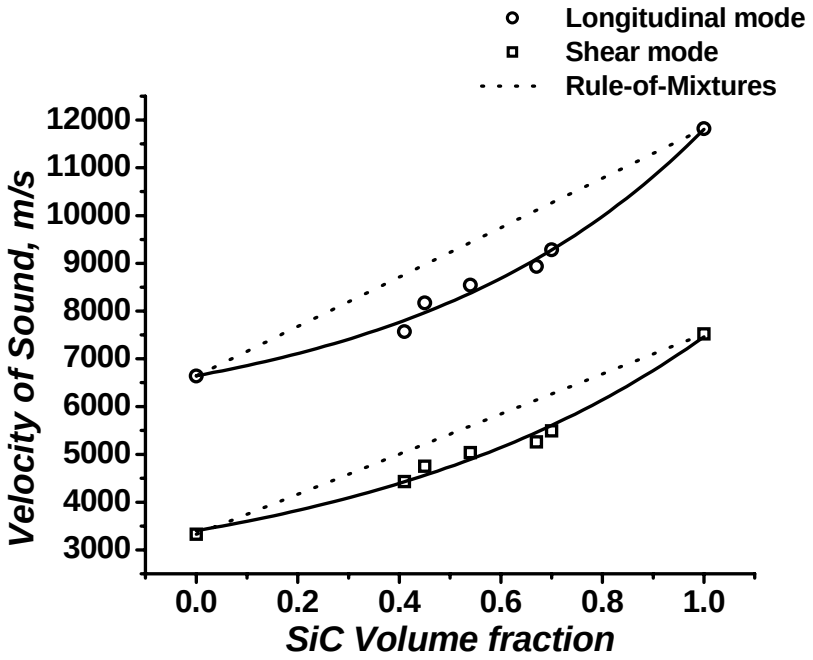

Figure 6.12 Velocity of sound in SiC_p/Al composites as a function of volume fraction of SiC along with extremes of volume fraction: 0.0 and 1.0 of SiC

Composite materials with fibers and whiskers as reinforcing materials project reasonable amount of anisotropy due to the pre-existing shape anisotropy in fibers and whiskers. However, a composite material with particulate reinforcement would not pose such anisotropy due to the shape of the reinforcement. Moreover, the method of fabrication of composite material would also introduce anisotropy in the composite. In the present case, composite materials were prepared using pressureless infiltration where the reinforcing material was stationary during the process of fabrication. As a result, anisotropy caused by the processing methodologies is excluded. Homogenous

distribution of SiC particulates can be observed from microstructures of SiC_p/Al composites with different volume fractions of SiC, shown in Figure 5.5. Isotropic nature of the composite materials was also confirmed from the fact that there were no substantial changes in the velocity upon rotating the shear probe. This reduces the number of elastic constants required for the description of a material. Ultrasonic velocities obtained as above were used to calculate the Poisson's ratio according to the relation.

$$\nu = \left[1 - 2(V_S/V_L)^2\right] / \left[2 - 2(V_S/V_L)^2\right] \qquad (6.7)$$

Poisson's ratio obtained in this manner was subsequently used for the determination of Young's (E), Shear (G) and Bulk (K) moduli of composites for all volume fractions using the formulae given below.

$$E = \rho V_L^2 \left[\frac{(1+\nu)(1-2\nu)}{(1-\nu)}\right] \qquad (6.8)$$

$$G = \rho V_S^2 \qquad (6.9)$$

$$K = \frac{E}{3(1-2\nu)} \qquad (6.10)$$

Where V_L – velocity of sound in longitudinal mode, V_S – velocity of sound in shear mode, ν - Poisson's ratio, E – Young's Modulus, G – Shear modulus and K – Bulk Modulus. The results are shown in Table 6.6 below. The uncertainty in the evaluation of elastic, shear and bulk moduli was found to be 2.00%, 0.12% and 2.02% respectively.

Table 6.6 Elastic moduli calculated from ultrasonic velocities.

Sl. No	Volume fraction	Poisson's Ratio, υ	Young's Modulus, E (GPa)	Shear Modulus, G (GPa)	Bulk Modulus, K (GPa)
1.	0.41	0.239	138.9	56.0	88.7
2.	0.45	0.245	161.4	64.8	105.5
3.	0.54	0.235	183.9	74.4	115.8
4.	0.67	0.234	205.5	83.2	128.7
5.	0.70	0.231	224.6	91.2	139.1

The variations in the moduli of SiC_p/Al metal matrix composites were then analyzed as a function of volume fraction of SiC. The observations are depicted in Figure 6.13 for Young's, Shear and Bulk moduli. It can be observed from the figure that these moduli increase with an increase in the volume fraction of silicon carbide in aluminum alloy matrix composites. The variation in the moduli is linear with volume fraction of SiC in the range: 0.41 to 0.70, studied in the present work. The experimental data for elastic moduli were plotted as a function of volume fraction including the extreme cases i.e. $\boldsymbol{V_f}$**:** 0.0 to 1.0. The data corresponding to individual phases is given in Table 6.7.

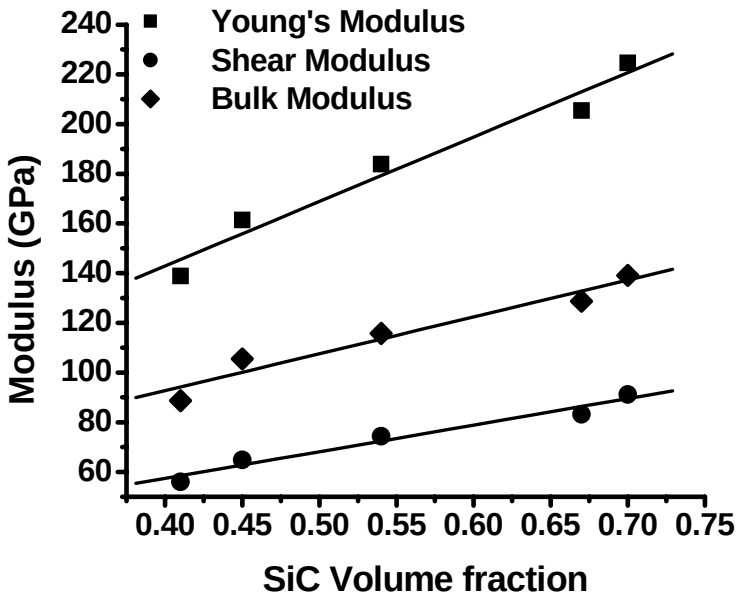

Figure 6.13 Variation of elastic properties of SiC_p/Al metal matrix composites as a function of volume fraction of SiC

Table 6.7 Calculated elastic properties of the residual Al and α-SiC

Sl. No	Volume fraction	Poisson's Ratio, υ	Young's Modulus, E (GPa)	Shear Modulus, G (GPa)	Bulk Modulus, K (GPa)
1.	0.00	0.333	76.8	28.8	76.6
2.	1.00	0.16	419.4	180.8	205.6

The variations in elastic moduli as a function of volume fraction were observed to be non-linear as shown in Figure 6.14. The experimental data for Young's modulus, accompanied by theoretical predictions from earlier works in this direction are shown in Figure 6.15. From the graph, it is clear that the experimental data could not be predicted by the basic models i.e., Parallel model and Series model. A schematic representation of the unit cells involved in the construction of composite microstructure is shown in Figure

6.16. The loading direction is parallel to the interface in the case of parallel model and normal to the interface in the case of series model. The effective Young's modulus is obtained from the parallel model by averaging stresses in the individual phases [15]. In the case of series model, the Young's modulus *E* is obtained by averaging the strains in the individual phases [16]. However, these models continue to serve as the lower and upper bounds, respectively for the elastic modulus of an isotropic and homogenous composite material. The expressions corresponding to these models are given below.

$$E_{c,parallel} = E_m V_m + E_d V_d \quad \text{(Upper bound)} \qquad (6.11)$$

$$\frac{1}{E_{c,series}} = \frac{V_m}{E_m} + \frac{V_d}{E_d} \quad \text{(Lower bound)} \qquad (6.12)$$

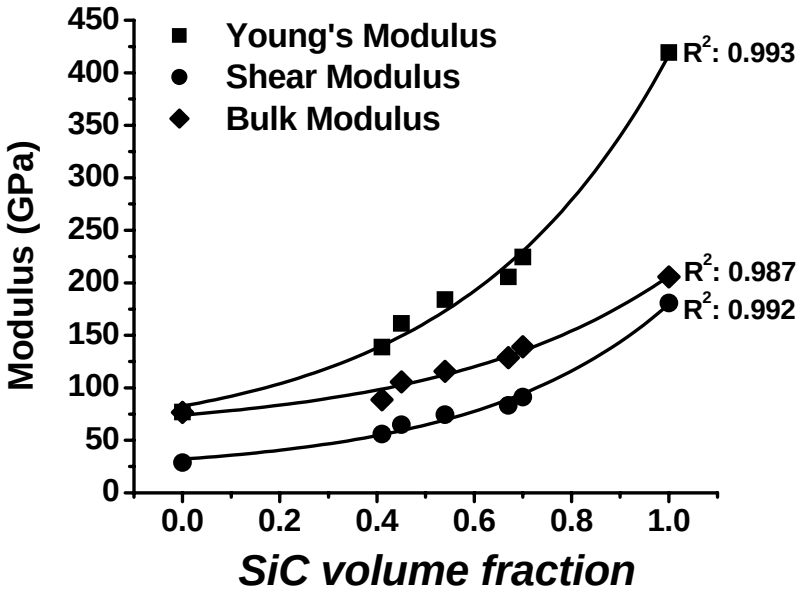

Figure 6.14 Variation of Young's, Shear and Bulk moduli as a function of volume fraction of SiC_p in composites of Al alloy matrix

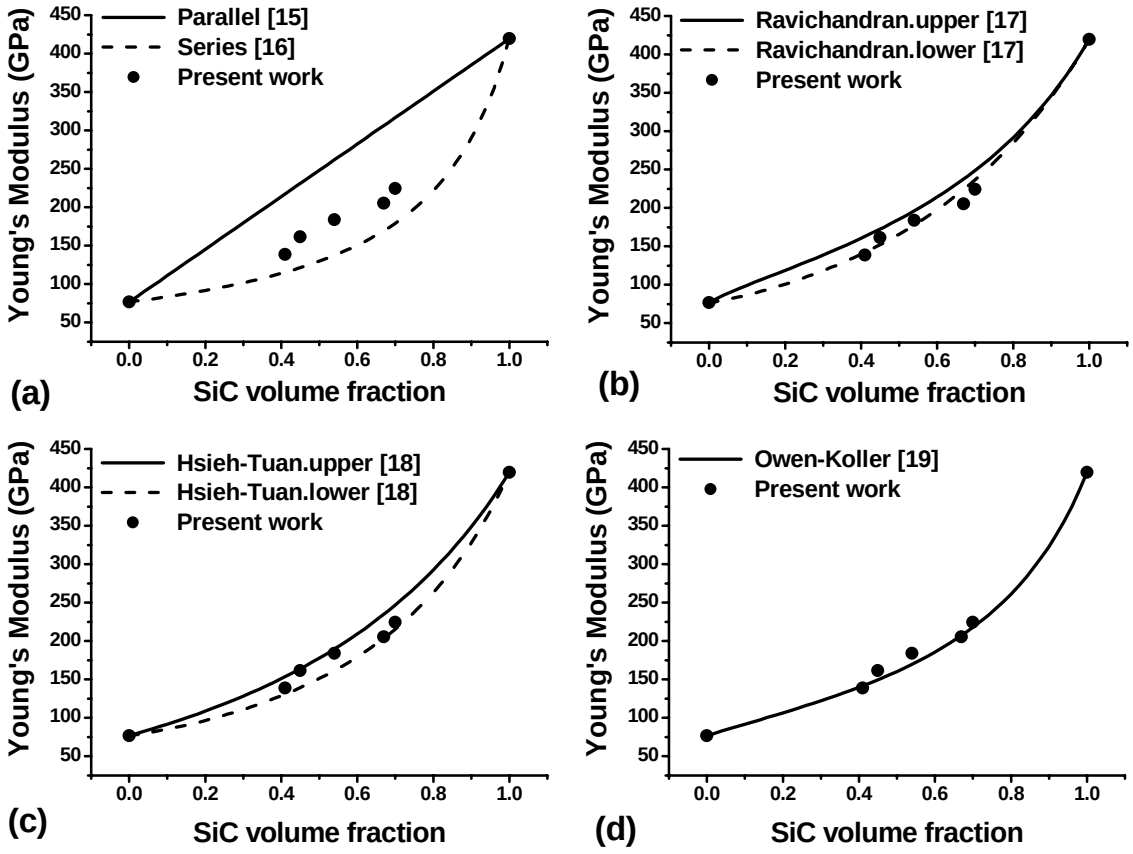

Figure 6.15 Comparison of experimental data with theoretical predictions for elastic moduli of two phase systems

The expressions 6.11 and 6.12 give the upper and lower bounds on effective elastic modulus of a two-phase composite and the curves pertaining to these relations are also shown in Figure 6.15(a). Later, models that are based on combinations of series and parallel configurations of a two phase composite system have been developed to estimate the bounds on effective elastic modulus. Effective elastic modulus was found to be a function of elastic modulus of matrix - E_m, elastic modulus of dispersed phase – E_d, Volume fraction of matrix – V_m, Volume fraction of dispersed phase – V_d, Poisson's ratio of matrix – ν_m and Poisson's ratio of dispersed phase – ν_d.

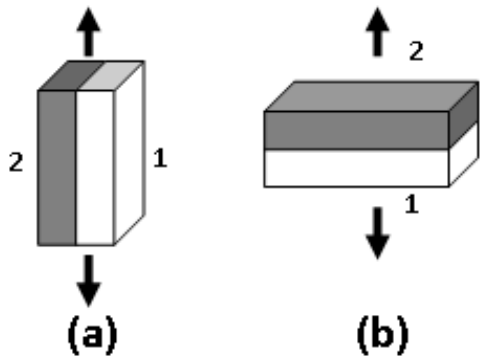

Figure 6.16 A schematic of composite unit cell loaded in (a) parallel and (b) series

The data was further compared with the predictions of Ravichandran [17] and Hsieh-Tuan [18]. In these models, it is assumed that a composite is a two-phase material with a periodic arrangement of inclusions of the second phase distributed in a continuous matrix. The unit cell of the periodic arrangement is further divided into parallel and series elements. These parallel and series elements are built up in two ways: (i) series – parallel combination and (ii) parallel – series combination. These schemes of building a unit cell out of series and parallel combinations as discussed above give lower and upper bounds respectively. However, there is a small difference in the shape of the inclusion in the unit cells of the two models. A pictorial representation of composite's idealized microstructure and the corresponding schemes of building the same out of the composite unit cells based on Ravichandran's model are shown in Figure 6.17 and 6.18 respectively [17]. Figure 6.19 and Figure 6.20 represent the scheme adopted by Hsieh-Tuan [18]. The inclusion is a cube in the case of Ravichandran's model and is a parallelepiped in the case of Hsieh-Tuan's model.

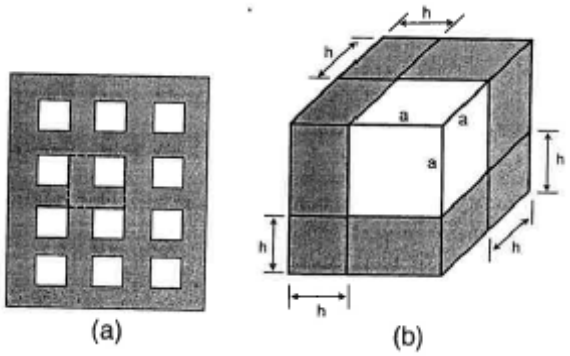

Figure 6.17 Schematic of (a) idealized microstructure and (b) unit cell of a composite, based on Ravichandran's model [17]

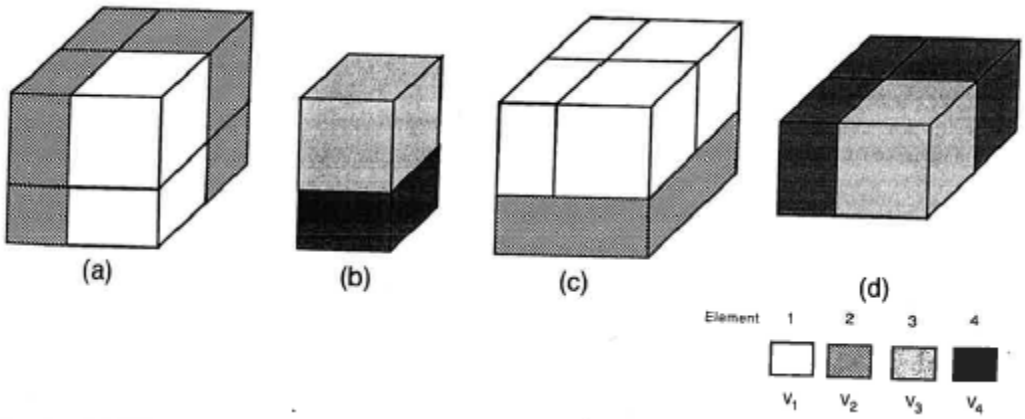

Figure 6.18 Schematics of divisions of the unit cell into several elements and the respective volume fractions: (a) and (b), Scheme – I; (c) and (d), Scheme – II, based on Ravichandran's model [17]

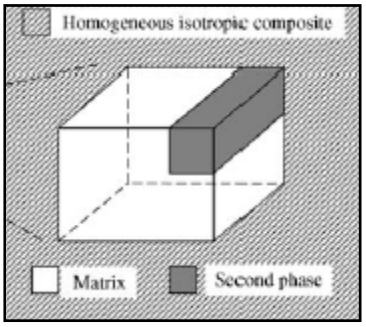

Figure 6.19 Schematic of unit cell of a composite, based on Hsieh-Tuan's model [18]

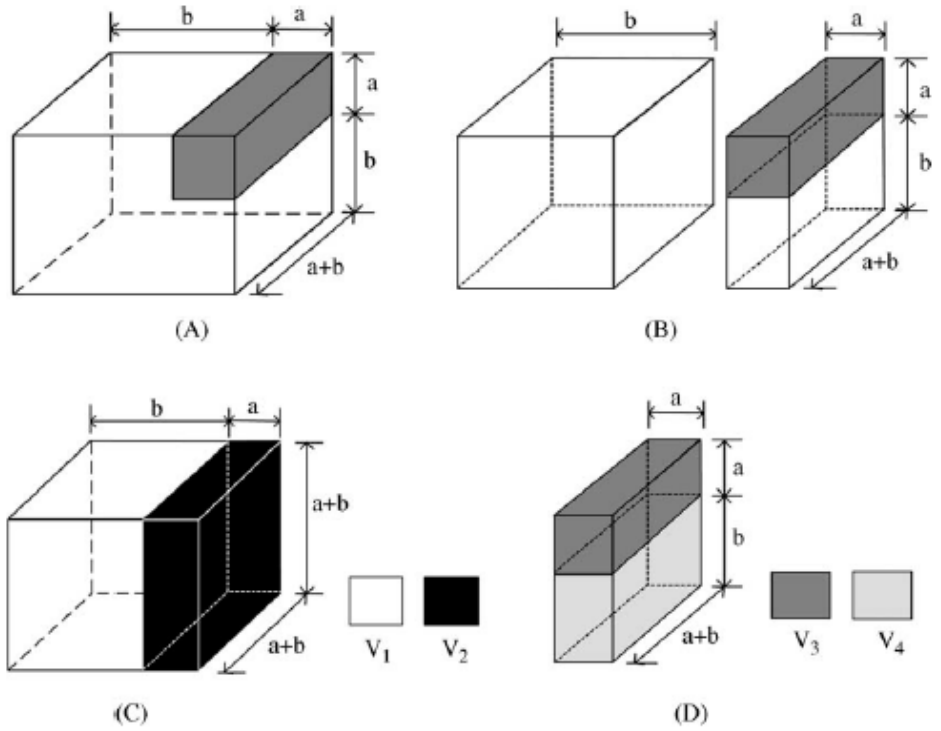

Figure 6.20 (A) Dimensions of one unit cell and (B-D) the subunits, based on Hsieh-Tuan's model [18]

Experimental results for composite materials namely WC-Co, Epoxy-Silica, Al-SiC, Polymer-Glass, Glass-W and Glass-Alumina were compared with the predictions of Ravichandran [17]. A marked deviation of the theoretical predictions from the experimental results at higher volume fractions of SiC can be observed [18]. The predictions of Hsieh-Tuan were also compared with the experimental results for different composite systems, namely Cu-Diamond, Al-SiC, WC-Co and Epoxy-Glass fiber. The bounds predicted by Hsieh-Tuan were found to confine the experimental results to a better degree than those predicted by Ravichandran.

In the present work, experimental results for effective elastic modulus of SiC_p/Al composites are compared with the theoretical predictions. Figure 6.15(b) shows a

comparison of the experimental data with the prediction of Ravichandran. It is observed that at higher volume fractions, the experimental data falls away from the predictions of bounds on effective elastic modulus. An observation similar to this is presented in a comparative study of variation effective elastic modulus of SiC_p/Al composites with volume fraction of SiC [18]. The lower (E_c^l) and upper (E_c^u) bounds for effective elastic modulus of a two phase composite material, predicted by Ravichandran are given below.

$$E_c^{\,l} = \frac{\left(cE_dE_m + E_m^{\,2}\right)(1+c)^2 - E_m^{\,2} + E_dE_m}{\left(cE_d + E_m\right)(1+c)^2} \tag{6.13}$$

$$E_c^{\,u} = \frac{\left[E_dE_m + E_m^{\,2}(1+c)^2 - E_m^{\,2}\right](1+c)}{\left(E_d - E_m\right)c + E_m(1+c)^3}, \tag{6.14}$$

$$\text{Where } c = \left(\frac{1}{V_d}\right)^{1/3} - 1 \tag{6.15}$$

Comparison of present experimental data with the predictions of Hsieh – Tuan bounds on the effective elastic modulus is shown in Figure 6.15(c). From the figure, it is observed that the present experimental data falls well within the bounds throughout the entire range of volume fraction. In the present case also, it is observed that the experimental data for effective elastic modulus of SiC_p/Al composites shows marginal deviations from the prediction of Ravichandran and a rather good agreement with those of Hsieh-Tuan. Hsieh and Tuan deduced bounds for effective elastic modulus of two phase composite material and are given below.

$$E_c^{\,l} = \frac{\left(1 + c + c^2\right)E_mE_d + cE_m^{\,2}}{(1+c)\left(cE_d + E_m\right)} \tag{6.16}$$

$$E_c{}^u = \frac{\left[\left(1+c+c^2\right)E_d E_m + cE_m{}^2\right]\left[(1-\nu_m)E_d + c(1-\nu_d)E_m\right] - 2c^2 E_m\left(\nu_m E_d - \nu_d E_m\right)^2}{(1+c)\left\{(cE_d + E_m)\left[(1-\nu_m)E_d + c(1-\nu_d)E_m\right] - 2c\left(\nu_m E_d - \nu_d E_m\right)^2\right\}} \tag{6.17}$$

$$\text{Where } c = \left(\frac{1}{V_d}\right)^{1/2} - 1 \tag{6.18}$$

The experimental data was further compared with the theoretical prediction of Owen and Koller for the Young's modulus of a two component isotropic composite, which takes into account the three dimensional nature of stress and strain coupling in the material [19].

$$\frac{1}{E_c} = \frac{V_m}{E_m} + \frac{V_d}{E_d} - \frac{2\left(\frac{\nu_m}{E_m} - \frac{\nu_d}{E_d}\right)^2}{\frac{1-\nu_m}{V_m E_m} + \frac{1-\nu_d}{V_d E_d}} \tag{6.19}$$

The above expression for effective elastic modulus of a two component isotropic composite is based on the assumption that the average normal stresses σ_i and strains ε_i (i = 1, 2, 3) for each phase obey the generalized Hooke's law. The model considers a constant uniaxial stress applied on the composite, series model. The result of this uniaxial stress is considered not only in the longitudinal direction but also the transverse constraints on the components due to Poisson contraction, thereby taking into account the three dimensional nature of stress and strain coupling in the material. Under the conditions of equivalent longitudinal stress and transverse strain in both matrix and reinforcement, the expression evolved for the effective Young's modulus was found to fall in between those predicted by the series and parallel models. The theoretical predictions of Owen-Koller were compared with the experimental results for different

composite systems like Epoxy-Silica, Starch-Poly 3 Hydroxy Butyrate and starch-Poly 3 Hydroxy Butyrate/3 Hydroxy Valerate. The experimental results for elastic modulus of Epoxy-Silica system was found to be in good agreement with the predictions of Owen-Koller. The agreement was extended to other systems of composites as well. However, the investigations on elastic modulus were limited to a volume fraction of 0.50 in the case of Epoxy-Silica system and 0.15 in the case of other systems. The experimental data for Al-SiC system investigated in the present work matches well with the predictions of Owen – Koller as shown in Figure 6.15(d). Non destructive ultrasonic testing of SiC_p/Al metal matrix composites with high volume fractions has been demonstrated for the first time in literature. The experimental results obtained were found to agree with theoretical predictions of Owen-Koller [19].

A simpler approach to fit the experimental data without considering the shape of the reinforcement or the degree of connectivity of the two phases or any other feature of the system would be to find a mathematical expression to fit the results. The trend in the experimental data points suggests exponential function dependence as given below.

$$y = y_o + A_1 \exp(x/t_1) \tag{6.20}$$

Where A_1, y_o and t_1 are the variables associated with the shape of the curve. Exponential fit of the experimental data for Young's, Shear and Bulk moduli are shown in Figure 6.14 and are given by the following expressions.

$$E_c = 49.08 + 34.22 * \exp(V_f / 0.4253) \tag{6.21}$$

Where E_c is the effective young's modulus and V_f is the volume fraction of the reinforcement ranging from 0.0 to 1.0. The experimental data was found to fit to the exponential curve with a square of regression coefficient of 0.993 and is shown in Figure 6.21 along with the predictions of Owen-Koller [19].

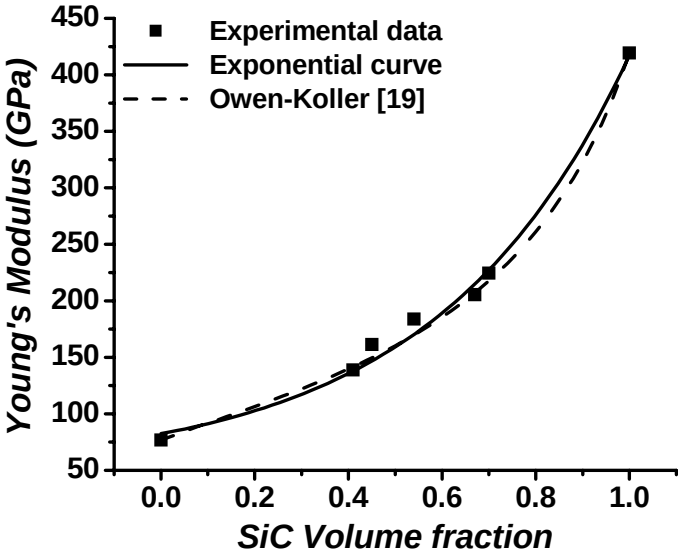

Figure 6.21 A comparison of exponential growth fit of the experimental data with the predictions of Owen-Koller model

This expression can thus serve to estimate the effective moduli of SiC_p/Al metal matrix composites at different volume fraction of silicon carbide so that the composite material can be tailored to possess desired modulus of elasticity.

d) Electrical Resistivity

The two phase composite materials of the SiC_p/Al system were evaluated for effective electrical resistivity. The results of four-probe electrical resistivity measurements on the composites are shown in Figure 6.22. The results include measurements on residual matrix metal which is a close representative of the matrix

within the composite material and resistivity data for sintered α-SiC. The uncertainty in the measurement of electrical resistivity was found to be 4.0%.

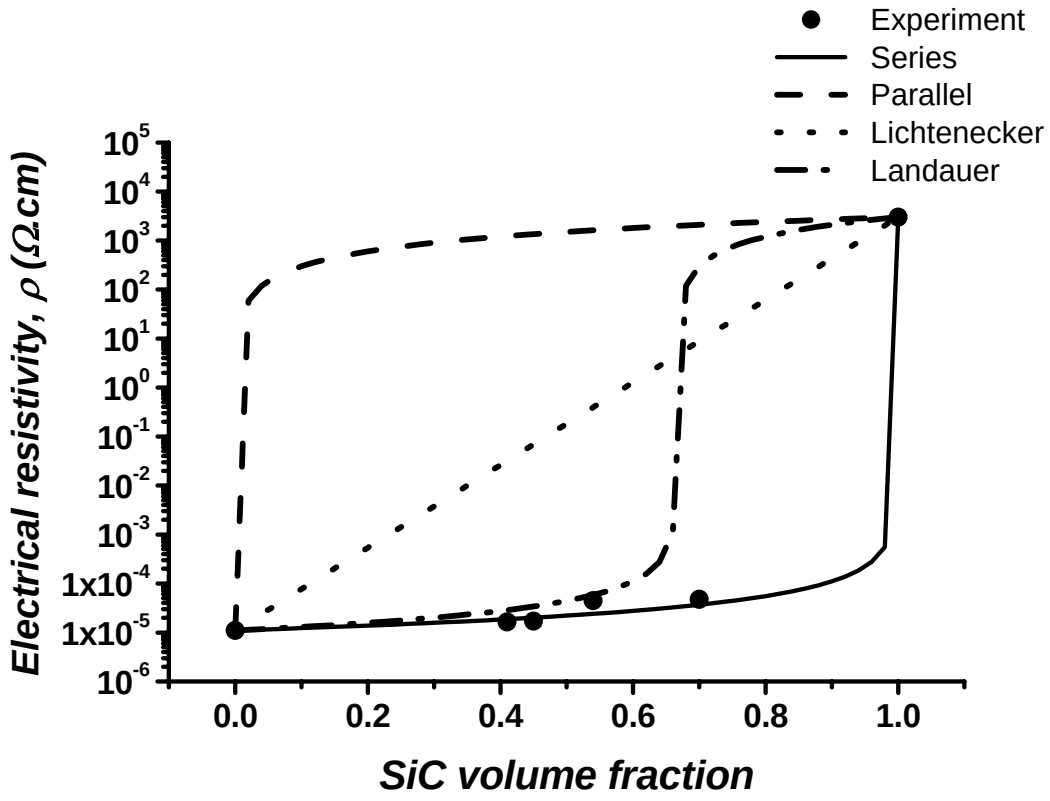

Figure 6.22 Electrical resistivity of SiC_p/Al composites: A comparison

The figure shows comparison of experimental results with other models such as Parallel [15], Series [16], Lichtenecker [20] and Landauer [21]. The effective electrical resistivity of two phase composite system according to the Parallel model is given by the following relation.

$$\rho_c = \rho_m V_m + \rho_d V_d \tag{6.22}$$

This would be the case where materials were arranged in alternate layers, perpendicular to the direction of electric filed. In such circumstances the current flowing

through the material cannot avoid regions of high resistance, which would be possible if the two phases were mixed at random. Thus, the parallel model prediction can serve as an upper bound in the determination of effective electrical conductivity of SiC_p/Al composites. The parallel model is not relevant in the case of effective electrical resistivity of a two phase composite system such as SiC_p/Al.

A better estimation of the effective electrical resistivity of a two phase composite system like SiC_p/Al can be obtained from Landauers's prediction.

$$\frac{1}{\rho_c} = \sigma_c = \frac{1}{4}\left\{(3V_d - 1)\sigma_d + (3V_m - 1)\sigma_m + \left[((3V_d - 1)\sigma_d + (3V_m - 1)\sigma_m)^2 + 8\sigma_m\sigma_d\right]^{\frac{1}{2}}\right\} \quad (6.23)$$

As seen from the figure, Landauer prediction yields a percolation point at a volume fraction that is closer to that observed from experimental results. Landauer projected a good agreement of the prediction with experimental results on effective electrical resistivity of some binary metallic mixture like Bi – Sn, Cd – Pb, Cu – Fe and Pb – Sb [21]. Landauer considered experimental results of Matthiessen for Bi – Sn, Cd – Pb and Pb – Sb metallic mixtures, where the ratio between the resistivities is 9.7, 0.3 and 0.5 respectively. Similar is the observation with other systems considered by Landauer. In the present case of SiC_p/Al composites, the ratio of resistivities between the matrix phase and the inclusion phase is 3.7×10^{-9}, indicating the huge difference in resistivities. This difference could play a major role in the behavior of effective electrical resistivity of two phase materials. It can be observed from the figure that the experimental results of effective electrical resistivity of SiC_p/Al composites is unaltered even up to volume fraction of 0.70 of SiC as evaluated in the present work.

Lichtenecker's model that is based on the crude assumption that the effective physical property of a two phase composite is given by the logarithmic rule of mixture is shown in concise form below. From Figure 6.22, it can be observed that the Lichtenecker's model is not valid.

$$\rho_c = \rho_m^{Vm} \rho_d^{Vd} \tag{6.24}$$

Electrical resistivity of SiC_p/Al composite was found to be best represented by the predictions of based on Series model. The effective electrical resistivity, according to Series model is given by the following relation.

$$\frac{1}{\rho_c} = \frac{V_m}{\rho_m} + \frac{V_d}{\rho_d} \tag{6.25}$$

This equation would correspond to a model in which a binary composite is visualized as an arrangement of material layers in a direction parallel to the direction of current flow. In which case current can pass through regions/layers of low resistivity and reflect in the resistivity of the composite. The behavior of effective physical property of a two phase composite material can be predicted by Series model, to a high degree of accuracy in cases where the physical properties of the individual phases differ largely in magnitude.

e) Thermal Conductivity

Thermal conductivity of SiC_p/Al composites was obtained from measurements of thermal diffusivity and specific heat along with knowledge of density. The results of thermal conductivity obtained in this manner are shown in Figure 6.23. From the figure it can be observed that there is no regular trend in the variation of thermal conductivity as a

function of temperature at various volume fractions. The uncertainty in the measurement of thermal diffusivity is ± 3% which enabled the determination of thermal conductivity within ± 5%.

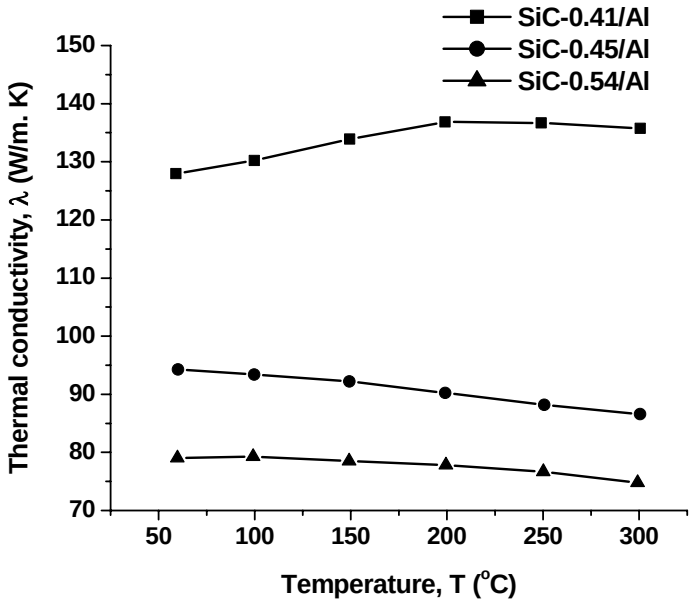

Figure 6.23 Thermal conductivity of SiC_p/Al composite as a function of temperature with different volume fractions of SiC

It can be observed that thermal conductivity decreases with volume fraction, at all temperatures between 50 – 300°C as expected.

References:-

1. F. P. Knudsen, *J. Amer. Cer. Soc*. **45** [2] (1962) 94.
2. M. I. Pech-Canul and M. M. Makhlouf, *J. Mater. Synth. Proc*. **8** [1] (2000) 35.
3. A. Zulfia and R. J. Hand, *J. Mater. Sci*., **37** (2002) 955.
4. R. Arpon, J. M. Molina, R. A. Saravanan, C. Garcia-Cordovilla, E. Louis and J. Narciso, *Acta Mater*. **51** (2003) 3145.

5. P. S. Turner, *J. Res. Natl. Bur. Stand.*, **37** (1946) 239.

6. E. H. Kerner, *Proc. Phys. Soc., B* **69** (1956) 808.

7. J. P. Thomas: *General Dynamics Report AD* 287-826 AQ4 (1960).

8. R. A. Schapery, *J. Compos. Mater.* **2** (1968) 380.

9. A. A. Fahmy and A. N. Ragai, *J. Appl. Phys.* **41** (1970) 5108.

10. S. Lemieux, S. Elomari, J. A. Nemes and M. D. Skibo, J. Mater. Sci., (1998) **33** p. 4381.

11. Alexander Evans, Christopher San Marchi and Andreas Moretensen, Metal Matrix Composites in Industry – An Introduction and a Survey, Kluwer Academic Publishers (2003).

12. W.D. Kingery, *Introduction to Ceramics,* Wiley, London and New York (1960) 502.

13. Jianping Zhang, Dang – Hyok Yoon and Burtrand I. Lee, *Mat. Res. Bull*. **38** (2003) 765.

14. R. G. Munro, Journal of Physical and Chemical Reference Data, **26**, (1997) 1195.

15. W. Voigt, *Lehrbuch der Kristallphysik*, Leipzig. (1928)

16. A. Reuss, *Z. Angew Math*. **9** (1929) 49.

17. K.S. Ravichandran, *J. Am. Ceram. Soc*. **77** [5] (1994) 1178.

18. C.-L. Hsieh and W.-H. Tuan, *Mat. Sci. and Eng*, **A 425** (2006) 349.

19. A. J. Owen and I. Koller, *Polymer* **37** [3] (1996) 527.

20. K. Lichtenecker, *Physik. Z*. (1924) **25** p. 225.

21. Rolf Landauer, *J. Appl. Phys*., (1952) **23** [7] p. 779.

7. Mechanical Properties of SiC_p/Al Composites

a) Flexural Strength

SiC_p/Al metal matrix composites were evaluated for flexural strength in a three point bending configuration according to standard procedures recommended by ASTM International. Composites with different volume fraction of SiC were evaluated at room temperature. The Load vs. Displacement curves for SiC_p/Al composites with SiC volume fraction, V_f **:** 0.41 – 0.70 are shown in Figure 7.1

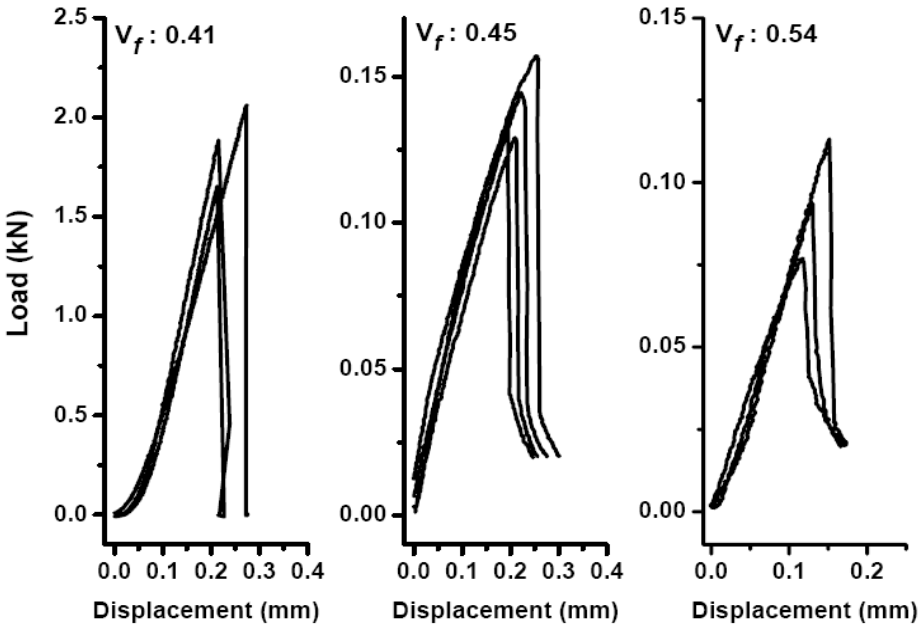

Figure 7.1 Load vs. Displacement curves for SiC_p/Al Metal Matrix Composites.

The flexural strength of SiC_p/Al composites fabricated in the present work was found to be in the range of 213 – 159 MPa for SiC volume fractions in the range of 0.41 – 0.54. The standard uncertainty in the measurement of flexural strength of SiC_p/Al metal matrix composites was estimated to be 2%. The flexural strength of SiC_p/Al metal matrix composites fabricated in the present work is listed in Table 7.1 for different volume fractions of SiC.

Table 7.1 Flexural Strength of SiC_p/Al composites under three point loading

Sl. No.	SiC Volume Fraction	Flexural Strength (MPa)
1.	0.41	213 ± 14
2.	0.45	234 ± 10
3.	0.54	159 ± 16

The strength of brittle material is more completely described with a statistical measure of this variability, e.g. Weibull modulus[§]. High Weibull modulus is indicative of little variation in measurements and the average strength is a representative of the potential sample-to-sample performance of the material. Low Weibull modulus reflects a high variation in measured strengths and an increase in the likelihood that flaws will tend to congregate and produce a weaker material. Weibull modulus (m) was deduced from following relations, where P_S is probability of survival at fracture stress denoted by σ and σo is the fracture stress at which the probability of survival is 1/*e*. See Figure 7.2.

$$\ln\left(-\ln\left(P_s\right)\right) = m\ln\sigma - m\ln\sigma_o \qquad P_S = 1 - i/\left(N+1\right)$$

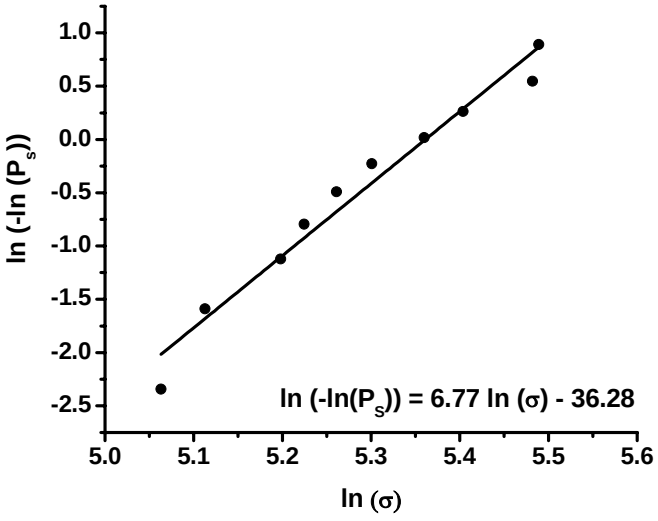

Weibull Modulus : 6.77

Average Strength : 213 MPa

Figure 7.2 Evaluation of Weibull Modulus of SiC_p/Al composites

In the present work, volume fraction was increased by using bimodal and trimodal size distributions in the preforms. As a result, SiC particle reinforced Aluminum

§ W. Weibull, *J. Appl. Mech.* 18 (1951) 293.

composites with a volume fraction ≥ 0.45 were comprised of SiC particulates of grit sizes 600, 220 and 36. The concentration of grit 36 is rather high in the case of SiC_p/Al composite with volume fraction 0.54 as is evident from the optical microstructures shown in Figure 5.5. Moreover, the coarse particulates possess more number of defects than finer particulates. As a result, greater is the concentration of internal defects in the case of a composite with higher concentration of coarser particulates as reinforcing phase. The main reason for lower flexural strength of SiC_p/Al composite with volume fraction of 0.54 can be attributed the very fact that it contains larger concentration of coarser particulates which possess porosity levels of up to 0.53%. The higher concentration of Si in the Al matrix could be another factor that has affected the flexural strength of SiC_p/Al composites prepared in the present work.

b) Fracture Toughness

Another most important mechanical property that is helpful in monitoring the health of a structural material is its fracture toughness. This is a measure of stress that would initiate the propagation of a pre-existing crack. Fracture toughness of SiC_p/Al metal matrix composites fabricated in the present work was determined by the single edge notched beam method under three point bending configuration. Standard test method, ASTM E-399 was used in the case of metal matrix composites. The corresponding Load vs. Displacement curves are shown in Figure 7.3 below. The fracture toughness of SiC_p/Al composites was determined and its variation was studied as a function of volume fraction of SiC. The uncertainty in the measurement of fracture toughness of SiC_p/Al metal matrix composites was estimated to be 2.3 %. The observed variation is shown in Figure 7.4 along with fracture toughness data for sintered α-SiC [1]. The results were compared with predictions of Parallel and Series models [2,3]

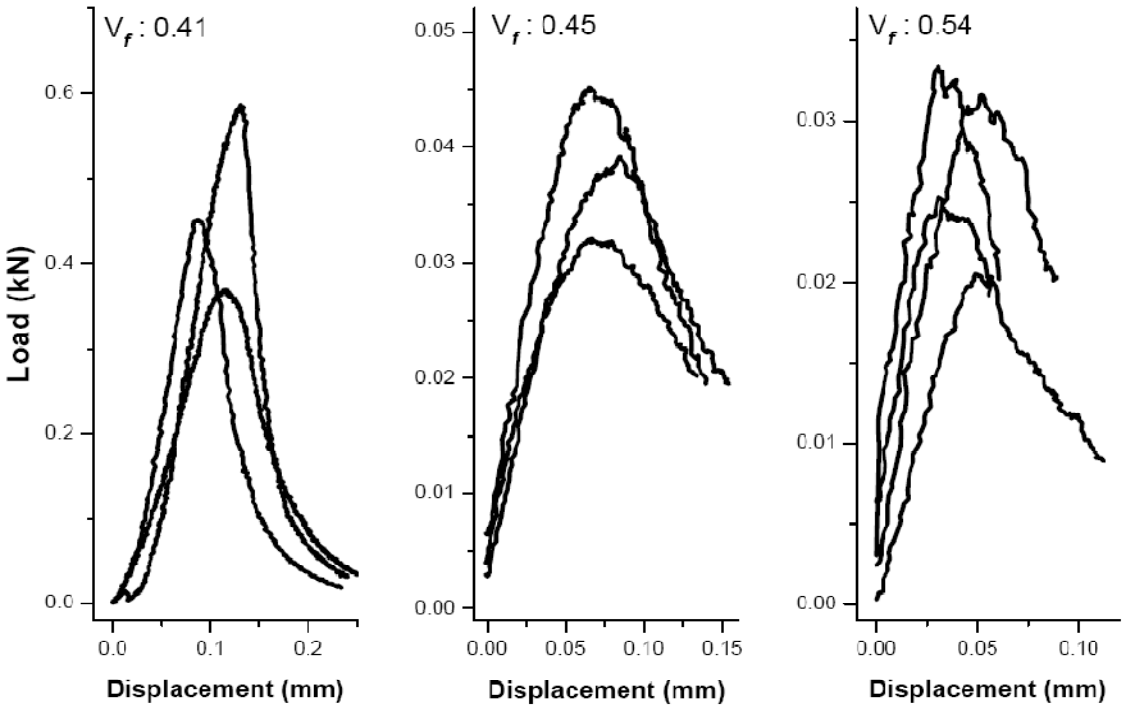

Figure 7.3 Load-Displacement curves for SiC_p/Al Metal Matrix Composites.

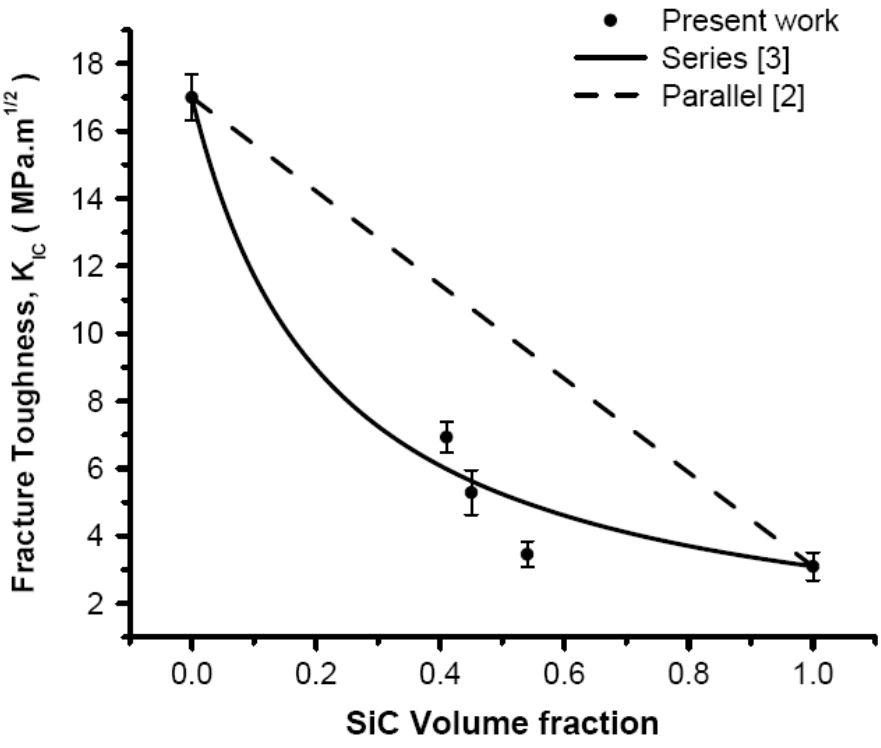

Figure 7.4 Variation of Fracture Toughness of SiC_p/Al Metal Matrix Composites.

A gradual decline was observed in the fracture toughness of SiC_p/Al MMCs with increase in volume fraction of SiC. The mode of fracture has changed from semi brittle to almost brittle. The dominant mode of fracture was found to be brittle in the case of high volume fraction SiC_p/Al MMCs with volume fraction in the range of 0.41 to 0.54 and beyond. The fractured surfaces were subsequently examined under SEM in order to throw light on the overall nature of fracture. These low levels of fracture toughness are basically unacceptable for structural applications. However, these high volume fraction SiC_p/Al composites possess requisite mechanical properties that are suitable for electronic packaging applications. The main reason behind the low levels of fracture toughness was supposed to be the reinforcement particle size. Metal matrix composites reinforced with fine particulates often offer high values of fracture toughness. This is so because of high density of dislocations developed around a finer inclusion than a coarser inclusion. In the case of fracture through the matrix region, it is these dislocations that offer resistance to propagation of an intrinsic or extrinsic crack. In the present work, the size of the reinforcement is quite large. As a result, the overall resistance to crack propagation through matrix region was rather limited. Moreover, the composition of the matrix phase too has an effect on the fracture toughness of SiC_p/Al MMCs. As a consequence of processing schedule, the composition of matrix phase has changed substantially. The matrix phase has developed a lot of Si resulting in hypo-eutectic Al-Si alloy, which possesses very low levels of fracture toughness. Further, at higher volume fractions of the brittle phase a deviation has been observed between the experimental data and the predictions of Parallel and Series models. This indicates that the role of matrix phase has ceased in arresting the propagation of cracks at volume fractions ≥ 0.45,

following which the composites have failed in a brittle mode of fracture. Reasons similar to those encountered in the analysis if flexural strength i.e., large size of reinforcement particulates, pores within the reinforcement which would act as stress concentrators and high Si content may be ascribed to the low levels of fracture toughness obtained for SiC_p/Al composites fabricated in the present work.

c) Hardness

Variation in the Vickers hardness of SiC_p/Al composites fabricated by the pressureless infiltration process was studied as a function of volume fraction of SiC. A plot of the same is shown in Figure 7.5 where the hardness data corresponding to residual matrix metal is included along with that of sintered α-SiC [1]. Hardness of SiC_p/Al metal matrix composites has increased with volume fraction of SiC which is expected. However, the increase in hardness was rather systematic up to a volume fraction of 0.54, beyond which a rapid increase in hardness was observed.

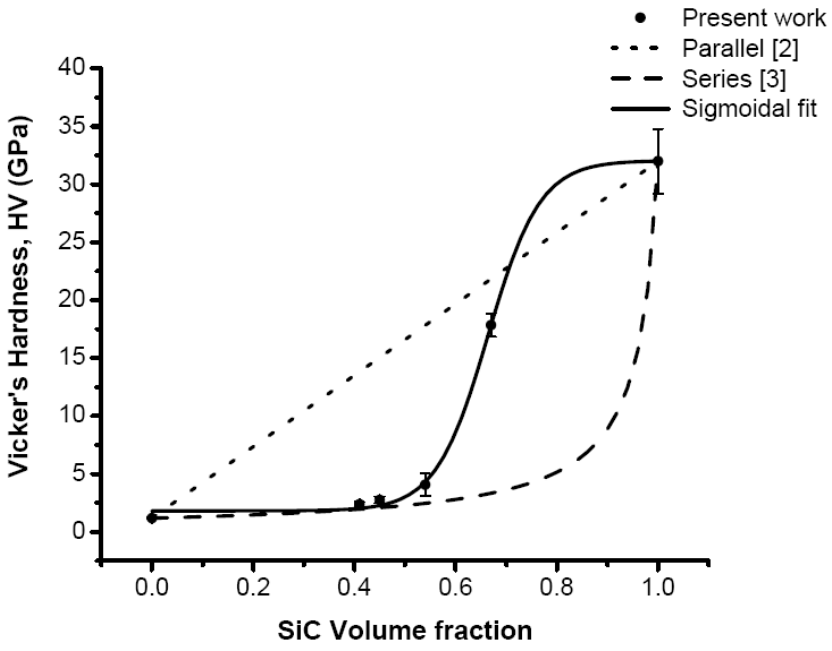

Figure 7.5 A Sigmoidal relationship between Hardness and volume fraction

Also shown in Figure 7.5 is a comparison of the experimental data with the predictions of Series and Parallel models [2, 3]. Sigmoidal relationship between hardness of SiC_p/Al MMCs and SiC volume fraction with a coefficient of square of regression, R^2: 0.998. The empirical fit between hardness and volume fraction depicts a nominal increase in the hardness for volume fractions up to 0.54 which is followed by a rapid increase in hardness. However, a fall in slope was observed after a certain volume fraction, ~ 0.74, beyond which there is no substantial increase in the hardness, as depicted by the empirical fit. Experimental data on hardness of SiC_p/Al composites was not available from the present work for volume fractions up to 0.40 of SiC. Restricting to the high volume fraction region of hardness vs. volume fraction plot, it should be understood that the indenting load shall be borne by the matrix and reinforcement phases together. Up to a volume fraction of 0.54, majority of the indenting load was borne by the matrix phase which is softer and has undergone deformation. At further higher volume fractions of SiC, both the experimental data and the empirical fit show very high values of hardness which are not encountered on usual basis. This indicates that at higher volume fractions of SiC with lower volume fraction of metallic (i.e., soft) phase, there is little room for the deformation of metallic phase which is basically entrapped within SiC particulate assemblies. As a result, most of the indenting load is borne by the reinforcement phase. Such a trend can be observed up to a volume fraction ~0.74 of SiC. Further extrapolation for volume fraction between 0.74 and 1.00, it is seen that there is hardly any increase in the hardness of SiC_p/Al composites. This can be understood in the following manner. It is well known that with increasing volume fraction the inter-particle spacing tends to come down. As a result, a situation arises in the case of discontinuously reinforced composites

wherein the reinforcement particulates tend to touch each other at higher volume fractions and the entire indenting load is borne by the reinforcement phase. This leads to a stage where the reinforcement particulates are almost interlocked which further results in a high hardness equivalent to that of reinforcing phase itself.

d) Fractography

Specimens fractured during three point bending test performed for the evaluation of flexural strength and fracture toughness of SiC_p/Al composites were examined under SEM for further investigations pertaining to the nature of fracture. Typical fractographs of few composites are shown in the following figures. The fracture of SiC_p/Al metal matrix composite is comprised of both brittle and ductile modes of fracture. Features of brittle mode of fracture are evident even at low magnifications as can be seen from Figures 7.6. From the figure it can be observed that the reinforcement phase has failed in a brittle manner with clear facets across the path of the crack. The matrix phase has failed in a ductile manner as can be seen from the dimples originated on the fractured surface. The fractographs viewed at higher magnification shown in Figure 7.8 would reveal the extent of elongation exhibited by the metallic phase in localized environments.

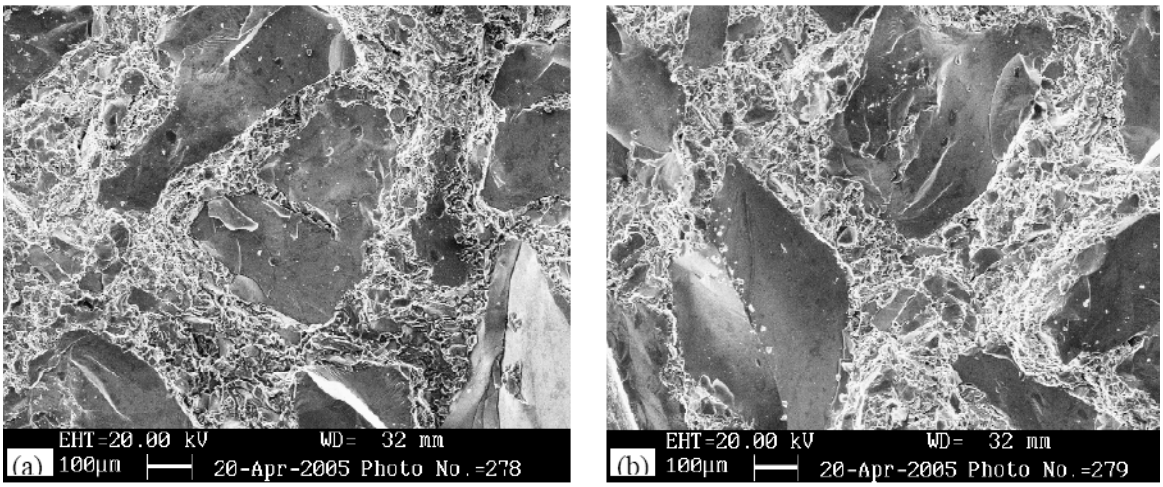

Figure 7.6 Fractographs of SiC_p/Al composites. (a) V_f : 0.45 and (b) V_f : 0.54.

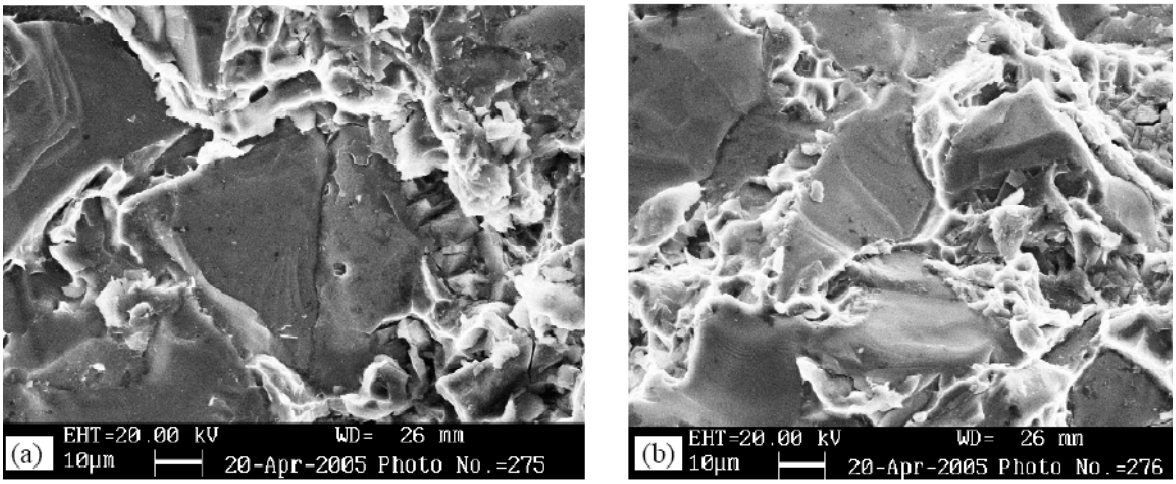

Figure 7.7 Fractographs of SiC_p/Al at high magnification. (a) V_f : 0.45 (b) V_f : 0.54

The average depth of dimples originated during fracture of a metallic phase is an indirect means of having a rough estimate of its fracture toughness. In the present case, it can be observed that the depth of the dimples is rather lower which indicates that the matrix phase itself possesses low fracture toughness. The very reason for the value of fracture toughness of the matrix shall be ascribed to high concentration of Si within the matrix phase.

Moreover, the lower levels of flexural strength obtained for SiC_p/Al metal matrix composites fabricated in the present work can be ascribed to more than one factors. The reinforcement phase used in the present work is a commercial grade SiC that is commonly used as an abrasive. As the pycnometric measurements suggest that the true density of SiC powder is 3.197 g/cc, it is evident that the rest is porosity in its different forms. Moreover, purity of commercial grade SiC is limited to 96%. Above all, the dominant reason behind lower levels of flexural strength is the larger size of the particulates employed in the preparation of powder preform, either loose or compact.

Apart from the reinforcement, the matrix phase too has a key role in resistance to deformation in the case of composite materials which are based on the principle of combined action. The matrix phase is the direct load bearing component of a composite material. The matrix phase is rich in Si which lowers the material's resistance to crack propagation. The load borne by the matrix phase is then transferred on to the reinforcement phase which is the indirect load bearing component of the composite material. In such a situation, the efficiency of load transfer would depend on bonding between the reinforcement and matrix phases i.e. the interphases, its nature and composition.

Interfacial reaction products between SiC and Al, such as Al_4C_3 are rather detrimental to the overall mechanical properties of SiC_p/Al composites. It is very essential to avoid the formation of Al_4C_3 that is not only a weaker interfacial reaction product but also hygroscopic. In the present work, appropriate care has been taken to prevent the formation of Al_4C_3 by providing more Si in the alloy and SiO_2 on SiC by

artificial oxidation in air. Absence of Al_4C_3 phase has been confirmed from various phase analytical techniques such as XRD, SEM-EDAX and SEPMA-WDAX. This observation then rules out the role of interfacial reaction product Al_4C_3 in lowering the flexural strength and fracture toughness of SiC_p/Al composites fabricated in the present work. Thus, high Si content in the alloy and large size of the reinforcement remain as the main reasons for lower levels of fracture toughness and flexural strength.

References:-

1. R. G. Munro, Journal of Physical and Chemical Reference Data, **26**, (1997) 1195.
2. W. Voigt, *Lehrbuch der Kristallphysik*, Leipzig. (1928)
3. A. Reuss, *Z. Angew Math*. **9** (1929) 49.

Summary and Conclusions

This chapter is comprised of summary and conclusions of the research work on the processing of SiC_p/Al two phase composite systems by the process of pressureless infiltration and its characterization.

The process of Pressureless Infiltration patented by the Lanxide Corporation could be reproduced to fabricate SiC_p/Al composites. Subsequent to the inventors, for the first time SiC_p/Al composites with dimensions 70 mm x 70 mm x 25 mm and beyond have been generated. These bulk composites were used for the purpose of various physical property measurements. The limitation on the volume fraction has been overcome and volume fractions as high as 0.70 of SiC were obtained in the present work. The conditions developed for pressureless infiltration were favorable to infiltrate molten Al into SiC preforms of higher volume fractions. These composites with a low coefficient of thermal expansion are adequate for thermal management applications.

By taking necessary precautions prior to thermal processing it was possible to protect the reinforcement from dissolution in molten Al and prevent the formation of Al_4C_3 phase. The absence of Al_4C_3 phase was confirmed using sophisticated analytical instruments such as electron probe micro analyzer. By identifying presence of extra phases developed as a result of processing schedule, it was possible to throw light on the stages involved in the process of reactive wetting that aids in spontaneous infiltration of Al alloy in to ceramic preforms. Also, the growth mechanism of extra phases was discussed.

It was observed that SiC_p/Al composites prepared in the present work were found to possess density that is in accordance with the density predicted by Rule-of-Mixtures. The composites were also found to be non-porous and thus, have qualified for further physical property measurements. An estimate of the total porosity present in the composites was made and it was observed that total porosity did not have any regular trend with increase in volume fraction.

The average coefficient of thermal expansion of SiC_p/Al composites prepared in the present work was found to have a non-linear relationship in the volume fraction range of 0.41 to 0.70 of SiC. Theoretical predictions of Kerner, Schapery, Fahmy-Ragai etc. were found to have deviation from experimental results. The overall behavior of the coefficient of thermal expansion of SiC_p/Al composites was found to be sigmoidal with volume fraction of SiC. Over the entire range of volume fraction, it was observed that theoretical predictions were valid up to a volume fraction ~ 0.55 of SiC. Nevertheless, the gross behavior of average coefficient of thermal expansion of SiC_p/Al two phase metal matrix composite system is governed by volume fraction in terms of a sigmoidal relationship.

SiC_p/Al composites with high volume fraction of reinforcement have been evaluated for ultrasonic velocity for the first time in literature. Measurements of velocity were performed in longitudinal and shear modes of vibration. It was found that the longitudinal wave velocity and shear wave velocity have a linear relationship with volume fraction of SiC in the volume fraction range of 0.41 and 0.70 of SiC. Elastic properties of SiC_p/Al composites were evaluated from ultrasonic velocity data.

Theoretical prediction by Owen and Koller is based on the fact that the transverse constraints on the two phases due to Poisson contraction need to be considered. It was observed that this kind of an approach towards the determination of effective physical properties of a two phase composite system is more realistic. Elastic properties determined from ultrasonic measurements were found to agree well with the predictions of Owen and Koller and have contributed in validating the basis of the model.

Electrical resistivity of SiC_p/Al composites was found to be invariant with volume fraction in the range of 0.00 to 0.70 of SiC. However, a drastic change in the electrical resistivity was observed for SiC volume fraction beyond 0.70. Because of the huge difference in the magnitudes of electrical resistivity of the two phases, the experimental data was found to be close to the predictions of Series model.

Thermal conductivity of SiC_p/Al composites was evaluated by Flash method and was found to range between 140 – 80 W/m. K for SiC volume fraction in the range of 0.41 – 0.54. It was concluded that thermal conductivity of SiC_p/Al composites decreases with volume fraction of SiC.

The composites fabricated in the present work were further evaluated for their mechanical properties such as flexural strength, fracture toughness, hardness followed by fractography of the fractured specimens. The flexural strength was found to decrease from 213 MPa to 159 MPa for SiC volume fractions ranging from 0.41 to 0.54. the fracture toughness of SiC_p/Al composites was found to decrease from 6.9 MPa$\sqrt{m}$ to 3.5 MPa$\sqrt{m}$ for SiC volume fraction ranging between 0.41 and 0.54. The decrease in flexural strength and fracture toughness was mainly attributed to the high concentration

of coarser SiC particles used in preparation of high volume fraction SiC_p/Al composites. Fracture toughness of SiC_p/Al composites fabricated in the present work were found to be bound by the predictions of Series and Parallel models up to a reinforcement volume fraction of 0.45, beyond which the fracture toughness was found to deviate from theoretical predictions. The hardness of SiC_p/Al composites was found to increase from 2.4 GPa to 17.8 GPa for SiC volume fraction between 0.41 and 0.67. The predictions of Series and Parallel models for hardness were found to function as bounds. Nevertheless, the hardness of SiC_p/Al composites was found to bear a sigmoidal relationship with volume fraction of SiC. From fractographic studies of SiC_p/Al composites, it was understood that the composites possess low levels of fracture toughness because of lower fracture toughness of the matrix phase which could be due to high Si content in the matrix alloy.

SiC_p/Al composites prepared in the present work were found to be free from defects/voids and undesired phases such as Al_4C_3. The composite specimens were large enough for physical property measurements and development of an electronic package shown in Figure 8.1. A brief comparison of various physical properties of interest for thermal management in electronic packaging applications is given below in Table 8.1 along with the physical property data for high volume fraction SiC_p/Al composites prepared in the present work.

Table 8.1 Thermal properties of Semi conductor, substrate and electronic packaging materials

Sl. No.	Material	Description	Density (g/cc)	CTE (x 10^{-6} /K)	Thermal Conductivity (W/m. K)
1.	Si	Device	2.3	4.2	156
2.	GaAs	Device	5.2	6.5	54
3.	Al_2O_3	Substrate	3.9	8.3	30
4.	AlN	Substrate	3.3	4.5	150
5.	Kovar	Package/ heat sink	**8.2**	5.6	**17**
6.	Al(6061)	Package/ heat sink	2.7	23	172
7.	Cu	Package/ heat sink	9	17	394
8.	W/Cu	Package/ heat sink	**16**	6.0 – 8.8	180 – 200
9.	Mo/Cu	Package/ heat sink	10	7.0 – 8.0	160 – 170
10.	SiC_p/Al* (70% SiC)	Package/ heat sink	**3.02**	**6.45**	**110**

* Present work

SiC_p/Al composites with features required for electronic packaging applications were developed and were found to be superior over other electronic packaging material like W/Cu in terms of density and Kovar in terms of both density and thermal conductivity. Machinability of these composites into specific designs was demonstrated.

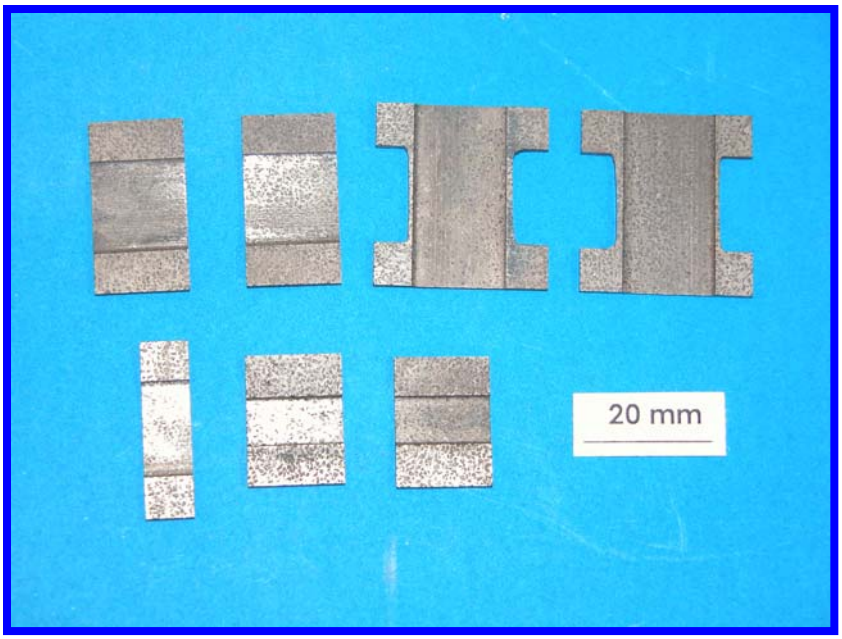

Figure 8.1 Electronic Packages made out of SiC_p/Al composites prepared in the present work

References:-

1. M. K. Aghajanian, M. A. Rocazella, J. T. Burke and S. D. Keck, *J. Mater. Sci*., **26** (1991) 447.
2. S. Elomari, M. D. Skibo, A. Sundarrajan and H. Richards, *Comp. Sci. & Tech*., **58** (1998) 369.
3. R. Arpon, J. M. Molina, R. A. Saravanan, C. Garcia-Cordovilla, E. Louis and J. Narciso, *Acta Mater*. **51** (2003) 3145.
4. P. S. Turner, *J. Res. Natl. Bur. Stand.,* **37** (1946) 239.
5. E. H. Kerner, *Proc. Phys. Soc.,* B **69** (1956) 808.
6. J. P. Thomas: *General Dynamics Report AD* 287-826 AQ4 (1960)
7. R. A. Schapery, *J. Compos. Mater.* **2** (1968) 380.
8. A. A. Fahmy and A. N. Ragai, *J. Appl. Phys.* **41** (1970) 5108.
9. W. Voigt, *Lehrbuch der Kristallphysik*, Leipzig. (1928)

10. A. Reuss, *Z. Angew Math*. **9** (1929) 49.

11. K.S. Ravichandran, *J. Am. Ceram. Soc*. **77** [5] (1994) 1178.

12. C.-L. Hsieh and W.-H. Tuan, *Mat. Sci. and Eng*, **A 425** (2006) 349.

13. A. J. Owen and I. Koller, *Polymer*, **37** [3] (1996) 527.

14. K. Lichtenecker, *Physik. Z*. **25** (1924) 225.

15. Rolf Landauer, *J. Appl. Phys*., **23** [7] (1952) 779.

16. C. Zweben, *Power Electronics Technology* **2** (2006) 40.

Curriculum Vitae

Name	: S. Santhosh Kumar
Father's name	: S. Subramanyam
Mother's name	: S. Suguna Mani
Nationality	: Indian
Religion	: Hindu
Date of birth	: 07.06.1980
Languages known	: Telugu, Hindi, Urdu & English

Educational Qualifications:

Name of the Examination	Board/University	Month & Year of Passing	Percentage of Marks
Secondary School Certificate	Board of Secondary Education – AP	May 1995	78.67
Intermediate Public Examination	Board of Intermediate Education – AP	May 1997	78.90
Bachelor of Science	Osmania University	April 2000	67.88
Master of Science	University of Hyderabad	May 2002	63.60
Doctor of Philosophy	University of Hyderabad	June 2008	

Extra Curricular Activities:

1. Passed out National Level NCC-B Certificate Examination in the year 1998 from No. 1 (Andhra) Air Squadron Unit held by the NCC Directorate, Secunderabad.
2. Represented No. 1(Andhra) Air Squadron Unit at the Republic Day Parade held at the Parade Grounds, Secunderabad in the year 1999.

Address for Correspondence:

S. Santhosh Kumar
H. No. 23-232, Brundavan Nagar Colony
Bhoodevinagar Extension
Trimulgherry P.O.,
Secunderabad – 500 015
Phone : 040 – 27993301, +91-9989691093
E-mail : dearsanthosh@gmail.com, santhosh_7@rediffmail.com

List of Publications

1. Aluminium matrix composites by pressureless infiltration: the metallurgical and physical properties.

   S. Santhosh Kumar, V. Seshu Bai and T. Rajasekharan *J. Phys. D: Appl. Phys*. **41** (2008) 105403 (6pp) doi:10.1088/0022-3727/41/10/105403

2. Elastic modulus of Al-Si/SiC metal matrix composites as a function of volume fraction

   S. Santhosh Kumar, V. Seshu Bai, K. V. Rajkumar, G. K. Sharma, T. Jayakumar and T. Rajasekharan (Accepted for publication in *J. Phys. D: Appl. Phys*.)

3. Characterization of W_p/Al-Si-Mg metal matrix composites fabricated by pressureless infiltration.

   S. Santhosh Kumar, V. Seshu Bai and T. Rajasekharan (Communicated to *Comp. Sci. Technol*.)

Conferences

1. Al/SiC_P metal matrix Composites.

   S. Santhosh Kumar and T. Rajasekharan. Oral Presentation at the National Conference on "Materials for Electrical, Electronic & Magnetic Applications: Characterization & Measurements - MEEMA 2005", September 2-3, 2005, Hyderabad, India.

2. Properties of Al/SiC_P metal matrix composites as a function of reinforcement content.

   S. Santhosh Kumar, K. Balkis Ameen and T. Rajasekharan. Accepted for Oral Presentation at the "30th International Conference & Exposition on Advanced Ceramics & Composites", January 22-27, 2006, Florida, USA.

3. Physical properties and microscopic features of Aluminum alloy reinforced with tungsten particulates.

   S. Santhosh Kumar and T. Rajasekharan. Oral Presentation at the International Conference on Advanced Materials & Composites - ICAMC 2007, Trivandrum, India. October 24-26, 2007

4. Al_2O_3-SiC ceramic matrix composite: Physical properties and microscopic features.

   S. Santhosh Kumar, M. Devaiah and T. Rajasekharan. Poster Presentation at the International Conference on Advanced Materials & Composites - ICAMC 2007, Trivandrum, India. October 24-26 2007

5. Ultrasonic properties of Al-Si/ SiC metal matrix composites prepared by pressureless infiltration technique.

   S. Santhosh Kumar, T. Rajasekharan, V. Seshu Bai, K.V. Rajkumar and T. Jayakumar. Oral Presentation at the International Symposium on Composites and Aircraft Materials - ACMA 2008, Agadir, Morocco. May 12-14, 2008

6. Mechanical and ultrasonic properties of Al_2O_3/SiC ceramic matrix composite prepared by directed metal oxidation of aluminum alloy.

   S. Santhosh Kumar, T. Rajasekharan, V. Seshu Bai, K.V. Rajkumar and T. Jayakumar. Oral Presentation at the International Symposium on Composites and Aircraft Materials - ACMA 2008, Agadir, Morocco. May 12-14, 2008

Seminars & Workshops

1. National Workshop on Non-Destructive Testing & Applications in Manufacturing Industries, 21-24 May 2008, Warangal, India.

2. National Workshop on Advances in Manufacturing Processes (AMP-2008), 8-10 August 2008, Warangal, India.

3. 22^{nd} National Convention of Metallurgical & Materials Engineers and National Seminar on Advanced Materials: Characterisation and Processing, 23-24 January 2009, Hyderabad, India.